NASA CR-132614

A STUDY FOR ACTIVE CONTROL RESEARCH AND VALIDATION USING THE TOTAL IN-FLIGHT SIMULATOR (TIFS) AIRCRAFT

By

Robert T.N. Chen
Hamilton Daughaday
Dominick Andrisani II
Robert D. Till
Norman C. Weingarten

AK-5560-F-1

April 1975

Prepared under Contract No. NAS1-13329 by
Calspan Corporation
Buffalo, New York 14221

for

NATIONAL AERONAUTICS AND SPACE ADMINISTRATION

FOREWORD

This study program was sponsored by the Langley Research Center, National Aeronautics and Space Administration. It was conducted by the Flight Research Department of Calspan Corporation, Buffalo, New York under Contract No. NAS 1-13329. The NASA project monitor was Mr. David B. Middleton and the Calspan project engineer was Dr. Robert T. N. Chen.

The authors would like to express their gratitude to the NASA personnel in the ACT project office for their helpful suggestions and stimulating discussions. Particular thanks are due to Messrs. L.W. Taylor, R.V. Hood, S. Hoffman, D.B. Middleton, and I. Abel. The authors also wish to express their appreciation to several members of the Flight Research Department of Calspan for their contributions. Special thanks are due to Messrs. Robert P. Harper, Jr., E.G. Rynaski, C.R. Chalk and L.S. Bloom. Grateful acknowledgement is also given to Mr. C.L. Mesiah, who was the project computer programmer and Mrs. J.A. Martino, Technical Editor for this report.

ABSTRACT

This report documents the results of a feasibility study and preliminary design for active control research and validation using the Total In-Flight Simulator (TIFS) aircraft. The objectives of this study program were to determine which active control functions can be demonstrated on the TIFS aircraft and to determine the cost of preparing, equipping, and operating the TIFS aircraft for active control technology development.

The study shows that the TIFS aircraft is a suitable test bed for in-flight research and validation of many ACT concepts. With the existing capability of the TIFS I (the Air Force TIFS), first phase flight programs can be initiated in a relatively short period of time and with a moderate cost for in-flight verification of potential benefits of such ACT functions as gust alleviation, precise flight path control, augmentation of relaxed static stability and envelope limiting system. With internal modifications on the mechanization of the ailerons to operate collectively as well as differentially (as they presently operate), first phase flight research programs for the maneuver load control and flutter control could then be initiated. With some external structural modifications, a more comprehensive second phase ACT flight research program using the TIFS aircraft could then follow.

Estimation of the cost for completing the TIFS II (Aero Space Lines, Inc. TIFS) to the present capability of the TIFS I has been performed. Also, some suggested improvements common to both TIFS I and TIFS II are presented in the report.

TABLE OF CONTENTS

TABLE OF CONTENTS (cont.)

LIST OF ILLUSTRATIONS

LIST OF ILLUSTRATIONS (cont.)

LIST OF ILLUSTRATIONS (cont.)

LIST OF TABLES

LIST OF SYMBOLS

b	wing span
$\bar{c}$	reference chord
g	gravity constant 9.8 m/sec^2 (32.2 ft/sec^2), also structural damping coefficients
h	altitude
$h_w^{(1)}$	1st symmetrical wing bending
$h_w^{(2)}$	2nd symmetrical wing bending
n_x, n_y, n_z	body axis components of accelerometer signals in g units
p, q, r	body axis components of angular velocity
q_i	generalized coordinates
s	Laplace operator
u	control vector
v	gust vector
v_m	discrete gust amplitude
w_g	vertical gust
$C_{r,i}$	in-phase control gains for active flutter control
C_l, C_m, C_n	body axis components of moment coefficient, $C_l = L/\bar{q}S$, etc
$-C_D, C_Y, -C_L$	wind axis components of aerodynamic force coefficient excluding thrust
D	drag, also dissipation function
F	matrix of dimensional stability derivatives
G	matrix of dimensional control derivatives
$G_{r,i}$	out-of-phase control gains for active flutter control
I	identity matrix

$I_{xx}, I_{yy}, I_{zz}, I_{xz}$	moments of inertia in the x , y , z body axis
J	matrix of dimensional turbulence input derivatives
$KCAS$	calibrated airspeed in knots
$KIAS$	indicated airspeed in knots
K_i	generalized spring constants
K_p	pilot gain, also feedback gain matrix
K_{ref}	reference reduced frequency
L	lift, number of control surfaces, also for scale
M	moment, also number of strips
$M_{i,j}$	generalized mass coupling coefficients
N	number of normal modes , Newtons
Q_i	generalized aerodynamic force acting in i^{th} degree of freedom
S	wing area
SM	static margin
T	thrust, kinetic energy, time constant, also for transformation matrix
U	potential energy
V_T, V	true airspeed
V_H	normalized tail volume
W	airplane weight
α	angle of attack
α_w	lst symmetrical wing, torsion
β	angle of sideslip
γ	flight path angle

$\delta_e, \delta_a, \delta_r, \delta_x$ $\delta_y, \delta_z, \delta_F$	control deflections of the TIFS elevator, aileron, rudder, throttle, side force surface, direct lift flap, and Fowler flap respectively
δ_{w_i}	control surfaces on the wing
$\delta_\theta, \delta_V, \delta_\gamma$	decoupling cockpit control for attitude, airspeed
$\delta_p, \delta_r, \delta_\beta$	flight path, roll, yaw, and sideslip respectively
λ	eigenvalue
τ	delay time
ζ	damping ratio
ω_n	undamped natural frequency
ω_i	uncoupled natural frequency of the i^{th} structural mode
ω_r	reference frequency
ω	frequency
t	time
ρ	atmospheric density
ϵ	downwash angle
σ_{w_g}	root mean square of the vertical gust
σ_{n_z}	root mean square of the normal acceleration
$\phi_{1/4}$	matrix of mode shapes at the 1/4 chord point, m x n
$\phi'_{1/4}$	matrix of slopes of mode shapes at 1/4 chord point, m x n
ϕ	bank angle
θ	pitch attitude
$[F]$	aerodynamic forces and moments per unit deflection of the normal mode coordinates
$[G]$	aerodynamic forcing terms due to deflection of control surfaces and atmospheric turbulence

$[K]$	diagonal matrix of generalized stiffness for the normal modes
$[M]$	diagonal matrix of generalized masses of the normal modes
$[Q]$	diagonal matrix whose elements are the $\mathcal{Z}$ force per unit deflection of each control surface
$[\zeta]$	generalized coordinate
$[u]$	external forcing terms such as control surface deflections or atmospheric turbulence

SYMBOLS AND ABBREVIATIONS

ATT	Advanced Technology Transport
TIFS	Total In-Flight Simulator
ACT	Active Control Technology
GA	gust alleviation
PFPC	precise flight path control
EL	envelope limiting
RSS	relaxed static stability
MLC	maneuver load control
FC	flutter control
cg	center of gravity
DOF	degrees of freedom
RMS	root mean square
DLF	direct lift flaps
SFS	side force surface
WB	wing bending mode
FB	fuselage bending mode
WT	wing torsion mode
psd	power spectral density
SCAS	stability and control augmentation system
CAS	control augmentation system
SAS	stability augmentation system
KIAS	indicated airspeed in knots
IPF	inboard plain flap
WRBM	wing root bending moment
RC	ride control

1. INTRODUCTION

The significant advancement in the active control technology of the past few years has been demonstrated in a number of experimental military aircraft flight programs sponsored by the Air Force and NASA (Reference 1). Using the B-52 aircraft as the test bed, a series of experimental programs have demonstrated, at selected flight conditions, the feasibility and the benefits of gust alleviation and ride control; flutter control, augmentation for relaxed static stability and the maneuver load control. Using the F-8 aircraft, NASA has demonstrated the feasibility of using the fly-by-wire digital flight control system. These flight programs, though experimental in nature, have given the impetus to a serious assessment of this emerging technology for possible application in the next generation transport aircraft.

System studies (Reference 2) for the Advanced Technology Transport (ATT) sponsored by NASA have been conducted by several airframe manufacturers which show that the application of ACT could reduce the weight and drag and improve ride quality, thus tending to reduce the direct operating cost of the commercial transport and to improve the ride comfort of both the passengers and the crew.

To prepare for the adoption of this technology for the next generation commercial aircraft designs, acceptable to both the commercial aircraft industry and the airline industry, NASA has been exploring possible avenues for gathering, cost effectively, flight test data under normal as well as extreme flight conditions for extensive verification of the benefits and operational practicality of the ACT systems, for identification of potential problem areas in the actual operational environment, and finally for the establishment of ACT system design criteria.

Under the sponsorship of NASA-Langley, Calspan has undertaken a feasibility study and cost estimate of using the total in-flight simulator (TIFS) to achieve the aforementioned purposes. The study shows that concept verification and gathering of valid data for design criteria development can be conducted for such ACT systems as gust alleviation (GA), precise flight path control (PFPC), envelope limiting (EL), and the augmentation of relaxed static stability (RSS) using the existing capability of the TIFS aircraft. With varying degrees of modifications, structurally and/or functionally, the TIFS aircraft can be used for more extensive flight research on the development of the above ACT systems and others such as maneuver load control (MLC) and flutter control (FC).

This report is organized as follows: Section 2 describes the two-phase program we recommend for an extensive ACT flight research program using the TIFS aircraft. Preliminary designs of some ACT systems illustrating the feasibility of mechanizing these systems on the TIFS aircraft are discussed in Section 3. Section 4 describes a preliminary development of the flexible equations of motion of the TIFS aircraft primarily for use in assessing the effect of structural modes on the gust alleviation and for structural mode stabilization study. Section 5 discusses the availability and cost of using TIFS as a test bed for the ACT system concept verification. Conclusions and recommendations are given in Section 6.

2. PRELIMINARY DEFINITION OF ACT FLIGHT PROGRAM USING THE TIFS

This section describes Calspan's preliminary definition of a two-phase flight research program using the TIFS aircraft, for ACT concept validation and for gathering test data to support development of ACT system design criteria. Before embarking on discussions of this suggested ACT flight program using the TIFS aircraft, a brief description of the TIFS aircraft will first be given.

2.1 The TIFS Airplanes

There are two TIFS airplanes: the USAF/TIFS (TIFS I), and the TIFS owned by the Aero Spacelines, Inc., Santa Barbara, California (TIFS II).

The TIFS I, as shown in Figure 1, is probably the most sophisticated and versatile variable stability airplane ever constructed. It is equipped with a large analog computer which can be patched for both response-feedback and model-following systems. The airplane has air data, control position, and inertial sensors and a digital tape data recording system. TIFS has independent control over the lift forces through large, nearly half span, direct-lift flaps which move both up and down. It has independent control over side force through large vertical surfaces built into the wings. The propellers are used for longitudinal force control and the conventional ailerons, elevator and rudder are used for roll, pitch and yaw control. All of these control surfaces are driven by full authority electrohydraulic servos. Aside from the side force control surfaces, TIFS most distinctive feature is the addition of a complete and removable second cockpit on the nose of the airplane. The capability of either masking the presently installed simulation cockpit, or easily removing it and adding a completely new one is unique. The instrument displays are readily changed. The airplane has been flown with a wheel controller, a side stick controller and with a center stick. The wheel controller, center stick and rudder pedals are equipped with variable feel systems including nonlinear functions. A more detailed description of this aircraft as well as its capability is given in Reference 3 and the references thereof.

A number of research projects and simulations of specific airplanes have been performed using the Air Force TIFS airplane. These include simulations of the space shuttle, the B-1 bomber and the Concorde supersonic transport; a flight research program to explore use of side force control in both automatic and manual modes, to counter crosswinds during crosswind landings; and flight demonstrations of multiplex techniques for flight control.

The TIFS II aircraft as shown in Figure 2, is basically similar to the Air Force TIFS with several notable differences. The evaluation cockpit is an actual 707 nose and includes pilot controls, seats and instrument panel of a 707. The Convair fuselage was shortened and the nose landing gear was

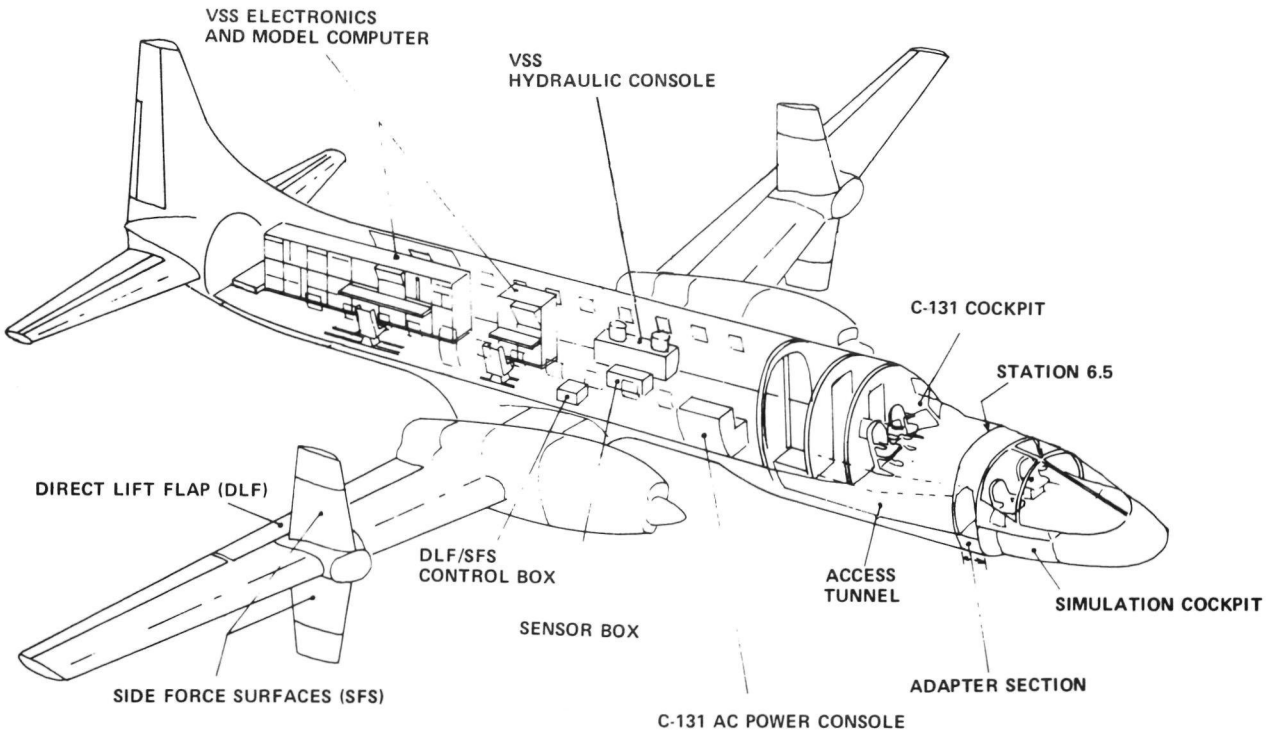

Figure 1 USAF FLIGHT DYNAMICS LABORATORY
TOTAL IN-FLIGHT SIMULATOR (TIFS I)

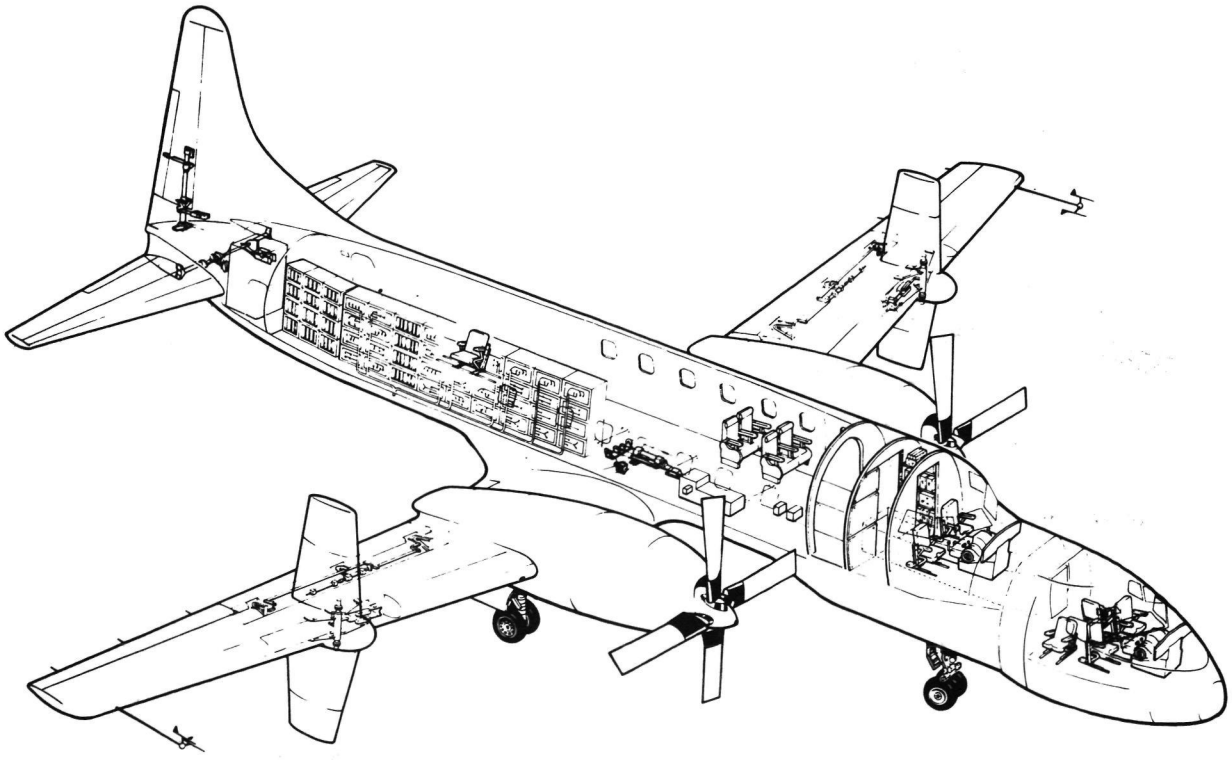

Figure 2 AERO SPACELINE INC. TOTAL IN-FLIGHT SIMULATOR (TIFS II)

relocated to maintain the same footprint, thus the fuselage structure and mass distribution are different. The electrical and hydraulic power supplies are driven by auxiliary power units mounted in the aft fuselage in TIFS II, rather than the engine mounted generators and pumps. The sensors, recording system and analog computer are basically the same as Air Force TIFS, except the analog computer potentiometers are automatically set by means of a card reader and the potentiometer settings are recorded on a paper printout (not yet completed). An engine thrust computer using multiplexed computation techniques is also included in TIFS II.

Although the TIFS II is basically similar in design to the Air Force TIFS, its control system is not completely installed and the TIFS II hardware has not been checked out or operated in flight; a cost estimate and time schedule are discussed in Section 5.

Several recommended improvements common to both TIFS airplanes, including installation of a digital computer to enhance the TIFS capability in on-line data analysis, safety monitoring of ACT systems, and digital flight control research are also discussed in Section 5.

2.2 A Two Phase ACT Flight Research Program Using the TIFS Aircraft

The ACT flight research program using the TIFS aircraft has been tentatively structured as a two-phase program. In the first phase of the program, which involves no external structural modifications of the TIFS aircraft, there are five ACT functions, i.e., Relaxed Static Stability (RSS), Maneuver Load Control (MLC), Gust Alleviation and Ride Control (GA/RC), Envelope Limiting (EL), and Precise Flight Path Control (PFPC) that can be validated in flight individually as well as in combination using the TIFS aircraft. The second phase of the program, which involves several structural modifications of the TIFS aircraft, will further validate some of these functions, such as MLC and GA/RD in a more complete manner as well as the concept of active flutter control(FC).

The major emphasis has been placed on the first phase program in this study. In fact, preliminary system design for several ACT functions that can be validated in flight using the TIFS aircraft in this phase has been performed, with varying degrees of completion as shown in Section 3. The ACT concept research and validation that are achievable in this phase of the flight program using the TIFS aircraft are shown in the upper half of Figure 3. Three internal modifications are involved, but there will be no external structural modifications. These internal modifications are the improvement of bandwidth of the elevator and rudder servos and the mechanization of the ailerons for collective as well as for the existing differential operation. Details of these modifications will be discussed in Section 5.

The fact that some flight programs for ACT functions such as GA/RC, PFPC, and EL can be initiated in a relatively short period of time in Phase I using the TIFS I aircraft permits an early in-flight verification of problem

areas and limitations that the presently configured TIFS might have. These flight test data will be very important for more definitive planning for the Phase II flight program.

The Phase II program will involve varying degrees of structural modifications of the TIFS aircraft as indicated in the lower part of Figure 3. Preliminary cost estimates for these modifications have been prepared and submitted to NASA in a separate letter.

Phase	Existing Control Surfaces & Devices	Modifications and/or Addition of Control Surfaces	ACT Functions					
			RSS	MLC	GA/RC*	EL	FC	PFPC
I	Ailerons	Collective operation		✓				✓
	Elevator	Bandwidth widened	✓		✓	✓		✓
	Rudder	Bandwidth widened			✓	✓		✓
	DLF			✓	✓			✓
	SFS				✓			✓
	Throttle				✓			✓
	Fowler flaps							
II	Ailerons (with collective oper.)	Splits			✓		✓	
	Elevator (bandwidth widened)							
	Rudder (bandwidth widened)							
	DLF							
	SFS							
	Throttle							
	Fowler flaps	Replaced plain flaps with wide bandwidth servos		✓	✓			
		Horizontal canards added with wide bandwidth servos			✓			
		Vertical canards added with wide bandwidth servos			✓			
		Wing tip surfaces added with wide bandwidth servos			✓		✓	

* Including structural mode stabilization

Figure 3 Control Surface for ACT Functions

3. PRELIMINARY DESIGN OF ACT SYSTEMS

Using the TIFS as the study aircraft, preliminary system design for several ACT functions has been performed. These ACT functions include gust alleviation, flutter stimulation and suppression, and precise flight path control. Considerations on the configuration that can be mechanized on the TIFS aircraft for in-flight research and validation of other ACT functions such as envelope limiting, augmentation of relaxed static stability and maneuver load control are also included in this section.

3.1 Gust Alleviation System

With incorporation of the active control technology into the design of the future generation transports, the airframe may be lighter, more flexible and hence, more sensitive to the turbulence. Also, with more all-weather operations anticipated in the future, there will be higher percentage of flight time in the rough air especially for the shorter-haul aircraft which operate at lower altitudes and have low wing loadings. As a result of these trends, it may be desirable to incorporate a gust alleviation system in the future transport to smooth the ride of both the passengers and the crew and to reduce the fatigue of the airframe structure.

The TIFS aircraft is a suitable air vehicle for developing gust alleviation systems and for gathering valid flight data for establishing the design criteria for the gust alleviation and ride control. The TIFS aircraft is equipped with control surfaces such as direct lift flaps (DLF) and side force surfaces (SFS) for generation of adequate direct forces. This feature together with the high resolution and wide bandwidth built into the servo actuators of the control surfaces, assures necessary gust alleviation capabilities for research and development of gust alleviation systems. Furthermore, the TIFS aircraft, because of its relatively low wing loading and high aspect ratio of the wings, is sensitive to gusts and thus more representative of the turbulence sensitive feature of the future STOL transports and more suitable for flight research in assessing gust alleviation system effectiveness.

3.1.1 Gust Sensitivity of the TIFS Aircraft

The TIFS airplane is relatively sensitive to turbulence as is evident from Figure 4, in which the rms of the normal acceleration response to unit rms of the vertical gust at the three stations (at 10.06m (33 ft) forward of c.g., at c.g., and at 10.06m (33 ft) aft c.g.) in landing, climb, and cruise conditions is shown. The longitudinal three-degree-of-freedom (DOF) rigid body representation for the TIFS aircraft was used in the calculation. The gust spectrum used in the calculation was of the Dryden form, which has similar characteristics as shown in Figure 7 for the von Karman form. Appendix A lists the data used in the calculation. The recommended satisfactory level shown in Figure 4 was calculated using the criterion for the vertical acceleration of 0.11 g (References 4 and 9) and the intensity for the clear air turbulence at

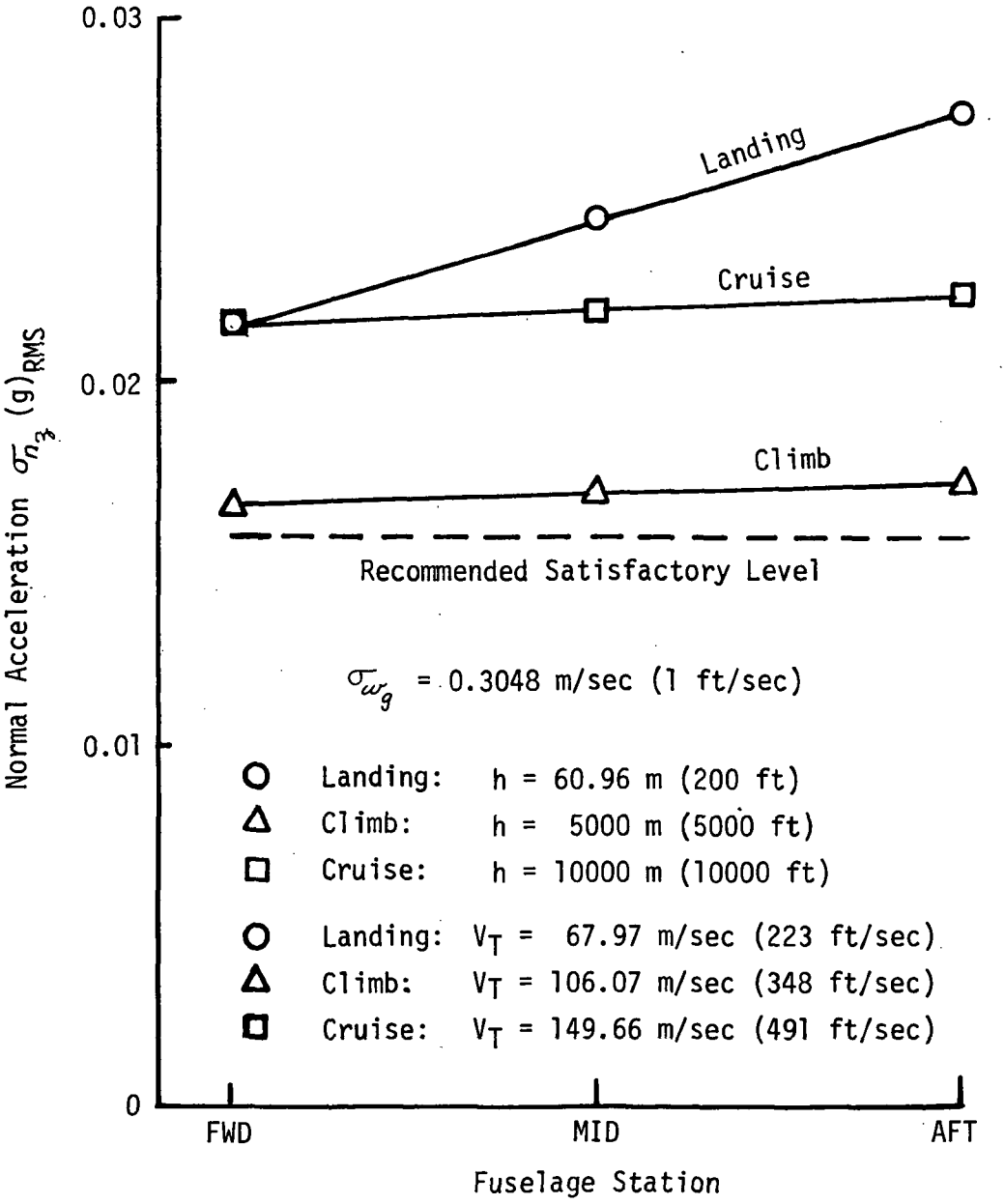

Figure 4 TIFS GUST SENSITIVITY, RIGID AIRPLANE

the landing configuration of σ_{w_g} = 2.04 m/sec (6.7 ft/sec) (Reference 7). As shown in the figure, the TIFS airplane exceeds the recommended satisfactory level for all of the three flight conditions considered.

Figures 5 and 6 show the gust sensitivity of the TIFS aircraft using a flexible representation which includes a total of 8 normal modes (2 rigid body and 6 structural modes)as described in Section 4. The von Karman form of the vertical gust spectra was used in this calculation as shown in Figure 7 for the three flight conditions. Considerable structural mode response is seen by comparing Figures 4 and 5. As indicated in Figures 5 and 6, the structural response is the largest in the forward position of the fuselage. Also, the landing configuration is the most gust-sensitive configuration considered, because the gust power in the frequency range of the short period and above is considerably higher for the landing condition than the other two conditions as is evident from Figure 7.

3.1.2 Gust Alleviation Capability of the TIFS Aircraft

The capability of a gust alleviation system depends on the following four major elements:

i. the bandwidth and the rate limits of the control surface servo actuators,
ii. the magnitude of the direct force generating capability,
iii. the control law employed in the gust alleviation system,
iv. the sensibility, response and accuracy of the sensors.

In developing the TIFS aircraft, particular attention has been paid to the first two elements (References 16 and 18). For example, in determining the maximum flow rate requirements of the TIFS hydraulic system, the gust alleviation and structural mode stimulation capability were analyzed, employing both deterministic and probabilistic approaches (Reference 16) to define the requirements of the rate limit and the bandwidth of the DLF and SFS servo actuators. The servo actuator characteristics of the DLF and SFS as well as other control surfaces are shown in Table 1. Note that both the DLF and SFS servos have wide bandwidth and high rate limit. The bandwidth of the elevator servo is the lowest, which is approximately 2 Hz. A proposed improvement on the bandwidth of this servo is discussed in Section 5.

The direct force generating capability of the TIFS aircraft with its DLF and SFS is shown in Figure 8b and 9b. The maximum incremental lift that the TIFS is capable of producing due to DLF's only ($\delta_F = 0$, $\delta_e = 0$) is limited by a combination of several factors as described in Reference 16. First of all, there is the surface limit of + .35 degrees, see Figure 8a. At + 35 degrees, ΔC_L =0.38 and at -35 degrees, ΔC_L =0.51.

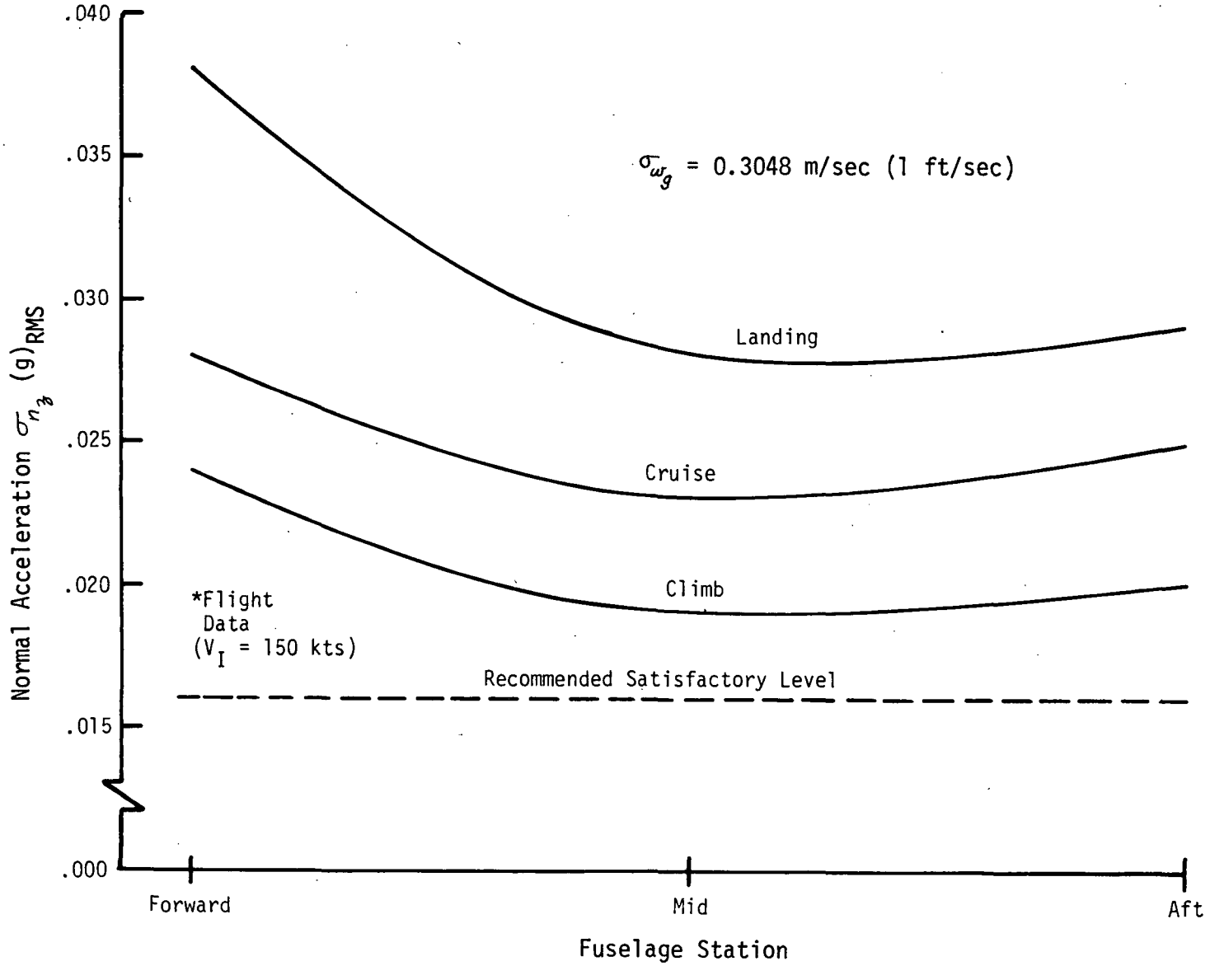

Figure 5 TIFS GUST SENSITIVITY, FLEXIBLE AIRPLANE , 8 NORMAL MODES

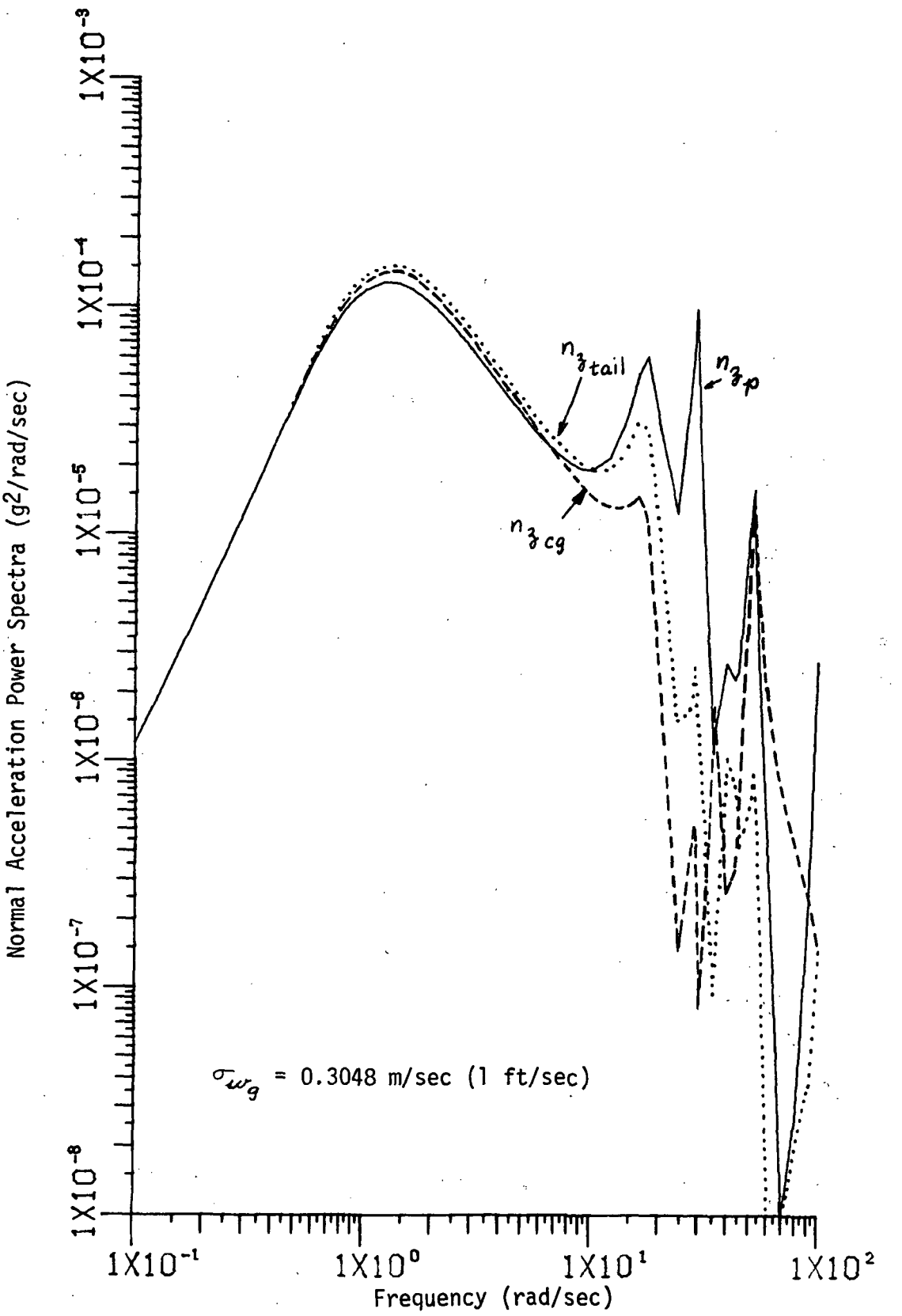

Figure 6 NORMAL ACCELERATION POWER SPECTRA, FLEXIBLE AIRCRAFT, LANDING 8 NORMAL MODES

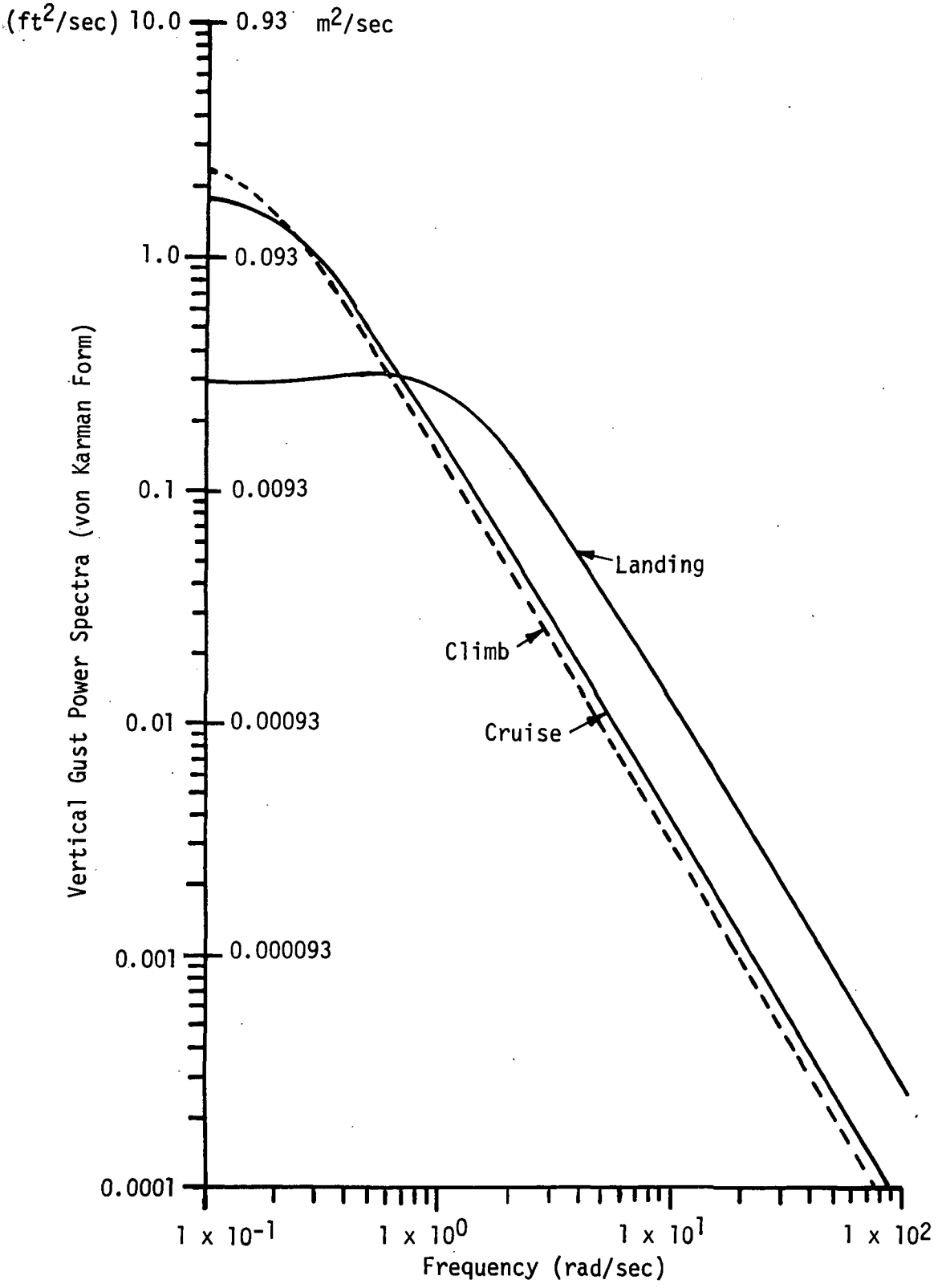

Figure 7 VERTICAL GUST POWER SPECTRA, VON KARMAN FORM

TABLE 1

CONTROL SERVO CHARACTERISTICS

Control	Surface Rate Limit (No Load) deg/sec	Surface Rate Limit Under Design Servo Hinge Moment deg/sec	Frequency For 90^{0} Phase Lag Hertz
Elevator	88.	60.	2.0
Total Aileron	77.	60.	3.7
Rudder	76.	60.	3.0
SFS	89.	60.	12.0
DLF	58.	40.	9.0
Throttle	NA	NA	.3

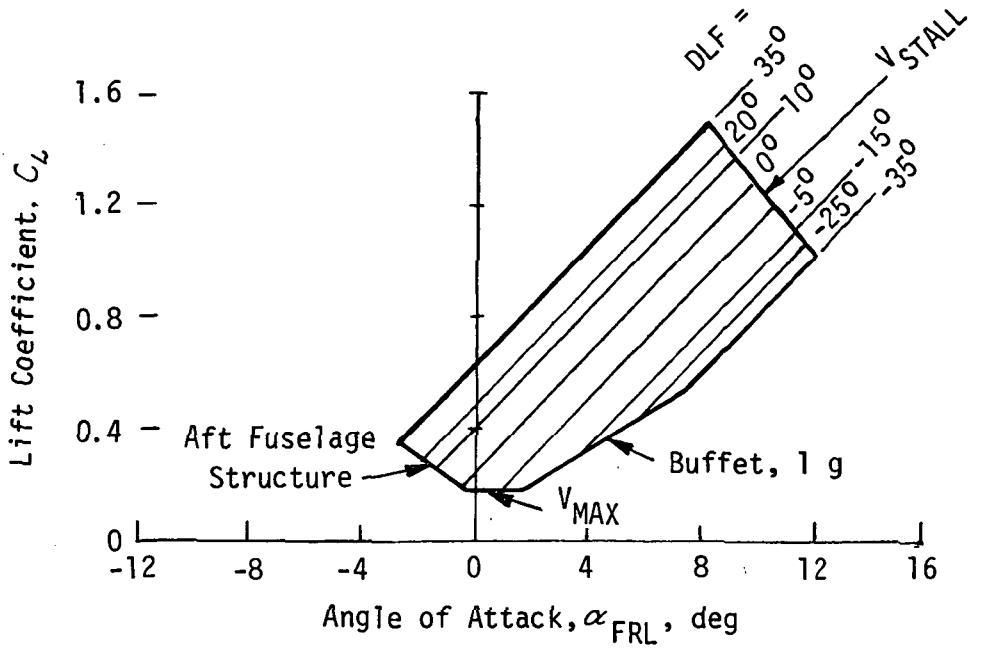

Figure 8a DIRECT LIFT FLAP CAPABILITY

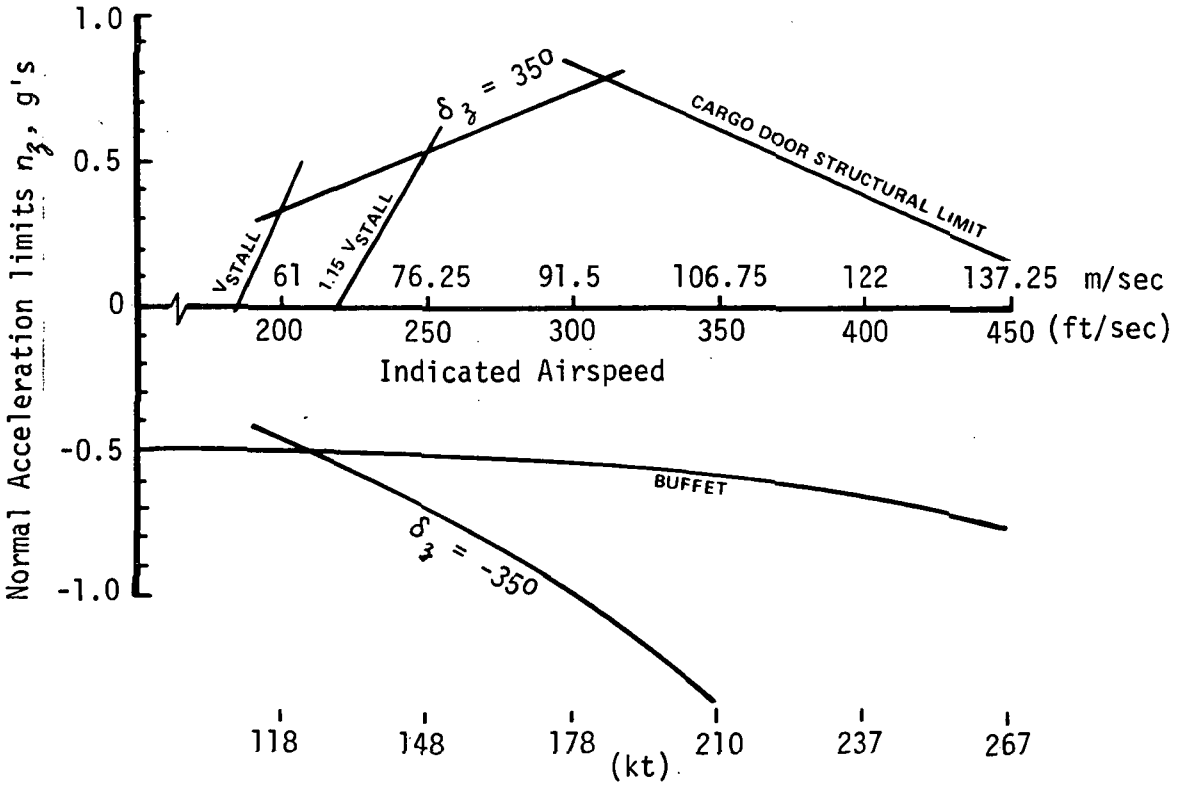

Figure 8b TIFS n_z CAPABILITY WITH DIRECT LIFT FLAPS ALONE
TRIMMED AT: $\delta_f = \delta_e = 0$

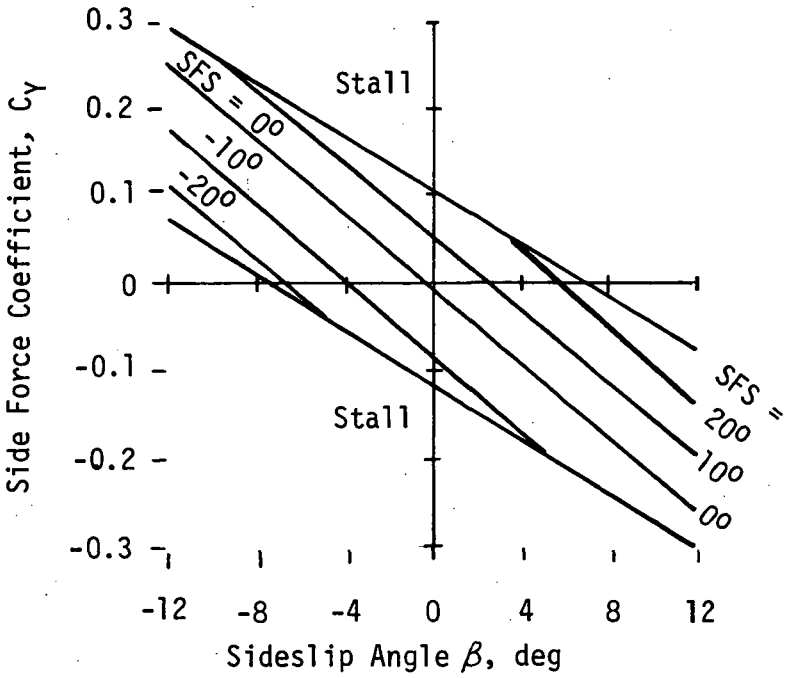

Figure 9a SIDE FORCE SURFACE CAPABILITY

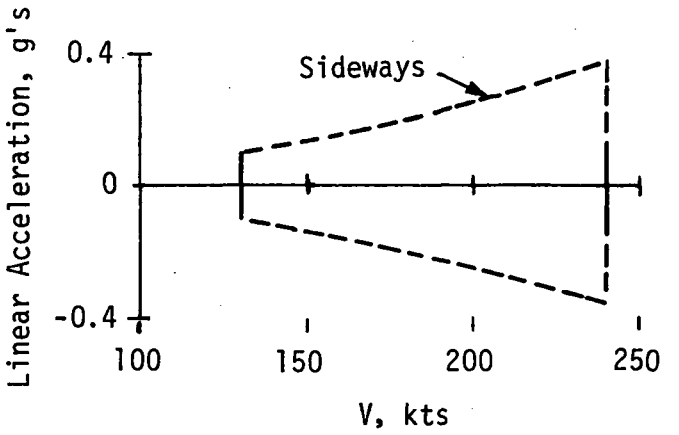

Figure 9b TIFS n_y CAPABILITY WITH SIDE FORCE SURFACES

However, these full deflections are not possible for all airspeeds. For negative δ_z an aerodynamic buffet is encountered before full deflection is achieved. This buffet boundary was determined from flight tests and limits ΔC_L from -.48 to -.175, depending on airspeed.

For positive δ_z , aircraft stall is encountered at low speeds, and a structural load limit is encountered at high speeds before full deflection is achieved. The stall boundary was determined from flight test. The structural limit is on the aft cargo door and only limits n_z at speeds above 94.5 m/sec (310 ft/sec). This structural limit was calculated from 75% of the allowable load rather than 100% to give some consideration to the point that TIFS as a simulator is maneuvered more frequently than a standard C-131. Figure 8b shows all of these limits on an n_z versus airspeed plot.

The maximum side acceleration that the TIFS is capable of producing due to side force surface deflections only ($\beta = 0$) is limited by the stall of the surfaces themselves. At β =0, stall of the SFS occurs at $\delta_y = 18°$ with ΔC_y =0.1 (see Figure 9a). For the TIFS at a gross weight of 222,111 N (50,000 pounds), this transforms into an acceleration of n_y =0.09 g at 118 kt to =0.42 g at 260 kt as shown in Figure 9b.

The development of the control law for gust alleviation will be discussed in the next section.

3.1.3. Preliminary Design of Gust Alleviation System for the TIFS Aircraft

There are two basic approaches for gust alleviation:

i. Using feedback to desensitize the aircraft response to the gust input by increasing both the damping ratio and the frequency of the natural modes, and
ii. Measuring the gust and using feedforward to cancel the gust effect by direct force surfaces such as DLF and SFS in conjunction with the conventional moment producing surfaces.

Use of Feedback Control

Consider first the use of feedback control for gust alleviation. Although use of feedback control can be very effective for gust alleviation, even with a simple control law, the maneuverability of the aircraft may be severely compromised, thus degrading the flying qualities. To illustrate this point, consider a simple control law with a feedback of the normal acceleration at aircraft c.g. to the DLF and a feedback of the pitch rate to elevator. Figures 10 and 11 show the effectiveness of the gust alleviation with the two levels of gain. The gust alleviation is very effective, as is evident from both the rms and the power spectral density of the normal acceleration in the frequency range of interest. However, the response of the aircraft to the pilot input

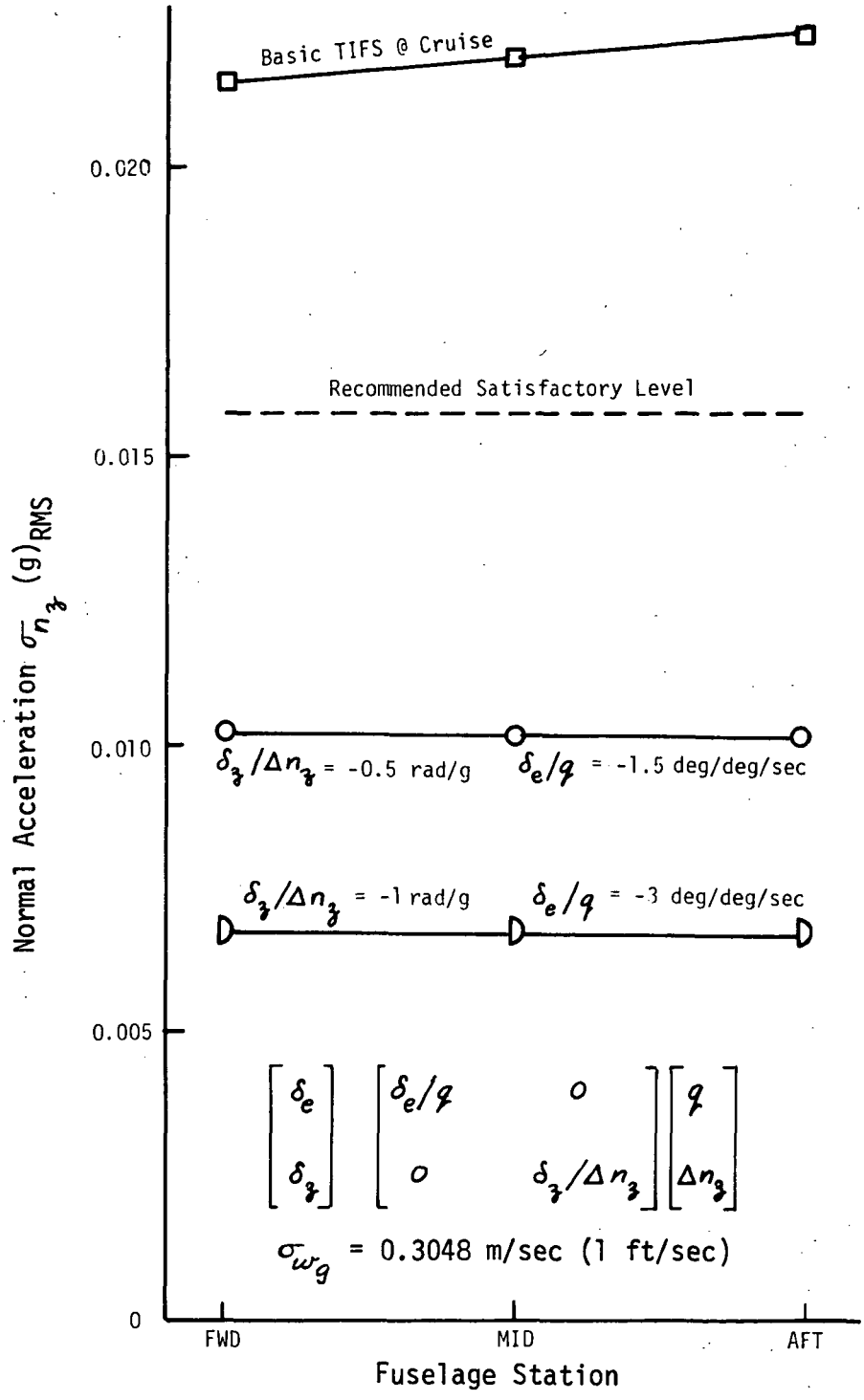

Figure 10 GUST ALLEVIATION, CONVENTIONAL DESIGN, RIGID AIRPLANE WITHOUT USING GUST MEASUREMENTS

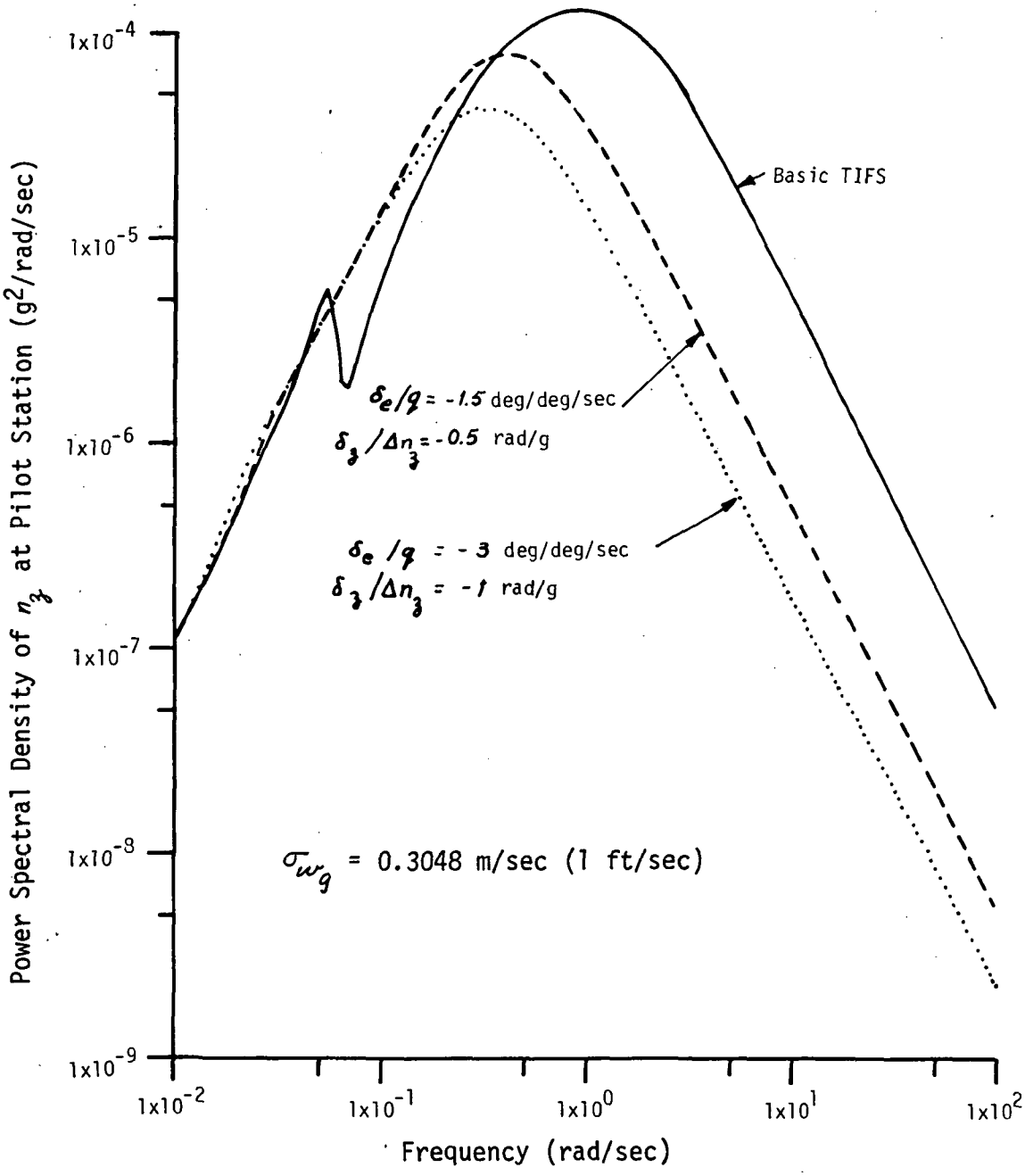

Figure 11 GUST ALLEVIATION, CONVENTIONAL DESIGN, RIGID AIRPLANE @ CRUISE

may be sluggish as is evident from the characteristic roots of the closed-loop system shown in Table 2. Clearly, a proper balance of the flying qualities and gust load alleviation is required, when a feedback control is used for gust alleviation.

Figure 12 shows another design example of using only feedback control for gust alleviation. The system uses inertia angle of attack, pitch rate, and pitch attitude as feedback variables. These variables are responsive mainly to the pilot input, not to the gust input. The results show that the gust alleviation is not effective even with the very high feedback gains as shown in Figure 12.

TIFS Gust Alleviation Using Gust Measurements.-

The TIFS aircraft is presently equipped with gust probes. It is therefore feasible and in fact it has been tested in flight to use the gust measurements to drive the control surfaces to cancel the gust effect, thus reducing the TIFS response to gust input (Reference 16).

Consider the small perturbation equations of motion of the TIFS using rigid airplane representation.

$$\dot{x} = Fx + Gu + Jv \tag{1}$$

It is theoretically possible with the ideal actuators (with infinite bandwidth and without rate limit) for the TIFS using the control law

$$u = -(G^T G)^{-1} G^T J v \tag{2}$$

to perfectly compensate the turbulence input v, since for the TIFS aircraft there is a controller in each degree of freedom of rigid body motion.

With the existing actuator dynamics, though, the compensation is not perfect, but the gust alleviation is still very effective as is evident from Figures 13 and 14. The actuator dynamic compensation indicated in these figures utilized a second-order lead-lag shaping filter and it effectively raised the bandwidth of the existing actuators by a factor of 10.

To further assess the gust alleviation capability of the existing DLF of the TIFS, discrete gust inputs with "1-cosine" shape were also used to obtain the time histories of the aircraft normal acceleration response, control surface deflection and deflection rate with gust alleviation system operating.

TABLE 2

CHARACTERISTIC ROOTS OF THE CLOSED-LOOP SYSTEM

Mode		Open Loop	Closed Loop	
			$\delta_z/\Delta n_z$ = -0.5 rad/g δ_e/q = 1.5 rad/rad/sec	$\delta_z/\Delta n_z$ = -1 rad/g δ_e/q = -3.0 rad/rad/sec
SHORT PERIOD	$\lambda_{1,2}$	$-1.778 \pm j\ 0.798$	- 0.39 -13.26	- 0.218 -24.35
	(ξ, ω_n)	(0.912, 1.949)		
PHUGOID	$\lambda_{3,4}$	$-0.9975 \pm j\ 0.0581$	$-0.0087 \pm j\ 0.0254$	$-0.0089 \pm j\ 0.018$
	$(\xi, \omega_n$	(0.128, 0.0586)	(0.324, 0.0269)	(0.439, 0.0202)

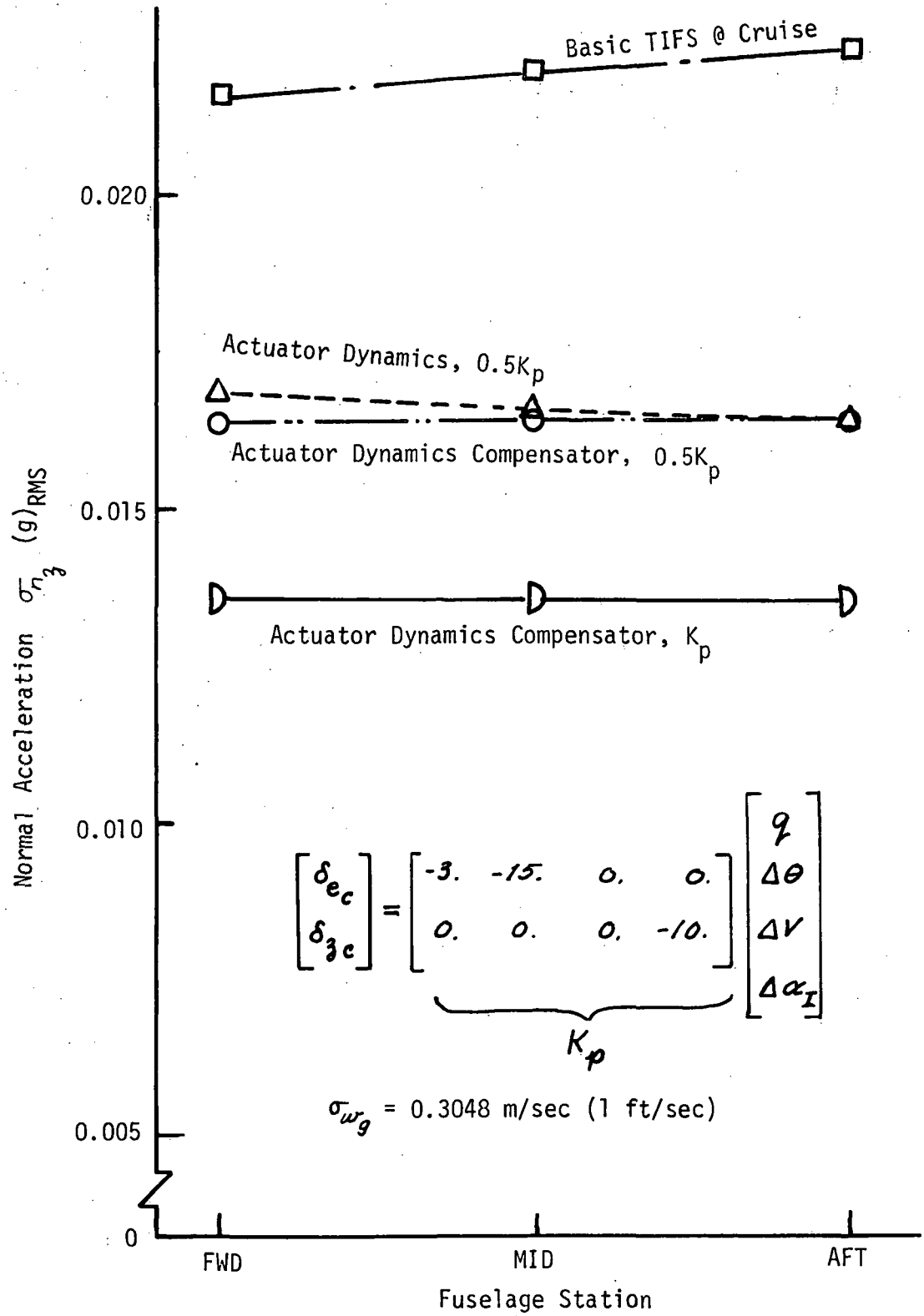

Figure 12 EFFECT OF FEEDBACK, NONCONVENTIONAL DESIGN, RIGID AIRPLANE WITHOUT USING GUST MEASUREMENTS

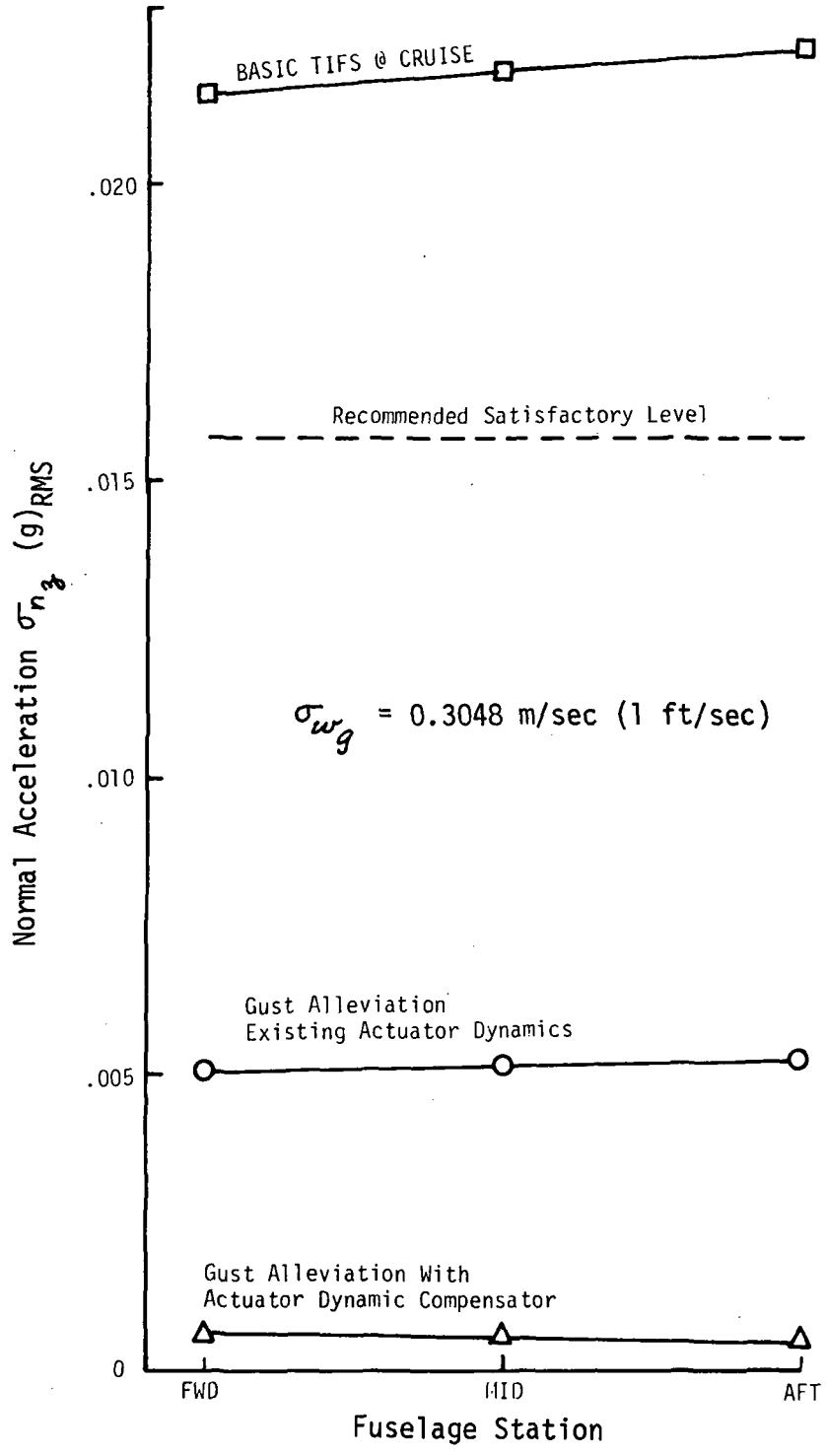

Figure 13 EFFECT OF ACTUATOR DYNAMICS ON GUST ALLEVIATION, RIGID AIRPLANE, USING GUST MEASUREMENTS

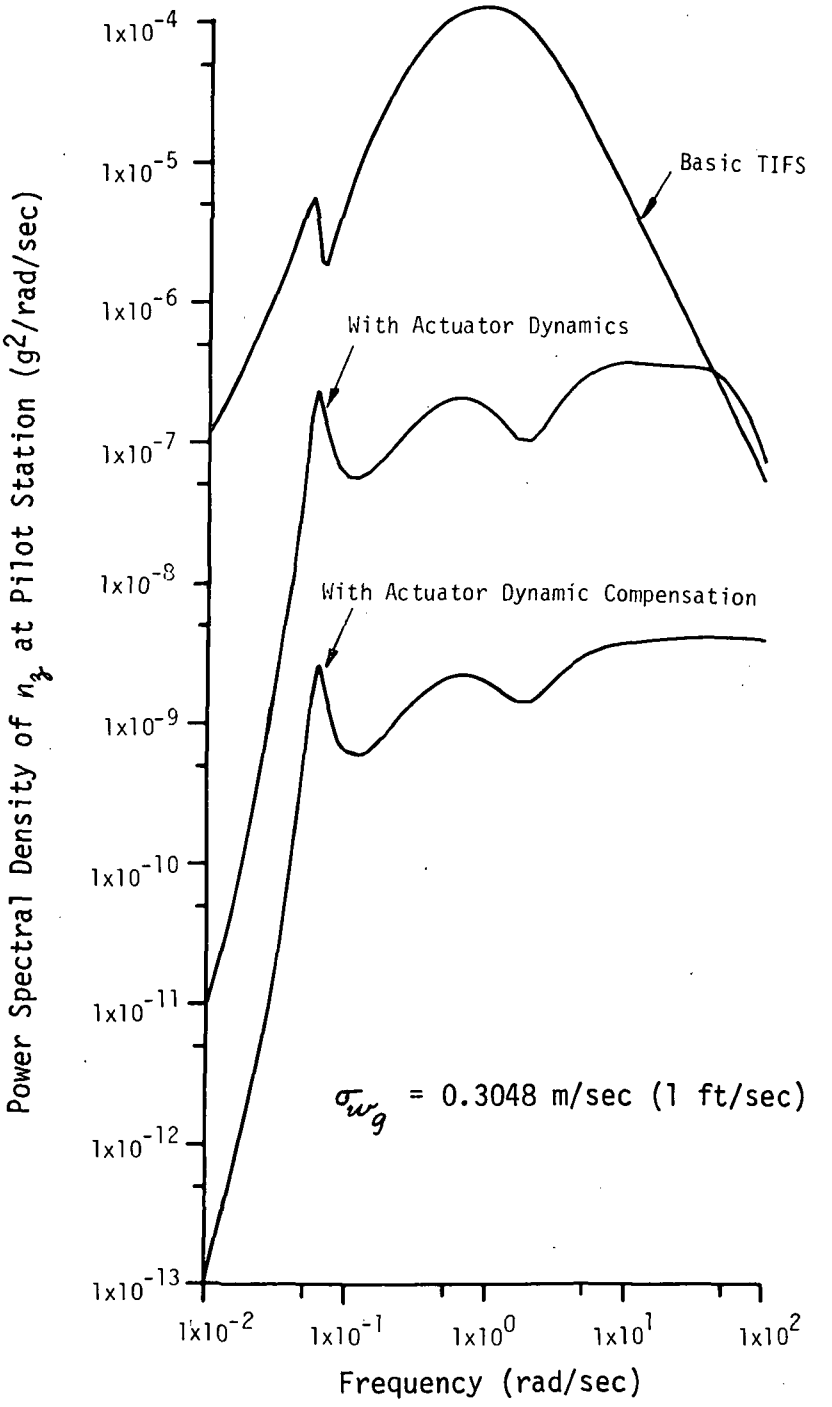

Figure 14 GUST ALLEVIATION USING GUST MEASUREMENT, RIGID AIRPLANE @ CRUISE

The procedure set forth in MIL-F-8785B(ASG) was used and cases of thunderstorm turbulence intensity (σ_{w_g} = 6.4 m/sec) were considered. First, the discrete gust shape was converted from spatial form in MIL-F-8785B into a temporal form as follows:

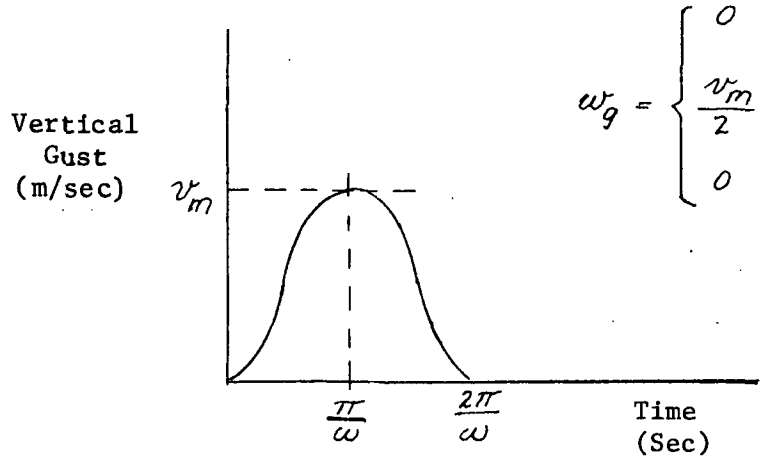

$$w_g = \begin{cases} 0 & t \le 0 \\ \frac{v_m}{2}(1-\cos\omega t) & 0 \le t \le \frac{2\pi}{\omega} \\ 0 & t > \frac{2\pi}{\omega} \end{cases}$$

The temporal frequency ω (rad/sec) was properly tuned in the vicinity of both damped and undamped natural frequencies of the short period modes (0.79 and 1.95 rad/sec, respectively). As the frequency ω varies, the peak of the discrete gust v_m changes accordingly. Five sets of v_m and ω were run in the computer simulation with and without the gust alleviation system operating.

CASE	v_m m/sec	(fps)	ω (rad/sec)
1	5.1	(16.8)	17.64
2	7.0	(23.1)	8.81
3	9.6	(31.5)	4.40
4	12.5	(40.9)	2.20
5	16.0	(52.5)	0.88

The results show that Case 1 has the largest deflection rate for the DLF and Case 5 has the largest DLF deflection, but they are within the limits of the existing DLF. Figures 14a and 15b show these two cases without gust alleviation system, and Figures 16a and 16b show the corresponding cases with gust alleviation system. The effectiveness of the gust alleviation system is clearly shown.

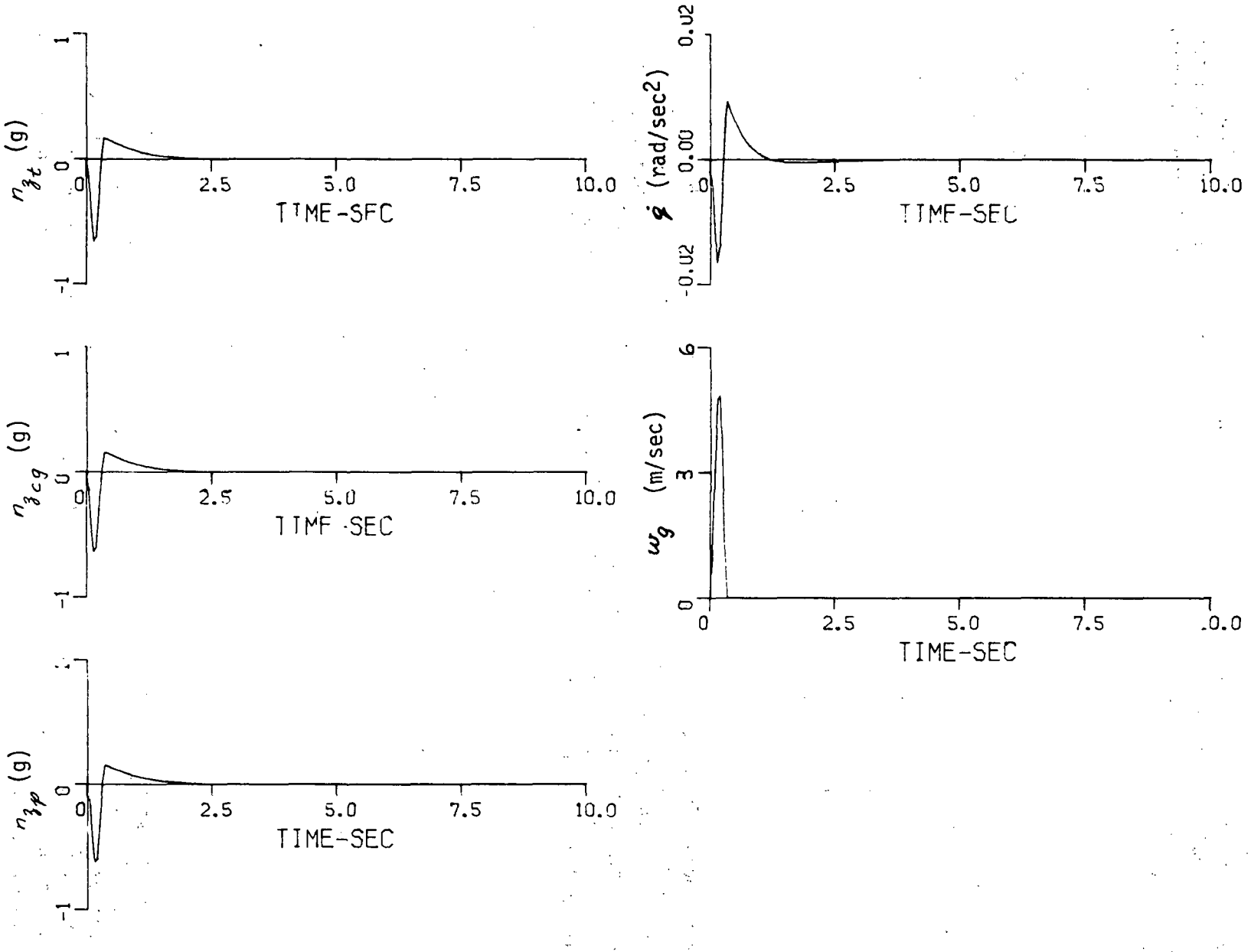

Figure 15a CRUISE THUNDERSTORM UPSET, CASE 1, NO GUST ALLEVIATION

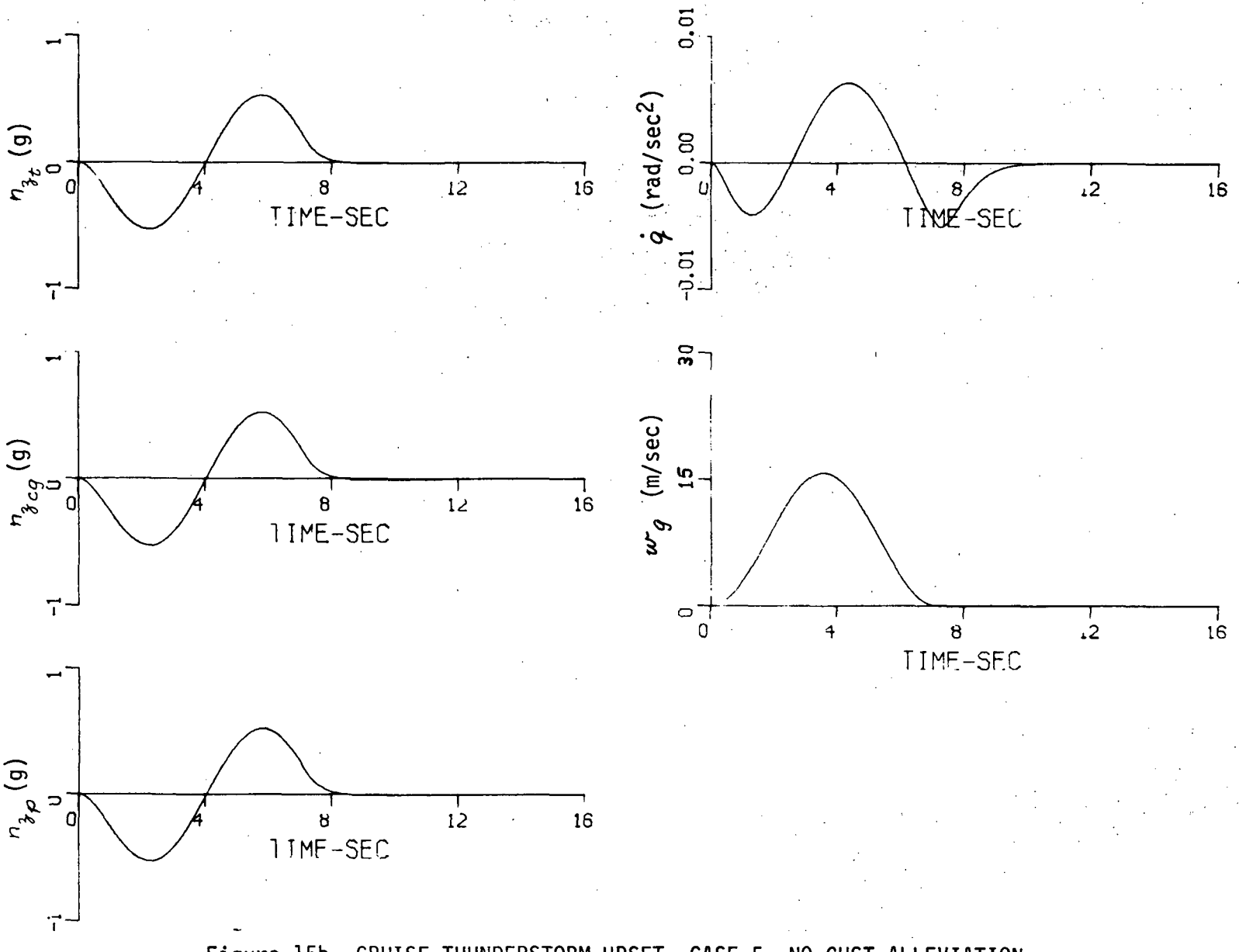

Figure 15b. CRUISE THUNDERSTORM UPSET, CASE 5, NO GUST ALLEVIATION

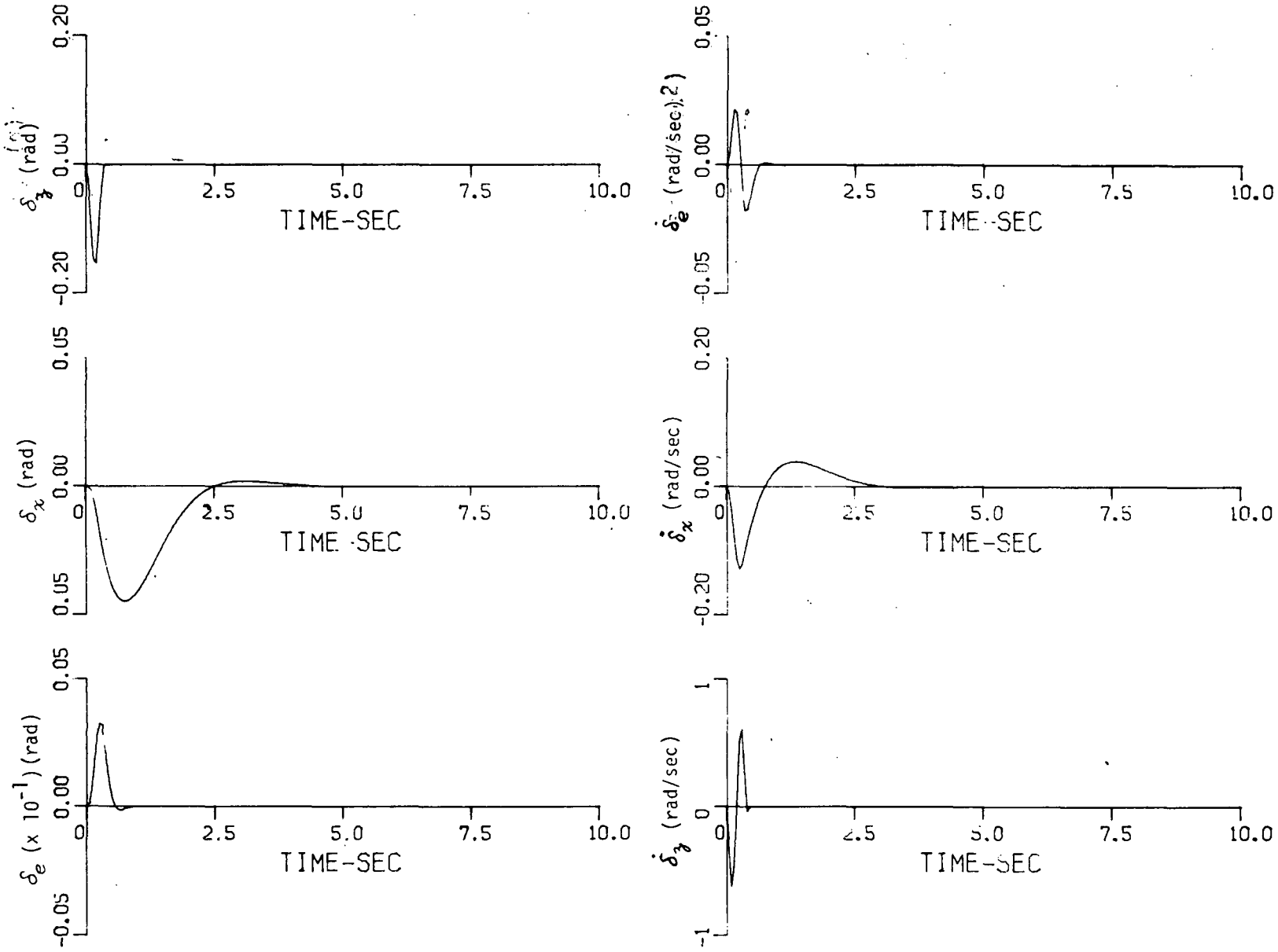

Figure 16a GUST ALLEVIATION WITH ACTUATOR DYNAMICS, CRUISE THUNDERSTORM, CASE 1

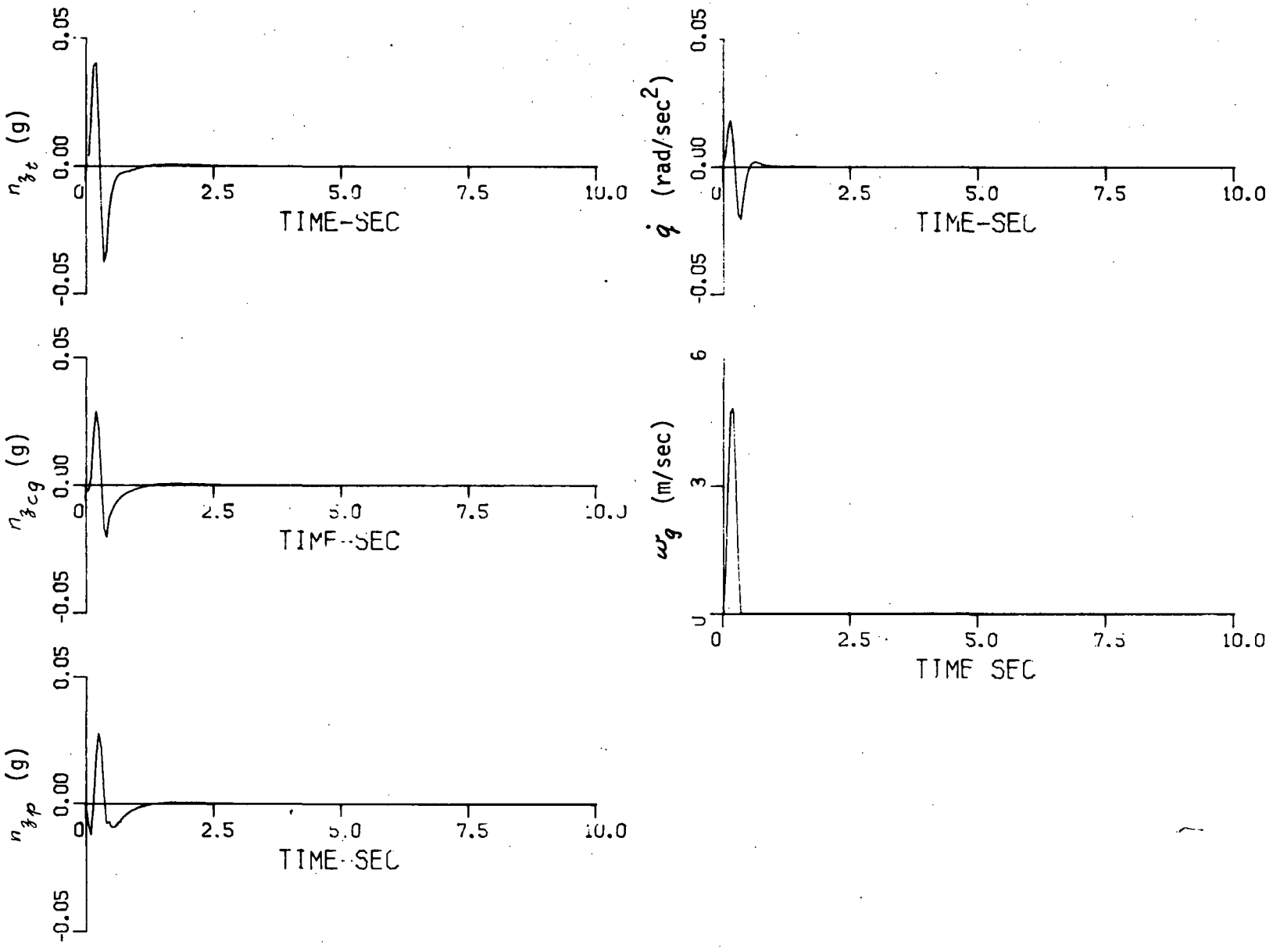

Figure 16a GUST ALLEVIATION WITH ACTUATOR DYNAMICS, CRUISE THUNDERSTORM, CASE 1 (Cont'd)

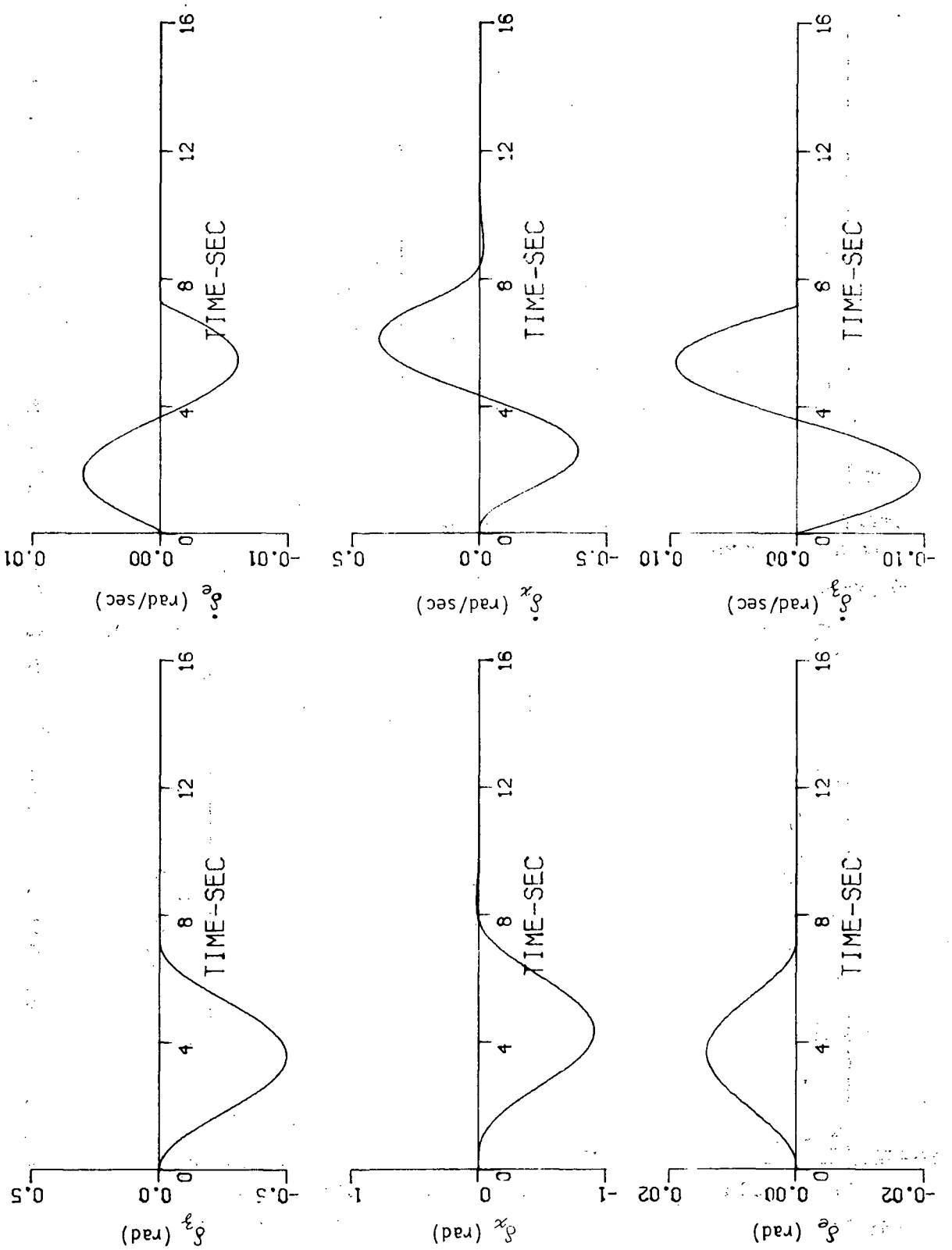

Figure 16b GUST ALLEVIATION WITH ACTUATOR DYNAMICS, CRUISE THUNDERSTORM, CASE 5

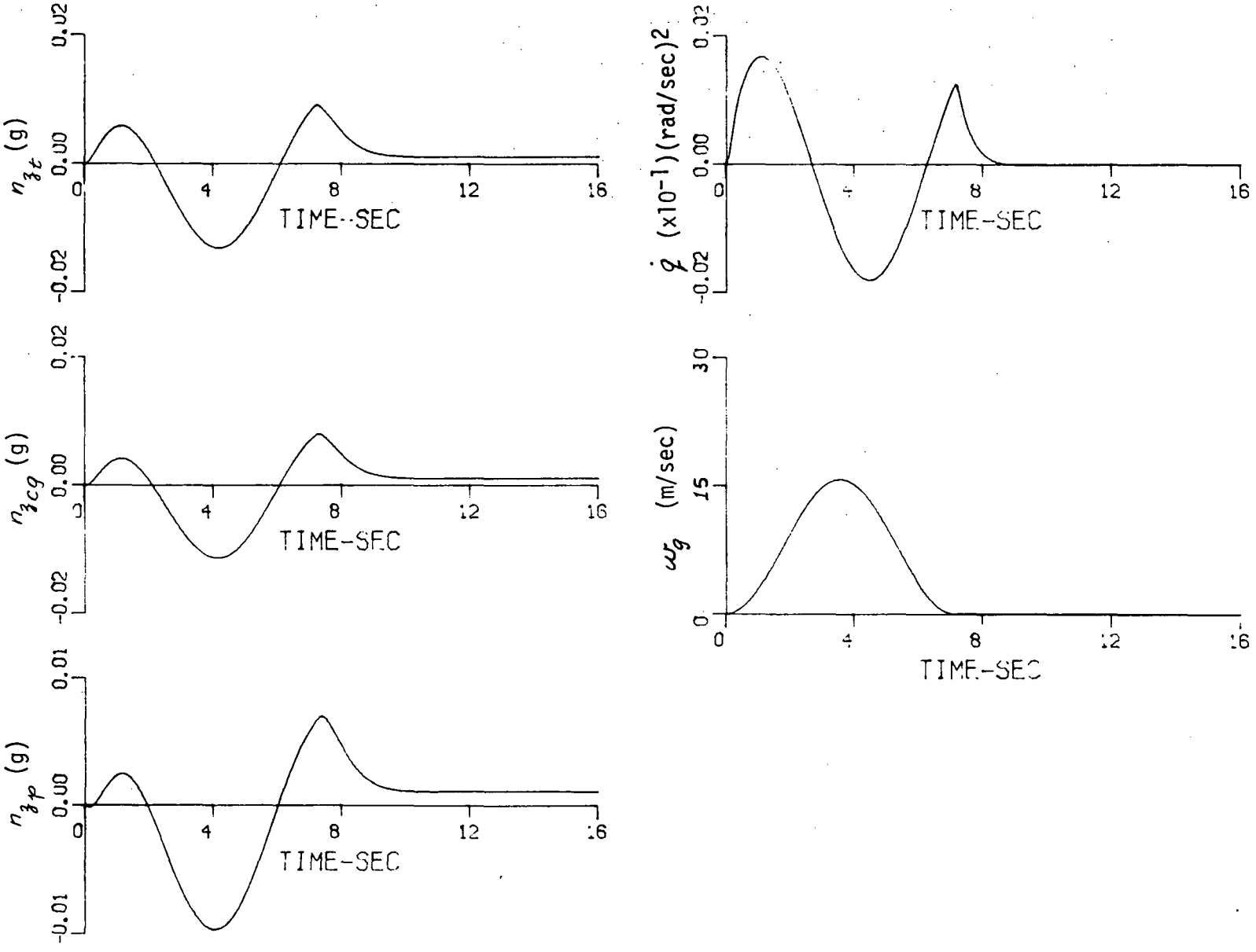

Figure 16b GUST ALLEVIATION WITH ACTUATOR DYNAMICS, CRUISE THUNDERSTORM, CASE 5 (Cont'd)

Aside from the fact that the gust alleviation using gust measurements is quite effective in the rigid body frequency range, an additional advantage is that the system does not have the conflicting requirements with the flying qualities. Therefore, the design of the gust alleviation system may be "decoupled" from the design of other systems such as augmentation of RSS whose function is to satisfy the flying qualities requirements.

The above discussions on the gust alleviation have been restricted to the rigid body representation of the TIFS aircraft. As indicated earlierr, in Section 3.1.1, the n_z response of structural modes of the TIFS can contribute as much as 30% of that of rigid body in terms of rms at the pilot station in the cruise condition. This suggests that the gust alleviation system designed for the rigid body representation can be less effective for the flexible airplane.

Figure 17 shows a comparison of the power spectral density of n_z at the pilot station with and without gust alleviation for the flexible TIFS representation using the eight normal modes. The gust alleviation system was designed to cancel the gust effect on the two rigid body modes. It is seen that within the rigid body frequency range, the gust alleviation system seems to be working properly, but in the frequency range of the structural modes, there appears to be some amplification in the aircraft response (because of the extremely high order system, with the 8 normal modes, the numerical solution obtained in Figures 17 and 18 were subject to further verification). To avoid possible numerical difficulties*, computer runs were also made for the TIFS flexible representation including only the three lower frequency structural modes, i.e., 1WB, 1FB, and 1WT. The results are shown in Figures 19 and 20. Again, there are some amplifications in the frequency range of the structural modes.

Further examination of Figures 19 and 20 suggests that there are three possible avenues that can be approached to suppress the power spectral density type (psd) of n_z in the frequency range of the structural modes:

(i) By comparing the type of n_{z_p} for the gust alleviation system with and without the actuator dynamics in Figure 19, it appears that a proper use of shaping filters to operate on the gust measurements (the existing servo actuators act as shaping filters) can significantly attenuate the type of n_z in the frequency range of the structural modes of the TIFS aircraft.

---

* A Leverrier algorithm was used to independently check the validity of the calculation of the numerators of the transfer functions with three structural modes included. A satisfactory check was achieved to assure the numerical accuracy.

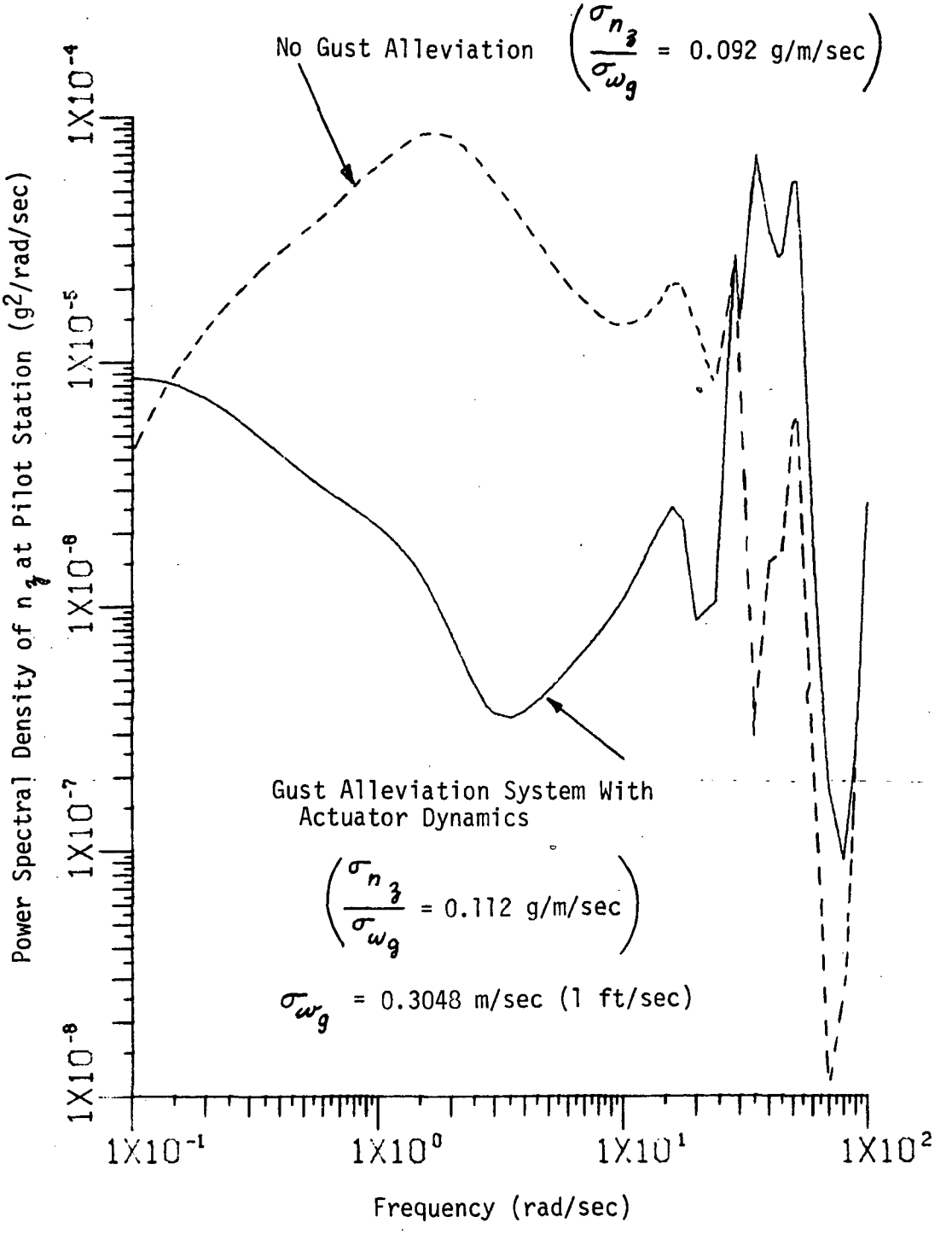

Figure 17 GUST ALLEVIATION USING GUST MEASUREMENT, FLEXIBLE AIRPLANE, CRUISE, 8 NORMAL MODES

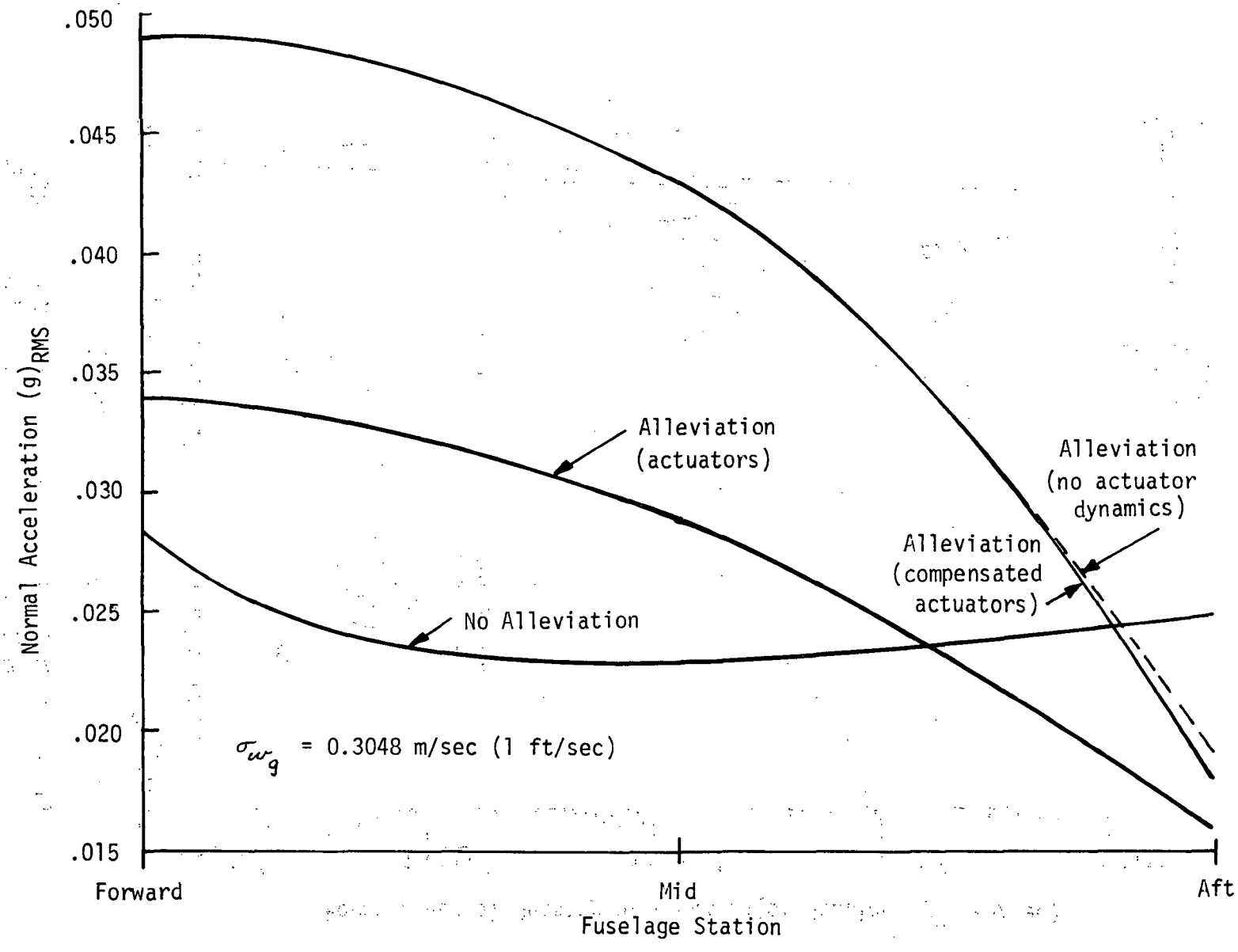

Figure 18 COMPARISON OF GUST ALLEVIATION SYSTEMS, FLEXIBLE AIRPLANE AT CRUISE, 8 NORMAL MODES

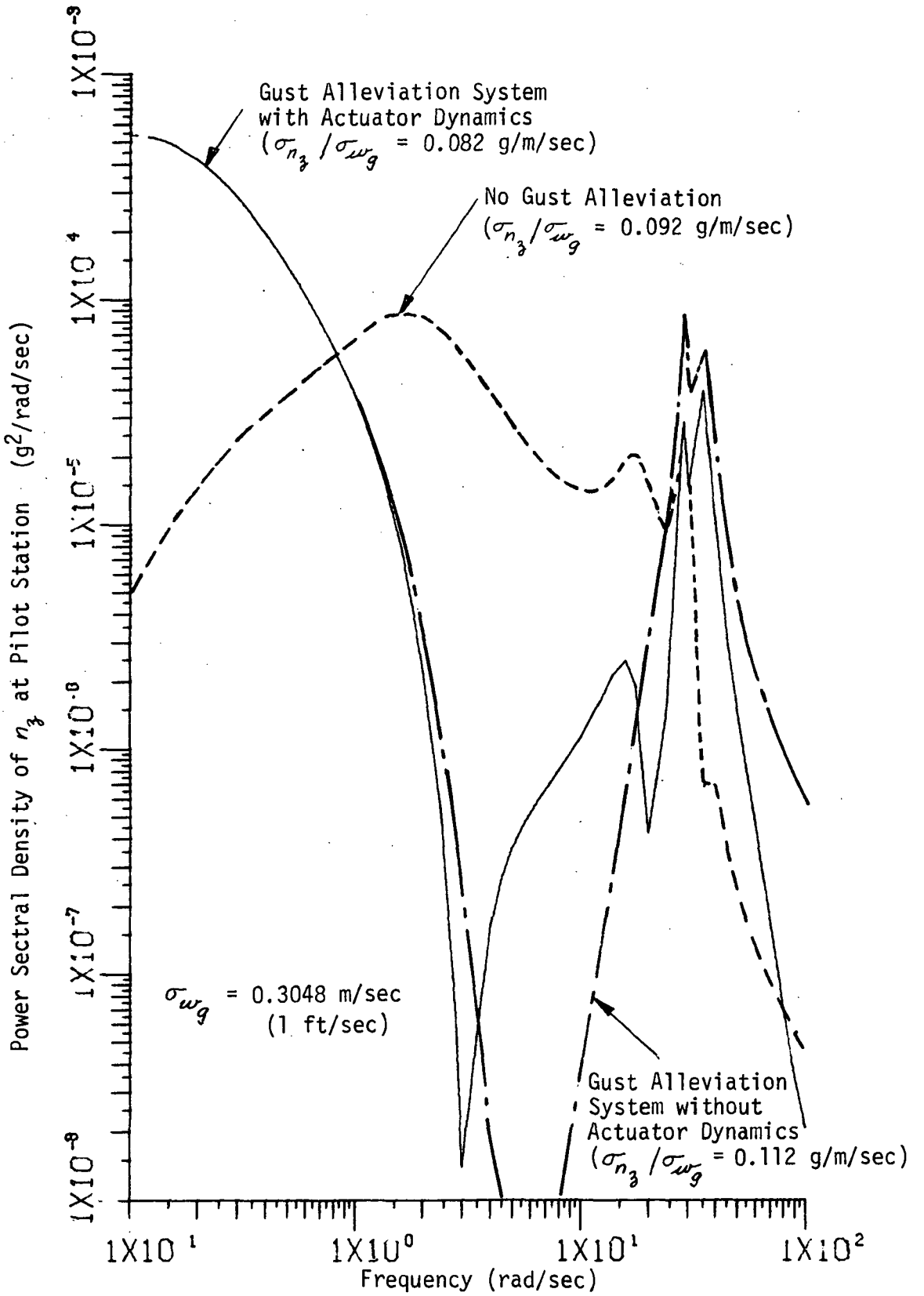

Figure 19 GUST ALLEVIATION USING GUST MEASUREMENT, FLEXIBLE AIRPLANE AT CRUISE, 5 NORMAL MODES

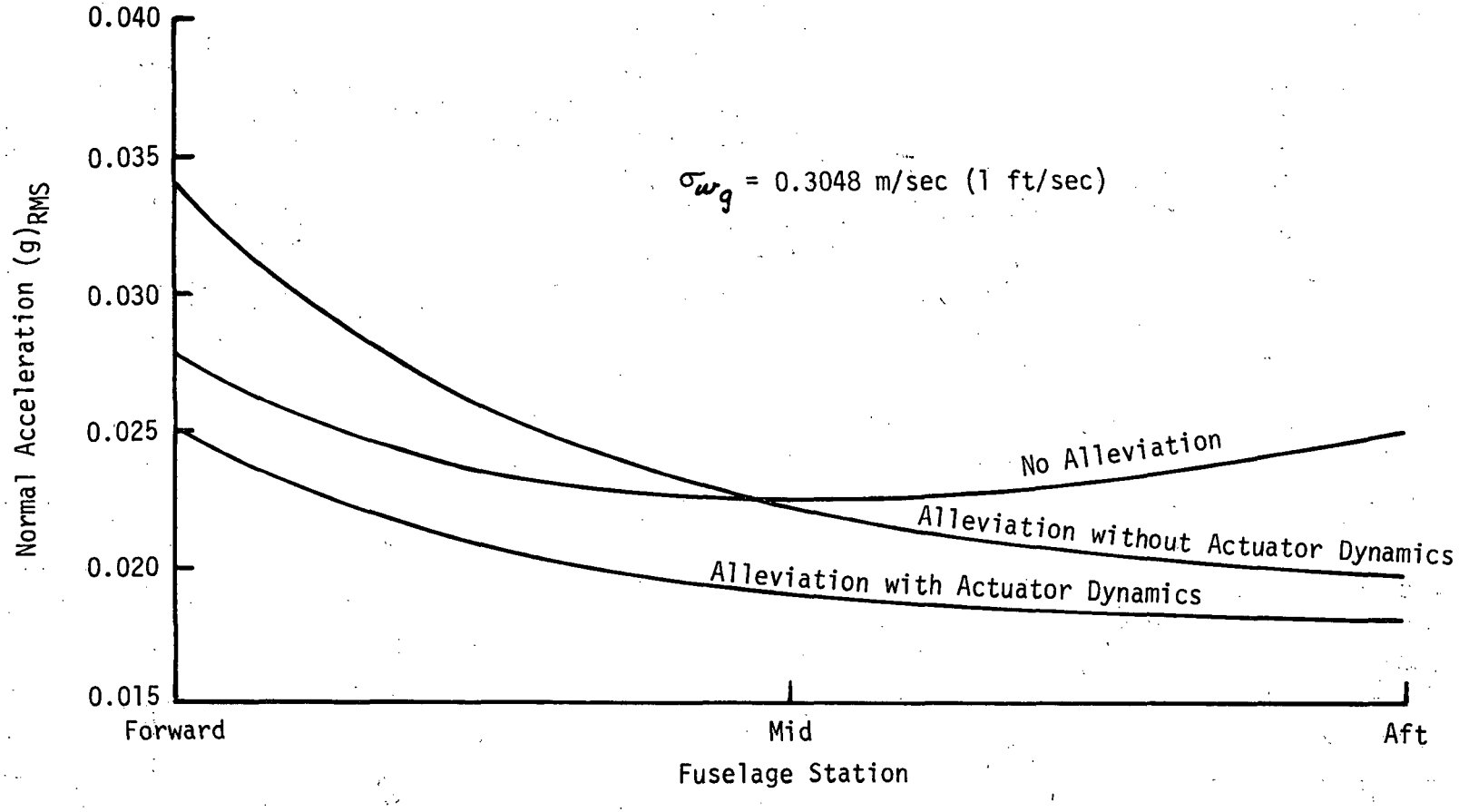

Figure 20 COMPARISON OF GUST ALLEVIATION SYSTEMS, FLEXIBLE AIRCRAFT AT CRUISE, 3 NORMAL MODES

(ii) The feedforward gains may be properly chosen to balance the cancellation of the gust effect on the rigid body and the structural modes, thereby reducing the excitation of the structural modes. This balancing task may be made easier and more effective if additional control surfaces with wide bandwidth servos are added on the wings and/or fuselage.

(iii) The feedback control may be used to increase the damping in the structural modes using sensors properly located on the wings and/or fuselage.

The effectiveness of last approach will be demonstrated in Section 3.2 in conjunction with the inducing and suppression of the flutter modes of the TIFS aircraft.

3.2 Flutter Stimulation and Suppression Using ACT Systems

One of the areas considered in the subject program was the application of the TIFS airplane for flight demonstration of active control concepts for flutter control. An immediate difficulty which is encountered in meeting this objective is that there are no critical flutter modes of the present TIFS configuration within the flight range of the airplane. Some modifications are required to bring a flutter point within a speed range suitable for flight testing before ACT can be used to suppress it.

A similar situation has existed in previous flight demonstrations of the use of ACT for flutter suppression. For example, Reference 11 considers flutter tests of the B-52 airplane which has a design airspeed of 420 KCAS. In this case, addition of ballast in the external tanks reduced the predicted flutter speed to 330 KCAS at 6400m (21,000 ft), and gave a placard speed of 285 KCAS where a damping ratio of $\zeta = 0.015$ was expected in the critical mode.

Calspan has considered two alternative fluttering systems for demonstrating active flutter control with the TIFS airplane.

(a) Flutter of a modified side force surface incorporating a flap.

(b) Flutter of TIFS wing when bending and torsional responses are modified by aileron and DLF inputs. These input motions would be governed by a dedicated ACT system for inducing flutter. (A separate ACT system which would operate on different control surfaces would be used to demonstrate active flutter suppression.)

Both of these approaches were selected with the aim of providing maximum safety in flight testing. In particular, they included means for limiting the severity of the flutter which might be encountered during flight testing.

A brief discussion is given in the following section of the possible application of a modified side force surface for demonstrating active flutter

control. Little investigation of this concept was carried out because it was decided early in the program to emphasize the second approach mentioned above.

The application of active control for inducing flutter as well as for suppressing it has been taken up in subsequent sections.

3.2.1 Application of Modified Side Force Surfaces for Demonstrating Active Flutter Control

Figure 21 indicates the side force surfaces on one side of the TIFS airplane and a hypothetical modification of the lower surface by the addition of an SFS flap. Some ATT designs have considered using all moveable horizontal tails with balance flaps. The modified SFS is clearly analogous to such an ATT configuration.

The weights of many aircraft are significantly increased by ballast weights used in control surfaces for flutter prevention. In principle, an alternative method would be possible in which the ballast weights would be removed and their function replaced by active flutter control systems. Study of this approach was not carried far enough in the present program to determine if it could lead to weight savings or if it could provide an economically feasible method of eliminating control surface flutter. In any case, it was believed that valuable experience in the operation and flight testing of active flutter control system might be obtained using a configuration such as shown on Figure 21.

The predominant degrees of freedom in the flutter mode of the modified SFS would be expected to be SFS rotation about its pivot and rotation of the SFS flap about its hinge line. The stiffness of the SFS actuating system would be adjusted to give a frequency of SFS rotation about the pivot axis which would result in flutter at a comparatively low forward speed. Active flutter control of this mode would be accomplished by moving an SFS tab in accordance with measured SFS and SFS flap rotations and an appropriate control law.

The difficulties of making accurate predictions of the aerodynamic flutter coefficients for the low aspect ratio SFS, flap, and tab were recognized. Thus, a semi-empirical design approach had been planned, utilizing data comparing theoretically and experimentally determined moments acting on low aspect ratio wings, flaps, and tabs (e.g., Ref. 12). Detailed design was to make provision for changing the static balance of the SFS flap by the tab.

Flutter calculations for the TIFS airplane have indicated that the presence of the unmodified SFS's has little effect on the primary flutter characteristics of the wing. The modification of the lower SFS alone as indicated on Figure 21 would result in some couplings between SFS rotation and the wing bending modes but these would be largely eliminated if both upper and lower surfaces were modified. The necessity of modifying both upper and lower surfaces would be evaluated in the course of the final design.

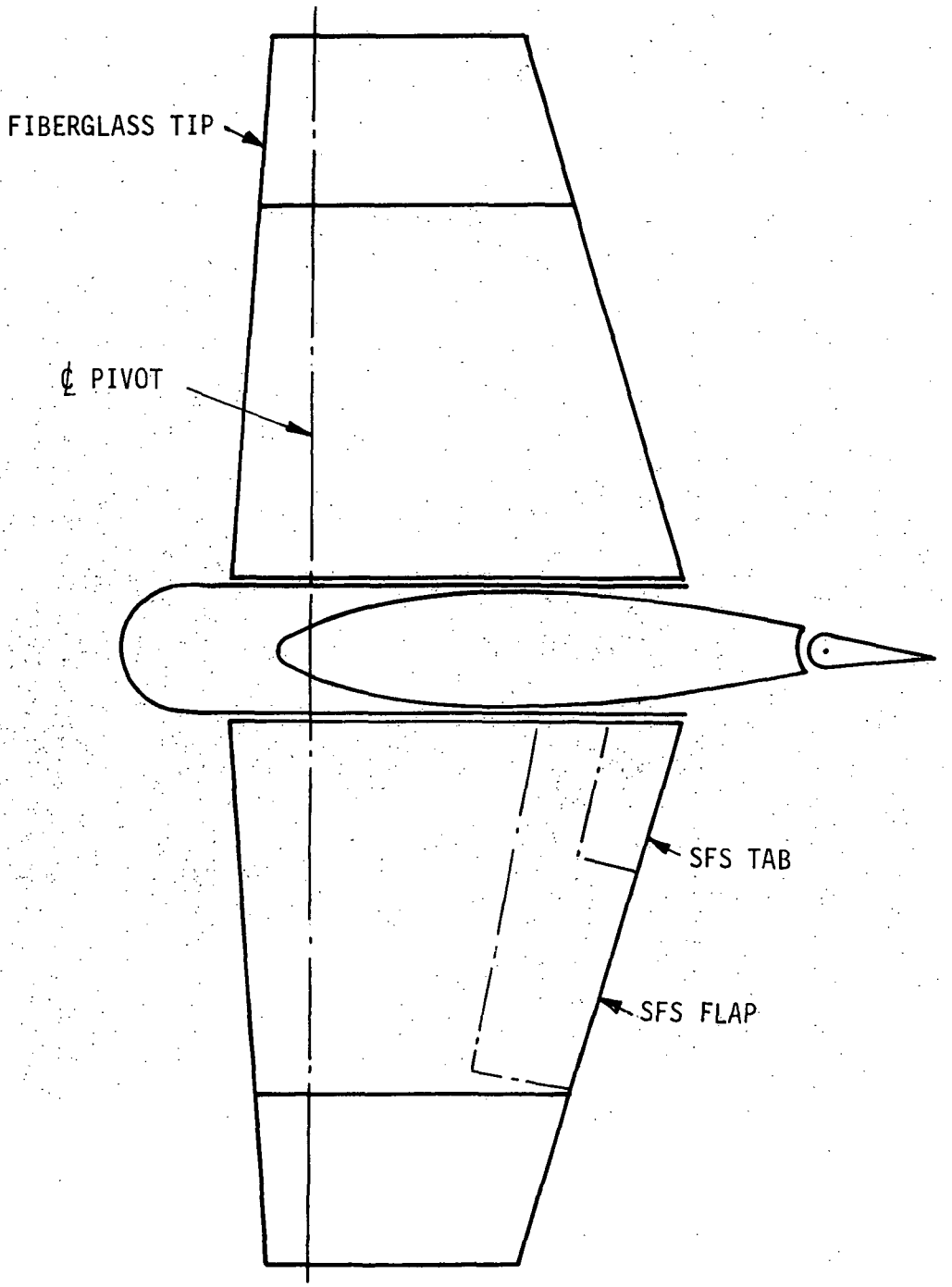

Figure 21: CONCEPT FOR DEMONSTRATING ACTIVE FLUTTER SUPPRESSION WITH A MODIFIED SIDE FORCE SURFACE

The preceding qualitative discussion of a possible application of the SFS's for demonstrating active flutter control has been included to document this concept as a possible future application of the TIFS airplane. As mentioned previously, work on a modified SFS was dropped early in the program in favor of study of a second method for demonstrating active flutter control.

3.2.2 Method for Analyzing Active Flutter Control

In the development of the TIFS airplane, flutter analyses were carried out to assure that the various structural modifications involved would not result in flutter. Subsequently, flight tests confirmed that the modified airplane was free from flutter instability up to the limit operating speed.

The TIFS wing flutter analysis which was used as a basis for the present work on active flutter control was carried out using classical methods. A sophisticated analysis employing more recent methods could not be undertaken within the scope of the program. However, it is believed that the results of a classical analysis are sufficient for a preliminary evaluation of the capability of TIFS for demonstrating active flutter control.

A brief description which is first given of the basic flutter equations used in developing TIFS and this is complemented by additional information and pertinent parameters presented in Appendix B. The method used for introducing the effect of active control in the flutter equations is taken up in a following section.

3.2.2.1 Basic Flutter Equations Used in Developing the TIFS Airplane

Flutter equations used in References 13 and 14 for analyzing the TIFS airplane were based on the classical methods of Reference 15 (which are also described in Reference 16). The following expressions for the kinetic energy, potential energy, structural dissipation function, and generalized aerodynamic forces of the system were written in terms of the generalized coordinates (q_i's) corresponding to several uncoupled vibration modes.

T = Kinetic energy

$$= \sum_{i,j=1}^{N} \frac{1}{2} M_{i,j} \dot{q}_i \dot{q}_j \qquad M_{i,j} = M_{j,i}$$

U = Potential energy

$$= \sum_{i=1}^{N} \frac{1}{2} K_i (q_i)^2 = \frac{1}{2} \sum_{i=1}^{N} \omega_i^2 M_{i,i} (q_i)^2$$

D = Dissipation function (following scheme in Ref. 16)

$$= \sum_{i=1}^{N} \frac{1}{2} \frac{g_i}{\omega} K_i (\dot{q}_i)^2 = \frac{1}{2\omega} \sum_{i=1}^{N} g_i \omega_i^2 M_{i,i} (\dot{q}_i)^2$$

δ_{W_i} = Virtual work done by aerodynamic forces in virtual deflection in the i^{th} degree of freedom

$Q_i = \dfrac{\delta_{W_i}}{\delta_{q_i}}$ = generalized aerodynamic force acting in the i^{th} degree of freedom

$$= \pi \rho \omega^2 \sum_{j=1}^{N} A_{i,j}\, q_j ; \qquad i = 1, 2, \cdots, N.$$

A straightforward application of Lagrange's equations of motion,

$$\frac{d}{dt}\left(\frac{\partial L}{\partial \dot{q}_i}\right) - \frac{\partial L}{\partial q_i} + \frac{\partial D}{\partial \dot{q}_i} = Q_i \tag{3}$$

followed by assuming sinusoidal motion ($\dot{q}_i = \sqrt{-1}\,\omega q_i = j\omega q_i$) resulted in flutter equations in the form:

$$-\omega^2 \sum_{k=1}^{N} M_{i,k}\, q_k + (1 + j g_i)\,\omega_i^2 M_{i,i}\, q_i - \pi \rho \omega^2 \sum_{k=1}^{N} A_{i,k}\, q_k = 0 \tag{4}$$

$$i = 1, 2, \cdots, N$$

The q_i's in the above expressions are generalized coordinates associated with the various uncoupled vibration modes. For example, analysis of symmetrical wing flutter in the present report is based on the following system of generalized coordinates:

q_1	=	$h_W^{(1)}$	1st symmetrical wing bending
q_2	=	$h_W^{(2)}$	2nd symmetrical wing bending
q_3	=	α_W	1st symmetrical wing torsion
q_4	=	δ_a	aileron rigid body rotation
q_5	=	δ_z	direct lift flap rigid body rotation

The weight of the fuselage and empennage were considered as a concentrated mass in determining the uncoupled bending modes and the fuselage pitching moment of inertia was considered to be infinite in computing the first torsion mode. The wing modes were not coupled with the fuselage modes in carrying out wing flutter calculations as was done in finding the dynamic response of the airplane to gusts. Data on the uncoupled wing modes is included in Appendix B.

The symbol ω_i is used for the uncoupled natural frequency in the i^{th} degree of freedom while ω is the flutter frequency. The definitions of the generalized masses ($M_{i,i}$'s), generalized mass coupling coefficients ($M_{i,j}$'s), generalized spring constants (K_i's) and structural damping

coefficients (q_i's) is evident from the expressions for the kinetic energy, potential energy and dissipation function.

The aerodynamic coefficients used in Reference 14 were obtained using strip theory aerodynamics based on tabulated results of unsteady two-dimensional aerodynamic theory as presented in Reference 15. This classical method was believed reasonable because of the high aspect ratio of the wing wing and the low operating speed of the TIFS airplane. However, the validity of this approach has not been checked with modified-strip-analysis or lifting surface theory.

In computing aerodynamic coefficients, a reference reduced frequency was defined

$$K_{ref} = \frac{\omega b_{ref}}{V} = \text{reference reduced frequency}$$

where

ω = frequency, rad/sec

V = velocity, m/sec

b_{ref} = 1.207m (3.959 ft) = reference semichord (at approximately 60% span)

The $A_{i,j}$ coefficients in the expressions for the generalized aerodynamic coefficients were computed for a series of $(\omega b_{ref}/V)$'s. For each reference reduced frequency, a corresponding local reduced frequency at each spanwise station was computed from

$$K_m = \left(\frac{\omega b}{V}\right)_m = \frac{b_m}{b_{ref}}\left(\frac{\omega b_{ref}}{V}\right) \tag{5}$$

where b_m is the local semichord at the m^{th} station. It was necessary to evaluate spanwise integrals of section aerodynamic coefficients depending on local reduced frequency and appropriately weight them with the vibration mode shapes in determining the $A_{i,j}$ coefficients.

A conventional solution procedure was used after arranging the flutter equation in the following matrix form

$$\left[f_{i,k}\right]\left\{q_k\right\} = \lambda\left\{q_i\right\} = (1+jg)\left(\frac{\omega_r}{\omega}\right)^2\left\{q_i\right\} \tag{6}$$

where

$$f_{i,j} = \frac{M_{i,j}}{M_{i,i}\left(\frac{\omega_i}{\omega_r}\right)^2} + \frac{\pi\rho A_{i,j}\left(\frac{b_r\omega}{V}\right)}{M_{i,i}\left(\frac{\omega_i}{\omega_r}\right)^2} = \text{Typical matrix element}$$

ω_r = is an arbitrary reference frequency

$g = g_i$ = structural damping coefficient (assumed the same for all degrees of freedom)

Then at a given reduced frequency $b_r\omega/V$, obtaining solutions amounts to solving an eigenvalue problem. The eigenvalues (λ's) and eigenvectors $\{q_i\}$'s are those required for sinusoidal oscillations of the system. Values of flutter frequency (ω), flutter velocity (V), and damping coefficient (g) corresponding to the k^{th} eigenvalue follow immediately from the equations:

$$\omega_k = 2\pi f_k = \frac{\omega_r}{\sqrt{Re(\lambda_k)}} \tag{7}$$

$$V_k = b_r\omega_k \Big/ \left(\frac{\omega b_r}{V}\right) \tag{8}$$

$$g_k = \frac{I_m(\lambda_k)}{Re(\lambda_k)} \tag{9}$$

and were used in obtaining V-g plots to indicate stability boundaries.

3.2.2.2 Introduction of Effect of Active Controls in Flutter Equations

Sinusoidal motion was considered in the analysis of the effect of active control on flutter as was done in the flutter analysis without active control. It was recognized that in final design it would be necessary to study the effects of real sensor and control system characteristics in both sinusoidal and transient motions.

A control law was postulated in which the control surface rotation was taken equal to the product of the generalized coordinate vector and a row matrix of control constants

$$q_r = \left[C_{r,i} + jG_{r,i}\right]\{q_i\} \tag{10}$$

q_r = aileron rotation, DLF rotation, or rotation of a wing tip control surface

$C_{r,i}$, $G_{r,i}$ = control constants

The possibility of using such a control law for inducing flutter was studied and also its application for flutter suppression by active control. Separate control surfaces and control laws would be used for inducing and suppressing flutter.

In order to clarify how the presence of active control modifies the flutter equations, a simplified example is written out below. Here a two-degree-of-freedom system (q_1 and q_2) is actively controlled by motion of a single control surface (q_3)

$$\begin{bmatrix} (f_{1,1} - \lambda) & f_{1,2} & f_{1,3} \\ f_{2,1} & (f_{2,2} - \lambda) & f_{2,3} \\ (C_{3,1} + jG_{3,1}) & (C_{3,2} + jG_{3,2}) & -1 \end{bmatrix} \begin{Bmatrix} q_1 \\ q_2 \\ q_3 \end{Bmatrix} = 0 \tag{11}$$

Flutter equations for the system modified by active control are obtained by eliminating control rotation, q_3 giving

$$\begin{bmatrix} \underbrace{\left[f_{1,1} + f_{1,3}(C_{3,1} + jG_{3,1})\right]}_{f'_{1,1}} - \lambda \Big]\Big[\underbrace{f_{1,2} + f_{1,3}(C_{3,2} + jG_{3,2})}_{f'_{1,2}}\Big] \\ \Big[\underbrace{f_{2,1} + f_{2,3}(C_{3,1} + jG_{3,1})}_{f'_{2,1}}\Big]\Big[\underbrace{f_{2,2} + f_{2,3}(C_{3,2} + jG_{3,2})}_{f'_{2,2}} - \lambda\Big] \end{bmatrix} \begin{Bmatrix} q_1 \\ q_2 \end{Bmatrix} = 0 \tag{12}$$

$$\lambda = (i + jg)\left(\frac{\omega_{ref}}{\omega}\right)^2$$

Some of the problems in using active control of existing TIFS control surfaces for modifying system flutter parameters are apparent when the equations are displayed in this form. For example, if it were desired to raise the uncoupled frequency of Mode 1,

$$\omega_1 = \omega_r \frac{1}{\sqrt{Re f'_{1,1}}} , \qquad (13)$$

the real part of $f'_{1,1}$ should be reduced. This could be accomplished by adjusting control constant $C_{3,1}$. On the other hand, it can be seen that $C_{3,1}$ also affects matrix elements $f'_{2,1}$ and thus the coupling between Modes 1 and 2. A more independent variation in the different flutter parameters could be obtained if active control of more than one control surface were possible or if additional control surfaces could be added at appropriate locations.

3.2.3 Active Control for Inducing and Suppressing Symmetric Wing Flutter

In the present study, emphasis was placed on methods for inducing and suppressing the symmetric flutter modes of the TIFS airplane. This was done because of the good response characteristics of the present symmetric DLF control system which could be incorporated in a flutter control system with little modification. However, there is reason to believe that it might be easier to induce antisymmetric flutter than symmetric flutter by active control as will be discussed later.

3.2.3.1 Basic Configuration

The results of a five-degree-of-freedom flutter analysis on the basic configuration considered in studying symmetric flutter of TIFS are indicated on Figure 22. The natural frequencies of the uncoupled vibration modes used in this analysis were:

Generalized Coordinate	Uncoupled Mode	Natural Freq. (Hz)
$h^{(1)}_{(W)}$	1st Symmetric Bending	2.981
$h^{(2)}_{(W)}$	2nd Symmetric Bending	7.253
α_W	1st Symmetric Torsion	4.583
δ_a	Aileron Rotation	7.75
δ_z	DLF Rotation	12

These parameters were for TIFS with the side force surfaces removed.

Figure 22 is a typical plot (i.e., velocity vs. structural damping required to give neutrally stable sinusoidal oscillations). The corresponding flutter frequencies are indicated at several points along the curve. The flutter stability equations for a five-degree-of-freedom system have five roots and a damping curve is obtained for each root. The principal motion

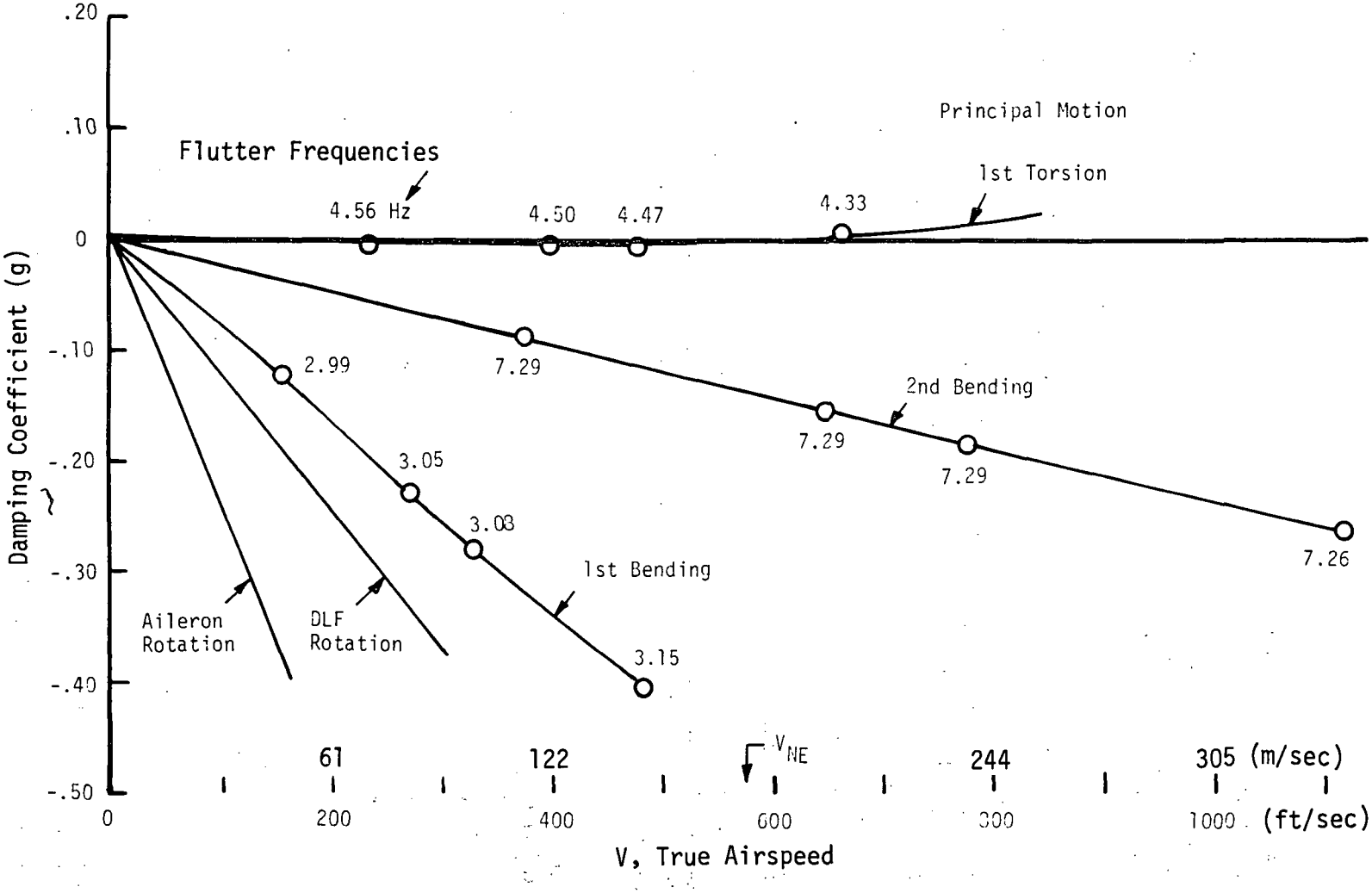

Figure 22 TIFS SYMMETRIC FLUTTER, BASIC CONFIGURATION

corresponding to each branch of the solution is indicated. When a control surface (e.g., the DLF) is driven by active control which constrains the surface rotation to a linear combination of other degrees of freedom, the number of degrees of freedom of the system is reduced by one, resulting in only four branches in the solution.

All values of g are negative in Figure 22 below V_{NE} . The never-exceed speed, V_{NE} , is taken to be a true airspeed of 176.8 m/sec (580 ft/sec) corresponding approximately to an indicated airspeed of 295 knots at 3048 m (10,000 ft) altitude.

3.2.3.2 Flutter of a Single Structural Mode

The simplest structural instability which might be induced by active control would be unstable oscillations in a single structural mode without appreciable coupling with the other degrees of freedom. Figure 23 shows the results of a study of such a case. Computations were made to show the effect of introducing a DLF rotation which is phased at 90° with respect to the first bending mode motion. This control law introduces effective negative damping of the first bending mode. The feedback constants have negative signs because downward motion of the wing tip and DLF trailing edge are both taken positive.

The DLF rotation also introduces generalized forces acting on the 2nd bending and torsional degrees of freedom. Nevertheless, feedbacks in quadrature with the first bending mode response and of the magnitudes considered do not result in significant changes in the damping curves for the modes characterized by second bending, torsion, or aileron rotation.

It should be pointed out that the results shown are for a pure feedback signal proportional to the response in the first uncoupled bending mode. In the implementation of this concept on the TIFS airplane it would be preferable to work with the coupled modes of the system. Then the feedback should be proportional to the response in the coupled mode primarily involving first bending.

Methods for generating the required control signal have not been analyzed in detail nor have computations yet been carried out to determine the effect of a contaminated feedback signal. However, it should be possible to obtain a reasonably pure first mode signal by appropriate combination of signals measured by pickups mounted on nodes for the second bending and torsional modes. Further refinement of the signal could be obtained by a band-pass filter tuned to the first bending mode frequency. It is believed that a satisfactory first mode signal could be obtained by the measures mentioned above in conjunction with empirical adjustments made in ground vibration tests.

Safety of the system would be assured by limiting the authority of the ACT system for controlling DLF rotation at flutter frequencies. Consequently, the DLF could not produce large enough wing oscillations to cause structural damage.

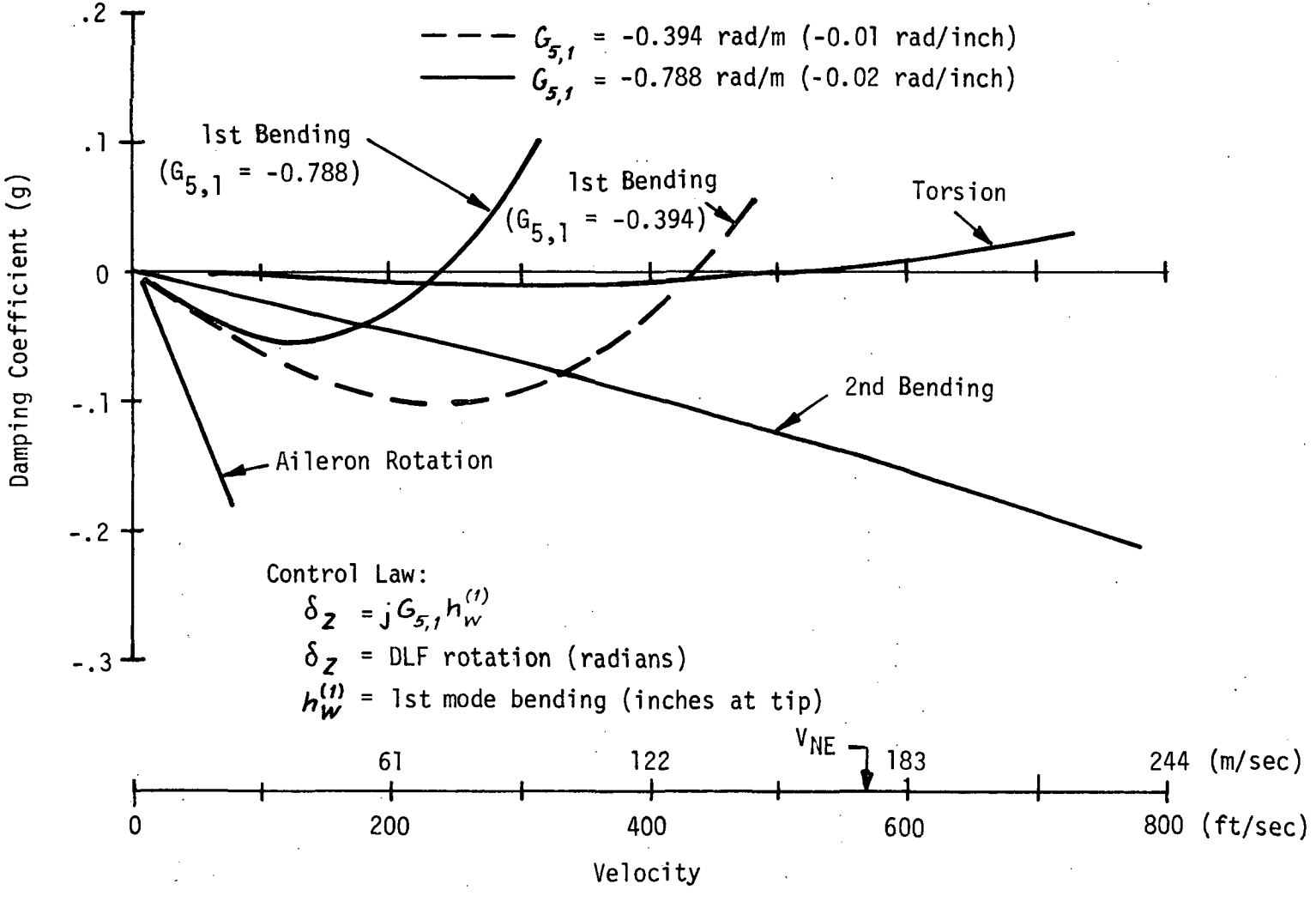

Figure 23 DESTABILIZATION OF FIRST BENDING MODE BY ACTIVE CONTROL OF DLF

Flutter tests involving destabilizing the first bending mode appear worthwhile for two reasons. First, it would demonstrate the ability to generate signals proportional to a particular modal response and to use them in active control of a particular control surface. This is a technique which is also required in active controls for reducing modal response or for inducing or suppressing flutter involving the coupling of two or more structural modes. Secondly, flutter modes primarily involving response in a single structural mode can result inadvertently in the design of active control systems for other functions. Consequently, it is desirable to develop methods for avoiding and suppressing flutter of this type.

The present DLF actuation system of the TIFS airplane is capable of destabilizing first mode bending when controlled with the proper feedback signal. The control servo characteristics of the DLF give a surface rate limit of 58 deg/sec with no load and 40 deg/sec under design servo hinge moment. At a first mode oscillation frequency of $2\pi(2.981) = 18.73$ rad/sec, a sinusoidal oscillation of the DLF of amplitude $40/18.73 = 2.14$ degrees could occur without exceeding the rate limit under design hinge moment. The corresponding tip deflection in first mode being for a control constant of $G_{s_1} = 0.788$ rad/m would be $h^{(1)}_{(w)} = 0.048$ m (1.9 in.). It is believed practical to work with deflections of this magnitude.

An alternative configuration might be envisioned in which a smaller DLF would be used in conjunction with larger flap angles. Such a configuration would minimize the problem of control surface backlash but might cause the control servo rate limit to be exceeded.

Preparation for flutter tests using the present DLF would involve installing pickups for measuring first mode bending and building equipment for processing the measured signals.

3.2.3.3 Symmetrical Wing Bending - Torsion Flutter Induced by Active Control of the DLF

The previous section has indicated how flutter in the first wing bending mode can be induced by driving the DLF in quadrature with the first bending mode response. Only a single structural mode is involved essentially in this type of flutter but coupling between two or more modes is usually required to cause flutter in most problems of practical interest. This section takes up calculations which were made to determine if coupled wing-bending torsion flutter could be induced with the DLF by using a different control law.

Results on Figure 24 were obtained using the following control law:

$$\delta_z = (.03 - j.0125)\, h_w^{(1)}$$

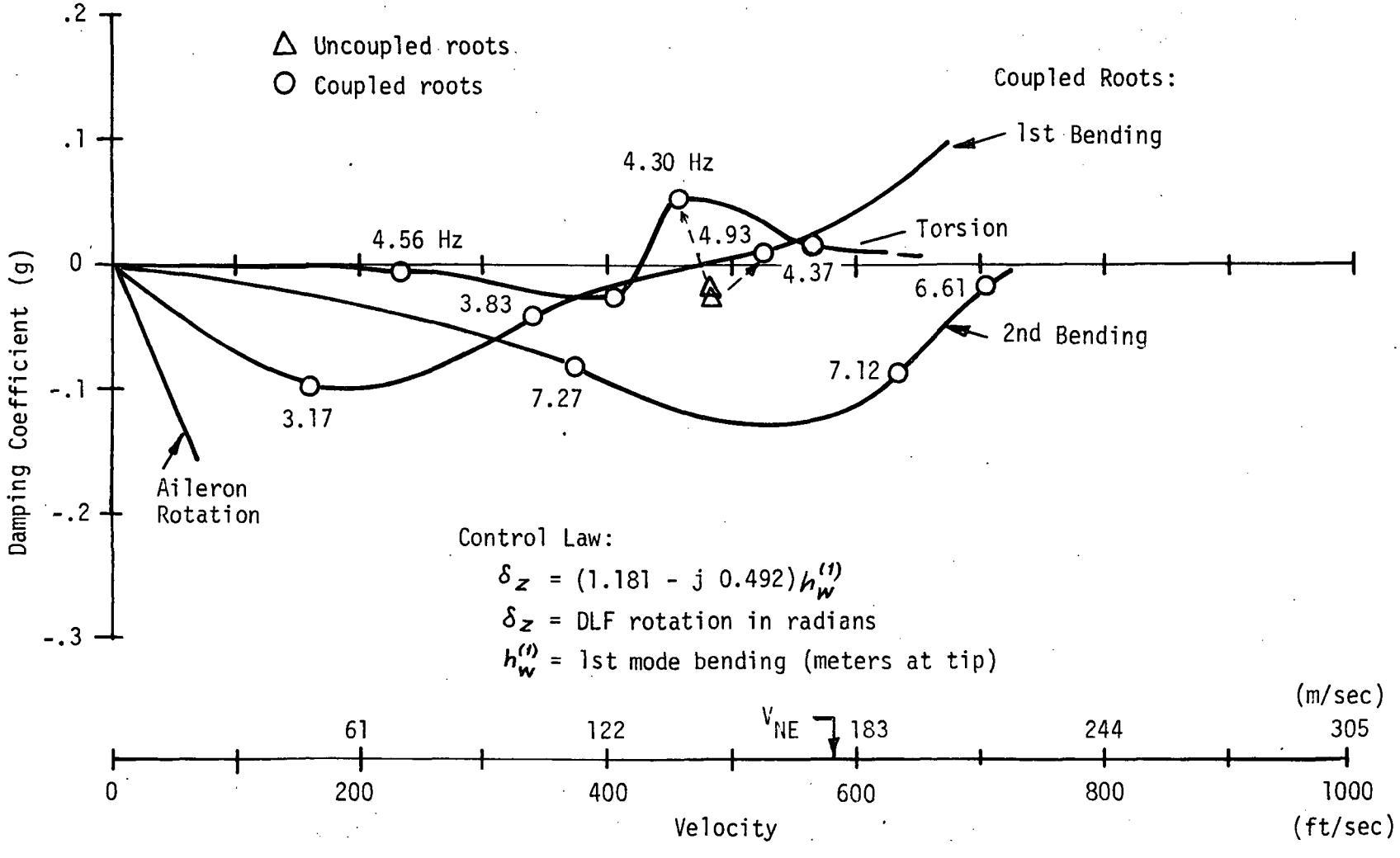

Figure 24 SYMMETRICAL FLUTTER INDUCED BY ACTIVE CONTROL OF DLF

DLF rotation (δ_z) is assumed to have a component in phase as well as in quadrature with the first mode bending response, $h_w^{(1)}$. The aerodynamic forces due to the in-phase component of DLF rotation act as an effective spring tending to stiffen the first bending mode. As the speed is increased, the aerodynamic spring force becomes larger, leading to the increases in frequency indicated along the damping curve associated with the first bending mode. However, the frequencies computed along the second bending and torsion damping curves did not change much below V_{NE}.

Flutter occurs in the torsion mode at approximately 140.2 m/sec (460 ft/sec) with the feedback constants used in computing Figure 24. The results were obtained using the generalized aerodynamic coefficients which were available from previous work on TIFS and which had been computed for a series of reduced frequencies. The values of reduced frequency were not spaced closely enough to give a good definition of the damping curve for the torsion mode in the critical velocity range. Further analysis of the shape of this curve could not be carried out in the present program. However, it is believed that a satisfactory determination of the shape of this curve could be obtained by using a spline fit of the variations in the aerodynamic coefficients with $b_r\omega/V$ as suggested by NASA personnel in Reference 17.

Further insight concerning the damping curves on Figure 24 can be obtained by an examination of Table 3 which shows how some of the flutter matrix elements are modified by active control of the DLF proportional to the first bending mode response. Only the first column of the flutter matrix is given because this is the only one affected by such a control law. The values given are all for $b_r\omega/V = .2326$. Calculations for this reduced frequency gave the critical point on Figure 24 of $g = .052$ at $V = 140.2$ m/sec (460 ft/sec).

The complex root for the first uncoupled bending mode obtained including the effect of the active control of the DLF but neglecting coupling with other modes is given by:

$$\lambda = (1 + jg)\left(\frac{\omega_r}{\omega}\right)^2 = f'_{h_w^{(1)}, h_w^{(1)}}$$

$$= f_{h_w^{(1)}, h_w^{(1)}} + f_{h_w^{(1)}, \delta_z}\left(C_{\delta_z, h_w^{(1)}} + jG_{\delta_z, h_w^{(1)}}\right) \tag{14}$$

where generalized coordinates have been used as subscripts rather than integers to simplify the identification of the various terms.

The corresponding velocity and structural damping coefficients required for uncoupled sinusoidal oscillation in the first bending mode are given by:

TABLE 3

Comparison of f_{q_i, q_j} and f'_{q_i, q_j}

Matrix Elements for Active Control of DLF

$b_r \omega / V = .2326$

(a) No Active Control

q_i	q_j	f_{q_i, q_j} REAL	IMAG	
$h_w^{(1)}$	$h_w^{(1)}$	2.26596D 00	-7.37021D-01	m/m
$h_w^{(2)}$	$h_w^{(1)}$	-1.58791D-02	-1.06227D-01	m/m
α_w	$h_w^{(1)}$	7.28577D-03	1.26475D-03	rad/m
δ_a	$h_w^{(1)}$	2.27103D-02	-1.03086D-01	rad/m

(b) Active Control of DLF , $\delta_z = (1.181 - j0.492)\, h_w^{(1)}$

q_i	q_j	f'_{q_i, q_j} REAL	IMAG	
$h_w^{(1)}$	$h_w^{(1)}$	1.03067D 00	-2.79736D-02	m/m
$h_w^{(2)}$	$h_w^{(1)}$	2.45184D-01	-2.50269D-01	m/m
α_w	$h_w^{(1)}$	-7.08806D-03	-4.82578D-04	rad/m
δ_a	$h_w^{(1)}$	2.27103D-02	-7.94636D-02	rad/m

(c) Active Control of DLF , $\delta_z = -1.181\, h_w^{(1)}$

q_i	q_j	f'_{q_i, q_j} REAL	IMAG	
$h_w^{(1)}$	$h_w^{(1)}$	3.57024D 00	-9.02617D-01	m/m
$h_w^{(2)}$	$h_w^{(1)}$	-2.89463D-01	-7.61781D-02	m/m
α_w	$h_w^{(1)}$	1.89129D-02	7.85672D-03	rad/m
δ_a	$h_w^{(1)}$	2.27103D-02	-1.03086D-01	rad/m

$$V = b_r \omega_r \Big/ \left(\frac{b_r \omega}{V}\right) \sqrt{Re\left(f'_{h_w^{(1)}, h_w^{(1)}}\right)} \tag{15}$$

$$g = I_m \left(f'_{h_w^{(1)}, h_w^{(1)}}\right) \Big/ Re\left(f'_{h_w^{(1)}, h_w^{(1)}}\right) \tag{16}$$

It follows from the data in Table 3 that the structural damping coefficient for the first uncoupled bending mode without active control is $g = -.737/2.27 = -.33$. At a reduced frequency of $b_r \omega / V = .2326$, computations for the first bending mode considered independently but including the active control law of Figure 24, give $V = 147.2$ m/sec (483 ft/sec) and $g = -.027$. These results and the corresponding data for the uncoupled torsion mode which is not affected by active control are indicated on Figure 24. Both of the points for the uncoupled modes are in the stable region requiring negative damping coefficients to maintain sinusoidal oscillations. However, the point for the torsion mode is moved into the unstable region when coupling with first bending and second bending are included.

The quadrature feedback tends to destabilize the first bending mode in the case shown on Figure 24 similar to the case on Figure 23, but the torsion mode becomes unstable at a lower velocity.

Inertia couplings between uncoupled bending and torsional modes are known to be significant flutter parameters. In particular, the inertia forces due to first mode bending often play an important role in establishing the equilibrium of generalized forces acting in the first torsion mode. This effect is introduced into the flutter computations through the matrix element

$$f_{\alpha_w, h_w^{(1)}} = \frac{M_{\alpha_w, h_w^{(1)}}}{M_{\alpha_w, \alpha_w}\left(\frac{\omega_{\alpha_w}}{\omega_r}\right)^2} + \frac{\pi \rho A_{\alpha_w, h_w^{(1)}}}{M_{\alpha_w, \alpha_w}\left(\frac{\omega_{\alpha_w}}{\omega_r}\right)^2} \tag{17}$$

where the contribution of the inertia coupling for symmetrical flutter of the TIFS wing is

$$\frac{M_{\alpha_w, h_w^{(1)}}}{M_{\alpha_w, \alpha_w}\left(\frac{\omega_{\alpha_w}}{\omega_r}\right)^2} = 6.768 \times 10^{-3} \tag{18}$$

It can be seen from Table 3(a) that the real part of $f_{\alpha_w, h_w^{(1)}}$ is primarily determined by inertia coupling when there is no active control. Case (b) of Table 3 shows modified matrix elements for the control law used in computing Figure 24. Here, active control has a dominant effect on the real part of $f_{\alpha_w, h_w^{(1)}}$ resulting in a change of sign. Nevertheless, this control law caused the effective uncoupled frequencies of the first bending and torsional modes to be approximately equal at $b_r\omega/V = .2326$ and gave a flutter point in the desired speed range.

Case (c) on Table 3 shows flutter matrix elements for a control law tending to make the real part of $f_{\alpha_w, h_w^{(1)}}$ more positive or to give an effective increase in the inertia coupling. However, this control law also tended to lower the uncoupled first bending frequency and did not give a flutter condition in a speed range suitable for flight testing.

3.2.3.4. Symmetrical Wing Bending - Torsion Flutter Induced by Active Control of Ailerons

Consideration was given to the possibility of using the ailerons rather than the direct lift flaps for inducing a symmetric wing flutter condition which could be suppressed in a flight demonstration of active flutter control. This would require modification of the present aileron control system of the TIFS airplane which can only introduce antisymmetric aileron motions.

Figure 25 shows the results of flutter calculations which were made assuming active symmetric control of the aileron according to the control law:

$$\delta_a = (0.394 - j\,0.098)\, h_w^{(1)}$$

δ_a = aileron rotation in radians

$h_w^{(1)}$ = tip bending deflection in first bending mode (meters)

It was assumed as in the preceding sections that the first mode bending deflection could be sensed. Flutter calculations were carried out using first uncoupled wing bending, second uncoupled wing bending, first uncoupled wing torsion and DLF rotation as degrees of freedom. The flutter matrix elements for these degrees of freedom were modified to include the effect of active control of the aileron by the scheme discussed earlier.

The component of aileron rotation in phase with the wing bending motion produces aerodynamic forces which increase the effective stiffness of the bending mode as was found with active control of the DLF. However, the aileron is more effective than the DLF in producing first mode bending and the first mode bending frequency can be raised to the frequency of the torsion mode with smaller feedback control constants than required with the DLF.

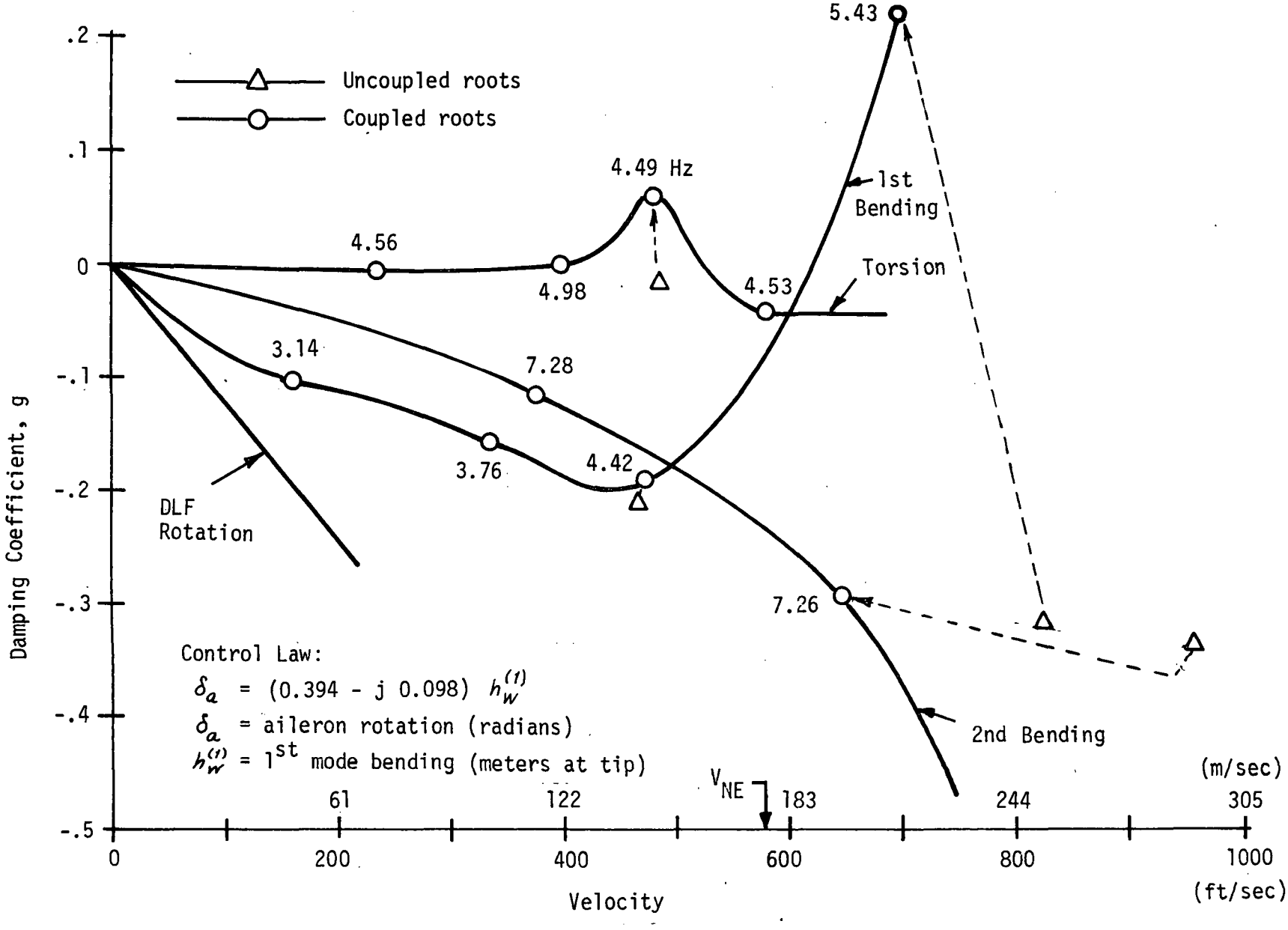

Figure 25 SYMMETRICAL FLUTTER INDUCED BY ACTIVE CONTROL OF AILERON

Computations for a reference reduced frequency of $b_r\omega/V = .2326$ gave the critical point on the torsion damping curve where g = .06 and V = 146.3 m/sec (480 ft/sec). The analysis was carried out for a limited number of reduced frequencies as discussed earlier. Consequently, the exact shape of the damping curve was not found in the critical region.

The aileron control law used in computing Figure 25 only influences the elements in the first column of the flutter matrix. Case (a) of Table 4 shows these elements when there is no active control while Case (b) of Table 4 shows these elements as obtained with the control law of Figure 25. All data on Table 4 are for a reference reduced frequency of $b_r\omega/V = .2326$ which gave the critical point on the torsion damping curve.

As discussed earlier, the element $f'_{h_w^{(1)}, h_w^{(1)}}$ is equal to the complex root of the flutter equation for the first uncoupled bending mode, assuming it is to be independent of the other degrees of freedom. The damping coefficient required to give sinusoidal motion in the first mode and corresponding velocity as determined from the root for Case (b) are

$$g = -.234/1.113 = -.21 \tag{19}$$

$$V = b_r \omega_r \Big/ \left(\frac{b_r\omega}{V}\right) \sqrt{\text{Re } f'_{h_w^{(1)}, h_w^{(1)}}}$$

$$= 141.6 \text{ m/sec } (464.5 \text{ ft/sec}) \tag{20}$$

A point corresponding to these results for the uncoupled bending mode is plotted as a triangle on Figure 25. It is found to be very close to the curve obtained for the root of the coupled system which is characterized by first bending. A point is also shown which was obtained in a similar manner for the torsion mode considered to be uncoupled from the rest of the system. It can be seen that the coupling of the torsion mode with the first and second wing bending modes leads to a considerable shift in this point.

It will be noted in Table 4 that the real part of $f_{\alpha_w, h_w^{(1)}}$ is reduced from 7.286×10^{-3} without active control to 5.619×10^{-3} with the control law $\delta_a = 0.394 - j\ 0.098) h_w^{(1)}$. Thus the effective mass coupling of first mode bending and torsion is reduced by approximately 25%. Nevertheless, the increase in first bending mode frequency with this control law resulted in a flutter condition.

Case (c) on Table 4 shows the matrix elements obtained with a control law which increases the effective mass coupling between the first bending and torsion modes but lowers the first bending mode frequency. The required damping coefficients corresponding to all roots of the flutter stability equation proved to be negative in this case.

TABLE 4

COMPARISON OF f_{q_i, q_j} AND f'_{q_i, q_j} MATRIX ELEMENTS

OBTAINED WITH ACTIVE CONTROL OF AILERON. $b_n \omega / V = .2326$

(a) No Active Control (Figure 22)

q_i	q_j	f_{q_i, q_j} Real	Imag	
$h_w^{(1)}$	$h_w^{(1)}$	2.26596D 00	-7.37021D-01	m/m
$h_w^{(2)}$	$h_w^{(1)}$	-1.58791D-02	-1.06227D-01	m/m
α_w	$h_w^{(1)}$	7.28577D-03	1.26475D-03	rad/m
δ_z	$h_w^{(1)}$	8.72490D-03	-5.01786D-03	rad/m

(b) Active Control of Aileron, $\delta_a = (0.394 - j\ 0.098)\ h_w^{(1)}$ (Figure 25)

q_i	q_j	f'_{q_i, q_j} Real	Imag	
$h_w^{(1)}$	$h_w^{(1)}$	1.11252D 00	-2.32375D-01	m/m
$h_w^{(2)}$	$h_w^{(1)}$	-1.99013D-01	-2.57042D-02	m/m
α_w	$h_w^{(1)}$	5.61865D-03	8.88065D-04	rad/m
δ_z	$h_w^{(1)}$	8.72490D-03	-5.01786D-03	rad/m

(c) Active Control of Aileron, $\delta_a = -0.394\ h_w^{(1)}$

q_i	q_j	f'_{q_i, q_j} Real	Imag	
$h_w^{(1)}$	$h_w^{(1)}$	3.47029D 00	-9.40584D-01	m/m
$h_w^{(2)}$	$h_w^{(1)}$	1.75429D-01	-1.38922D-01	m/m
α_w	$h_w^{(1)}$	8.76620D-03	2.01154D-03	rad/m
δ_w	$h_w^{(1)}$	8.72490D-03	-5.01786D-04	rad/m

It is noted that Figure 25 indicates a second flutter condition which occurs at a speed greater than V_{NE} and involves considerable coupling between first and second bending.

3.2.3.5 Active Flutter Suppression

The preceding sections have been concerned with methods for using active control for inducing flutter conditions of the TIFS airplane at relatively low operating speeds suitable for demonstrating systems for active flutter suppression. It was postulated that the active control system for flutter suppression should operate with a different control surface than the one used to induce flutter.

Limited calculations were made of a possible active control system for the ailerons for suppression of flutter induced by the direct lift flaps. The problem considered was the suppression of the torsion mode flutter condition shown in the V-g curve on Figure 26.

The critical portion of this curve has been redrawn on the V-g diagram on Figure 26. Damping curves are also plotted on this figure which were obtained from flutter calculations made assuming active control of the aileron to eliminate the instability. The active control law used for the aileron was of the form,

$$\delta_a \ (radians) = j G_{\delta_a, h_w^{(1)}} h_w^{(1)} \ (\text{meters}) \qquad (21)$$

It was found in this case that a feedback constant giving as little as $G_{\delta_a, h_w^{(1)}} = 0.197$ rad/meter would be sufficient to give a considerable increase in flutter speed. This suggests that a control surface smaller than the present TIFS aileron might be used for flutter suppression possibly with greater angular movement.

Analyses were not made of methods for suppressing the flutter mode induced by active control of the aileron as indicated on Figure 25. However, it will be remembered that comparatively small active control feedback constants were required to induce this type of flutter. Consequently, it should be possible to employ a split aileron configuration as indicated in the hypothetical modification shown on Figure 27 where the inboard portion of the aileron would be used to induce flutter and the outboard aileron used for active flutter suppression.

3.2.4 Active Control of Antisymmetric Wing Flutter

Computations have been carried out to determine if active control can be used to lower the speed for symmetric flutter of the TIFS wing because this approach for demonstrating active flutter control would require

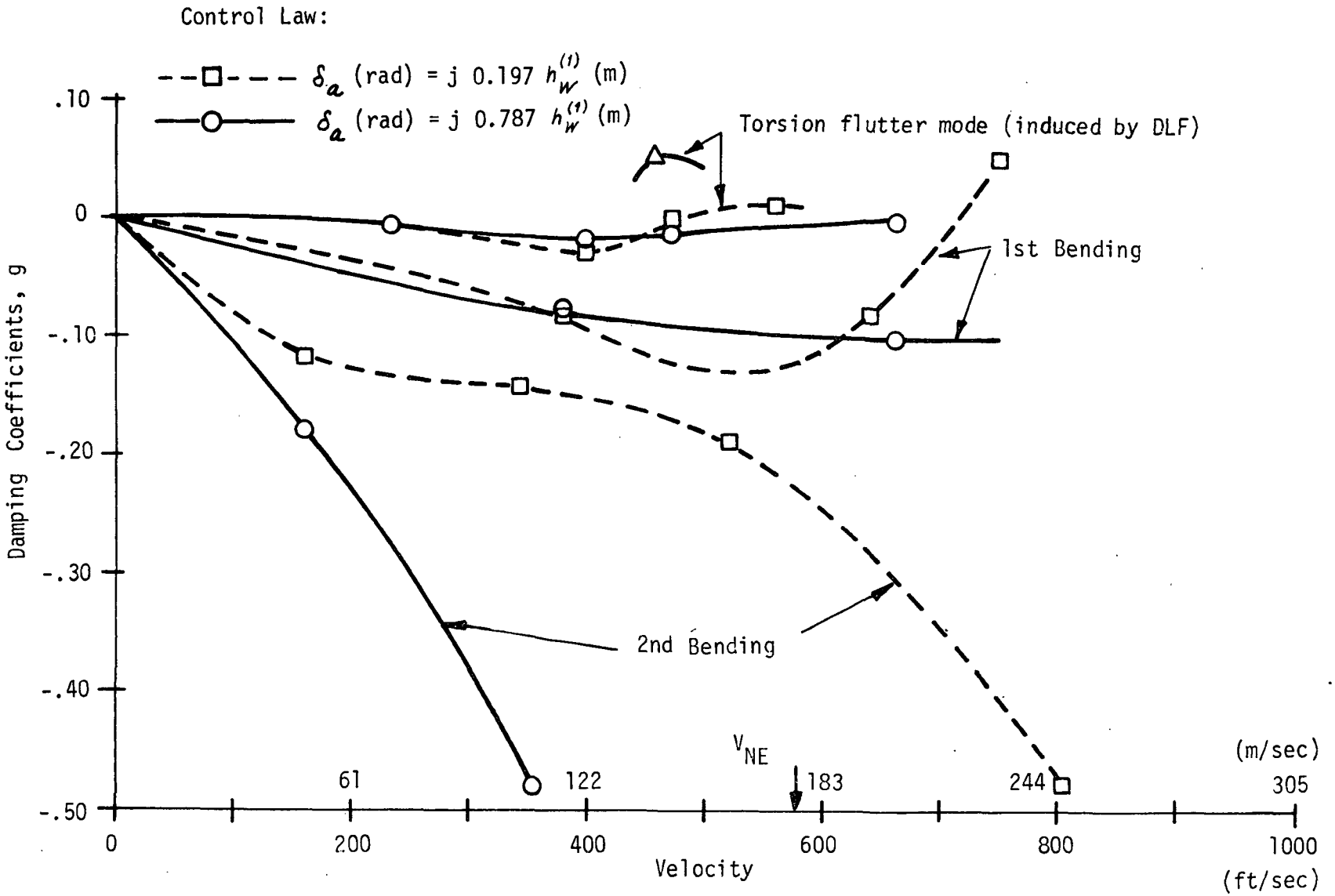

Figure 26 SUPPRESSION OF SYMMETRICAL FLUTTER BY ACTIVE CONTROL OF AILERON

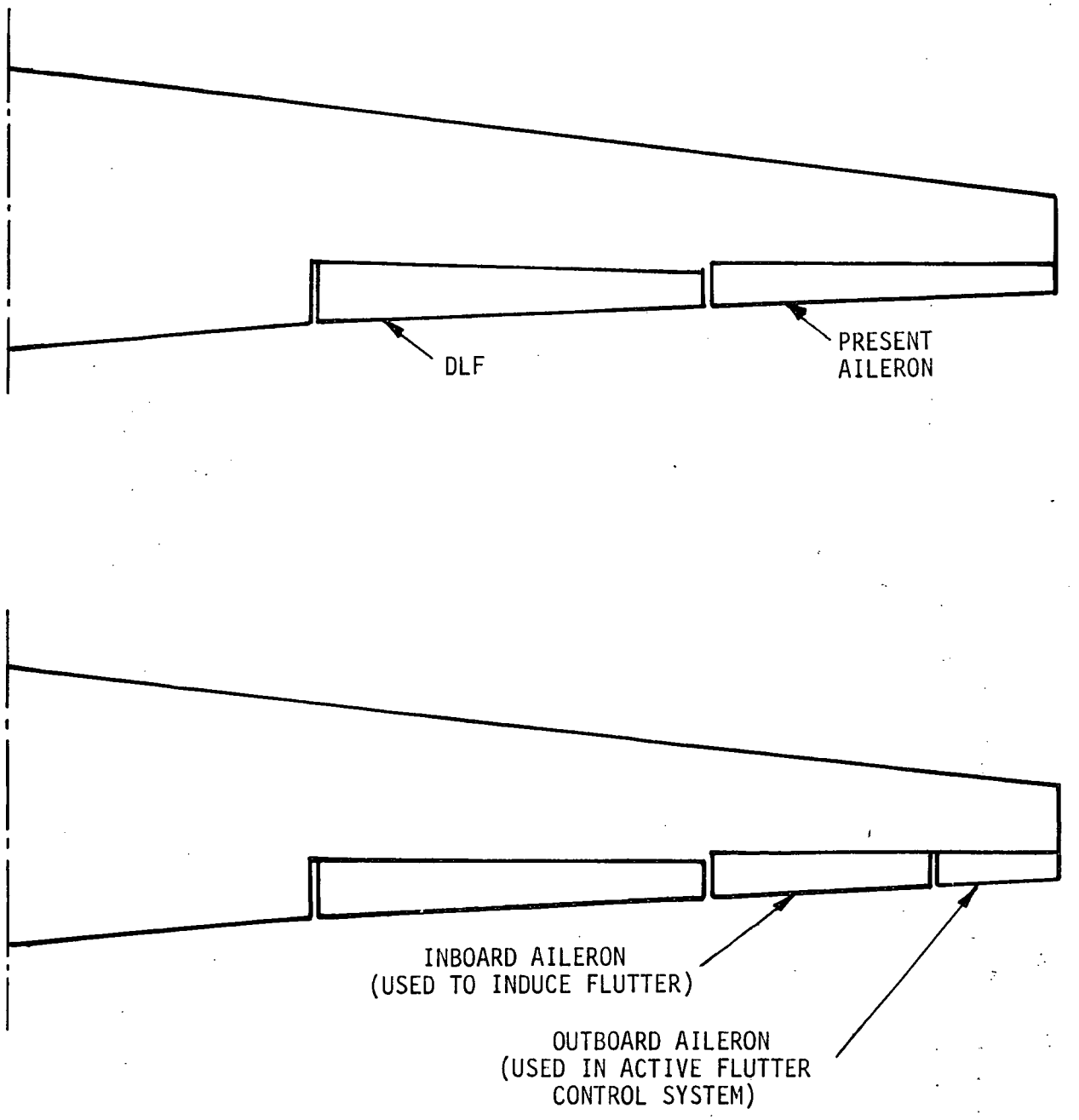

Figure 27 HYPOTHETICAL AILERON MODIFICATION

minimum modification of the airplane. Similar computations have not yet been made for the antisymmetric case which might provide more interesting flutter modes for flight investigation.

The frequencies of the uncoupled elastic modes which would be expected to be of primary importance in antisymmetric wing flutter are as follows:

Mode	Frequency (Hz)
First antisymmetric wing bending	4.85
Second antisymmetric wing bending	11.02
First antisymmetric wing torsion	4.57

The proximity of the first antisymmetric wing bending and torsional frequencies should be conducive to a flutter condition. Consequently, active control tending to increase the effective mass coupling between these modes should be able to induce flutter at an intermediate flight speed. If the DLF actuation system were modified to permit antisymmetric control, the active control of the DLF's could supply the required coupling by introducing torsional moments in accordance with the first antisymmetric bending mode response. Since the node line of the first antisymmetric bending mode is approximately at the midspan of the DLF, control movements of the DLF should not be very effective in exciting first antisymmetric bending. Thus it should be possible to use active control of the DLF to modify the coupling between bending and torsional motions without detuning the first antisymmetric wing bending and first antisymmetric wing torsion frequencies.

3.2.5 Conclusions and Recommendations

Two concepts have been considered for utilizing the TIFS airplane for demonstrating active flutter control. The first was flight test of a flutter mode coupling rigid body rotation of a side force surface and rotation of a side force surface flap. Work on this was dropped in favor of the second concept.

This second concept involved using active control for both inducing and suppressing flutter. This approach appears attractive from a safety standpoint because nonlinearities in the control system could be used to limit the amplitude of the flutter motion and it would always be possible to switch the system back to a flutter free configuration.

Flutter calculations have been carried out to study the feasibility of using active control for inducing flutter at an intermediate flight speed. It was found that single-degree-of-freedom flutter of the first symmetric

wing bending mode could be induced by active control of the DLF's. It is recommended that this system be implemented as a first step in utilizing the TIFS airplane for active flutter control tests.

The present DLF servo actuator system is capable of driving the DLF surfaces at the required frequencies and amplitudes to induce instability of the first bending mode. However, it would be necessary to install sensors to measure the first bending mode response and to develop equipment to filter and process the measured signals in the active control system. It is recommended that flight tests of this system would be conducted using active control constants both for suppression and for destabilization of the first bending mode response. A primary objective of the test would be to show that desired active control of the first bending mode could be obtained in spite of some contamination of the sensor signals due to response in other structural modes. It is recommended that in initial flutter tests only, the DLF's would be subject to active control and separate control surfaces would not be actively controlled to suppress the first mode response. DLF amplitudes would be limited to small values to avoid structural damage to the airplane.

Flutter analyses have shown that it is possible to induce coupled symmetric bending-torsion flutter of the TIFS wing by active control of either the DLF's or ailerons. It is believed that coupled antisymmetric bending-torsion flutter could also be induced by active control but computations have not yet been carried out for this case.

Although these results on bending-torsion flutter are encouraging, further analytical work is required to obtain better definitions of the velocity-damping curves for critical modes which could be used in planning a flight test program. It is recommended that additional flutter calculations be made to determine the best methods for using active control for both exciting and suppressing bending-torsion flutter. The results of this analysis would be used as a basis for selection of a particular configuration to be employed in future active control flutter tests of coupled bending-torsion flutter.

Work discussed in this report has been limited to the application of active control for controlling particular flutter modes of the TIFS airplane. This is believed to be the best approach when the objective is to induce flutter. However, for the problem of suppression of flutter, it might be preferable to apply the more general concepts of aerodynamic energy proposed by Nissim in Reference 18. The implementation and extension of these concepts was discussed in References 3 - 9 and it was shown that a flutter dynamic pressure increase could be obtained with a single trailing-edge control surface as well as with the combined leading edge and trailing edge control surface system discussed in Reference 18. It is recommended that additional computations of the application of active flutter control to the TIFS airplane include consideration of control laws analogous to those used in References 18 and 19.

3.3 Precise Flight Path Control System

The direct lift flaps, direct side force surfaces, and the thrust control of the TIFS aircraft can be effectively used for providing the pilot with the capability to easily achieve precise flight path control. The capability of achieving a precise flight path control is essential, if more demanding approach paths, such as steep, curved, decelerated paths are to be used to alleviate the noise and congestion problems facing today's terminal operations.

The design of a flight control system, which can provide the pilot with more precise flight path control and with reduced workload, may be achieved by using a decoupled flight control system in which each control affects only single output (e.g., a flight path control without disturbing the speed; control of bank angle without sideslip). Since in each control action by the pilot, his attention is focused only on a single response, a more precise flight path control may be achieved. Further, since proper coordination of controls is not required, the pilot workload may be significantly reduced.

In theory, it is always possible, through use of feedback and control crossfeed, to synthesize a precise decoupled control system having desired response characteristics, if the aircraft has independent and adequate force generating devices (direct lift and side force devices such as in the TIFS aircraft) in addition to the conventional moment generating devices. In practice, however, these independent force generating devices may either have only limited authority or be entirely lacking, it becomes only possible to design approximate decoupled control systems. While experience has shown that a precise decoupling is not required, the clear trade-offs involved in the design of approximate decoupled systems for a satisfactory pilot-vehicle performance and pilot workload are yet to be fully explored.

Two major steps are involved in the design of the decoupled flight control system.

(i) Definition of the "model" or the desirable decoupled system. This model is dictated by the flying qualities requirements or determined using manual control theory.

(ii) Determination of the control law for the decoupled flight control system. Calculation of the feedback gains and the control crossfeed gains for the decoupled control system that best match the model may be done either using conventional control theory or optimal control theory.

3.3.1 Decoupled Model and the Selection of Model Parameters

Consider first a decoupled model for the longitudinal motion of the TIFS aircraft. In this model there are three independent cockpit controllers, i. e., the pitch attitude controller, the speed controller, and the flight path controller, each of which affects only a single output. The model that provides this sort of airplane response characteristics has the following form:

$$\dot{y} = F_y y + G_y \delta \tag{22}$$

where

$$\left.\begin{aligned} y^T &= (q,\ \Delta\theta,\ \Delta V,\ \Delta\gamma) \\ \delta^T &= (\delta_\theta,\ \delta_V,\ \delta_\gamma) \\ F_y &= \begin{bmatrix} -2\zeta_0\omega_0 & -\omega_{n_0}^2 & 0 & 0 \\ 1 & 0 & 0 & 0 \\ 0 & 0 & \lambda_V & 0 \\ 0 & 0 & 0 & \lambda_\gamma \end{bmatrix} \\ G_y &= \begin{bmatrix} b_1 & 0 & 0 \\ 0 & 0 & 0 \\ 0 & b_2 & 0 \\ 0 & 0 & b_3 \end{bmatrix} \end{aligned}\right\} \tag{23}$$

The selection of the parameters in the decoupled model parameters in Equation 23 must be based on the flying qualities considerations. Consider the pilot-vehicle closed-loop system for each decoupled control loop. One possible choice of the model parameters is to assume that the closed-loop pilot-vehicle performance in each loop will meet certain performance measures, e.g., closed-loop stability and bandwidth, that the pilot requires no dynamic compensation to achieve a preset performance standard, and that the channel interaction is negligible. We shall call the dynamic model of the pilot without the dynamic compensation the "comfort" pilot model, which has the mathematical representation in each loop as follows:

$$G_p(s) = K_p(e)^{-\tau s} \tag{24}$$

where K_p is the pilot gain and τ, the effective time delay, in seconds, is usually in the range of

$$0.2 \leq \tau \leq 0.4$$

To assure that the pilot does not use dynamic compensation to achieve a desirable level of performance measures, the "comfort" pilot model may be imposed in each of the decoupled manual control loops. Figures 28 and 29 show the effect of model parameters on the closed-loop performance measures as expressed in terms of the dominant branch are adequate for the simple structure of the decoupled model considered here (Reference 22).

The requirements of the pilot-vehicle closed-loop stability and bandwidth depend to a large extent on the task and/or flight phase (Reference 23). For the numerical example studied, the following parameters were used in the longitudinal decoupled model considered.

Pitch Control Loop	$\zeta = 0.7$ $\omega_{n_o} = 2.5$ rad/sec $b_1 = 1$
Speed Control Loop	$\lambda_v = -1$ 1/sec $b_2 = 10$
Flight Path Control Loop	$\lambda_\gamma = -0.5$ 1/sec $b_3 = 1$

One decoupled model for the lateral-directional motion of the TIFS was also studied. This model permits the TIFS aircraft to turn without having to bank. To be specific, the cockpit control functions are as follows:

$$\delta_p \xrightarrow{control} p$$

$$\delta_r \longrightarrow r$$

$$\delta_\beta \longrightarrow \beta$$

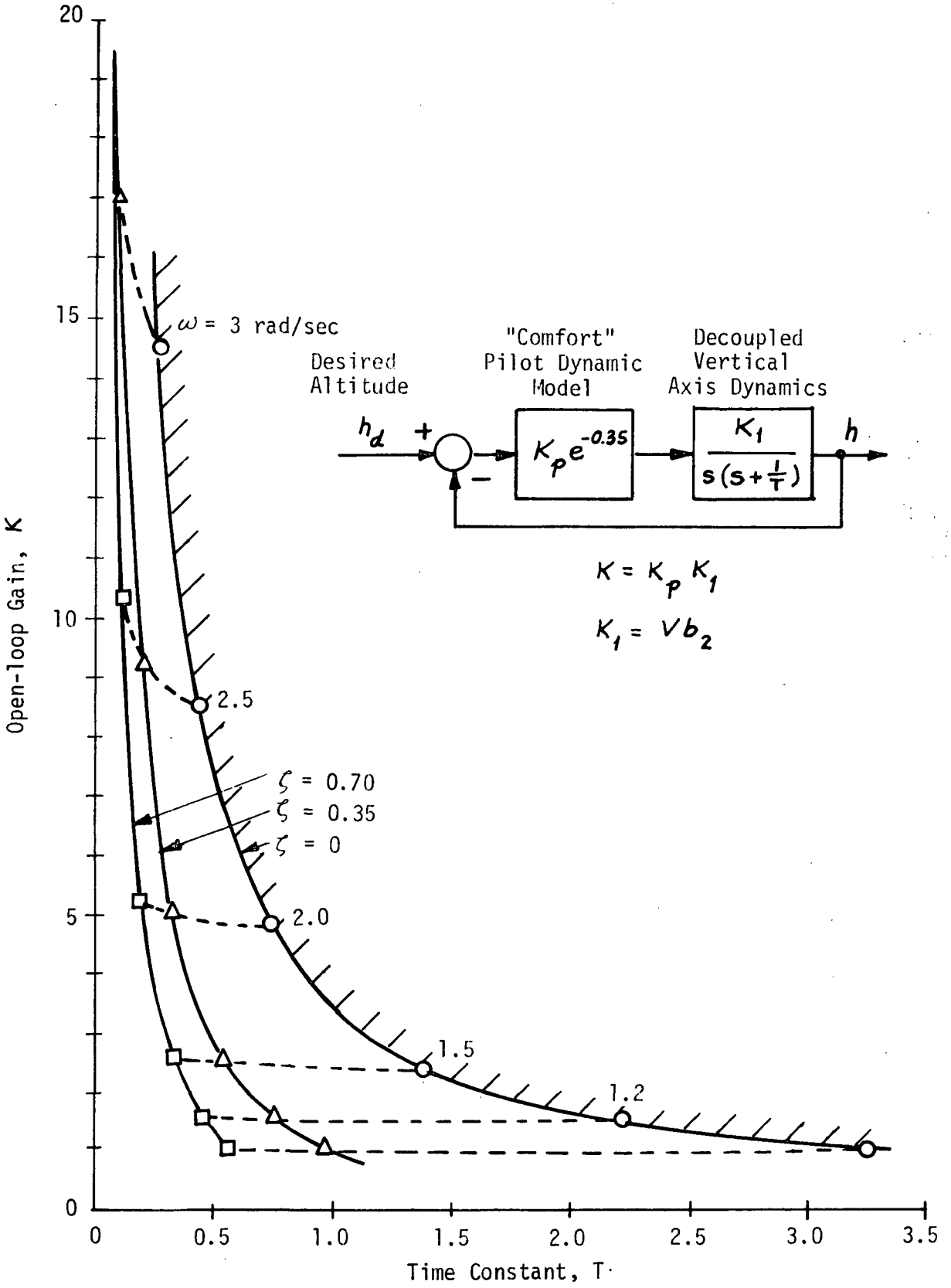

Figure 28 EFFECT OF THE TIME CONSTANT ON THE DOMINANT BRANCH CLOSED-LOOP ω_n AND ζ, NO DYNAMIC COMPENSATION BY PILOT

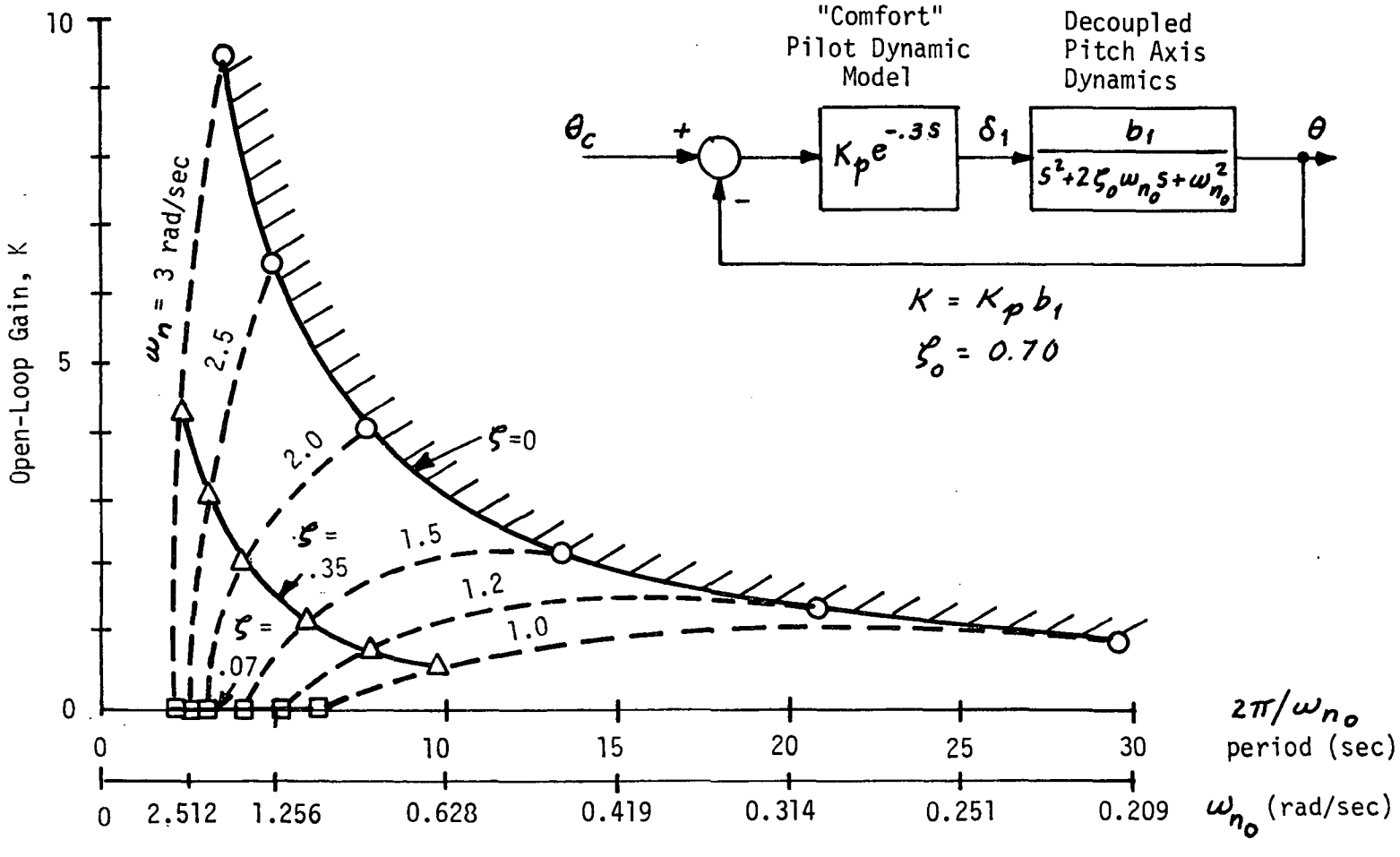

Figure 29 EFFECT OF THE OPEN-LOOP PARAMETERS, ω_{n_o} AND ζ_o ON THE DOMINANT BRANCH CLOSED-LOOP ω_n AND ζ, NO DYNAMIC COMPENSATION BY THE PILOT

To achieve these control functions, the decoupled model takes the following form:

$$y^T = (p, \Delta\phi, r, \beta)$$

$$\delta^T = (\delta_p, \delta_r, \delta_\beta)$$

$$F_y = \begin{bmatrix} \lambda_p & 0 & 0 \\ 1 & 0 & \\ \hline 0 & & \begin{matrix} \lambda_r & 0 \\ 0 & \lambda_\beta \end{matrix} \end{bmatrix} \qquad (25)$$

$$G_y = \begin{bmatrix} c_1 & 0 \\ 0 & \\ \hline 0 & \begin{matrix} c_2 & 0 \\ 0 & c_3 \end{matrix} \end{bmatrix}$$

The model parameters used are as follows

Roll Control Loop	λ_p = -3 1/sec c_1 = -2.3
Yaw Control Loop	λ_r = -0.2 1/sec c_2 = -0.8
Sideslip Control Loop	λ_β = -0.2 1/sec c_3 = 0.06

Other decoupled models for the lateral-directional motion, such as those for a more conventional coordinated turn, may also be studied using the existing capability of the TIFS aircraft.

3.3.2 Decoupling Control Law

The control law which permits achieving the desired decoupled response characteristics of the TIFS airplane will be synthesized using feedback and control crossfeed of the following form

$$u = -K_p x + K_\delta \delta \tag{26}$$

where K_p and K_δ are the feedback gain matrix and the control crossfeed gain matrix, respectively.

The equations of motion of the TIFS aircraft are given by:

$$\dot{x} = Fx + Gu \tag{27}$$

It is desirable, therefore, to transform the desired decoupled model expressed in the y coordinate into that in the state vector x using the similarity transformation

$$\left.\begin{aligned} F_x &= T F_y T^{-1} \\ G_x &= T G_y \end{aligned}\right\} \tag{28}$$

where the transformation matrix T relates the state x to the y coordinate (or output vector) by

$$x = Ty$$

For example, in the longitudinal motion, the state vector is

$$x^T = (q, \Delta\theta, \Delta V, \Delta\alpha)$$

and the transformation matrix T becomes,

$$T = \begin{bmatrix} 1 & 0 & 0 & 0 \\ 0 & 1 & 0 & 0 \\ 0 & 0 & 1 & 0 \\ 0 & 1 & 0 & -1 \end{bmatrix}$$

for the lateral-directional example, since $x = y$, $\tau = I_4$. But substituting the control law, Equation 26, into the state equation, Equation 27, and equating the resultant equation with the decoupled model equations expressed in the state x, the desired gain matrices K_p and K_δ may be found to be

$$K_\delta = (G^T G)^{-1} G^T G_x$$

and

$$K_p = (G^T G)^{-1} G^T (F - F_x) \tag{29}$$

The above decoupling control law yields the perfect dynamic decoupling desired for the TIFS aircraft if the actuator dynamics are neglected and the control authorities are not saturated. Using the equations of motion for the selected landing configuration as shown in Appendix A, the gain matrices K_p and K_δ were calculated using Equation 29. The results are shown in the following table.

Longitudinal Decoupling Control Law at the Landing Condition

$$K_\delta = \begin{bmatrix} -0.4878 & 0.0002 & -0.2082 \\ 0.1101 & 0.1511 & 2.4221 \\ 0.2308 & -0.0028 & 5.0769 \end{bmatrix} *$$

$$K_p = \begin{bmatrix} -1.0933 & -0.3264 & -0.0004 & 0.5074 \\ 0.2468 & -1.7517 & 0.0762 & 2.3796 \\ 0.5173 & 6.6093 & 0.0053 & -0.7034 \end{bmatrix}$$

* The dimensions are in ft/sec and rad.

Lateral-Directional Decoupling Control Law at the Landing Condition

$$K_\delta = \begin{bmatrix} 0.9520 & 0.2314 & -0.003 \\ -0.1177 & 0.9022 & 0.0834 \\ 0.0853 & -0.6541 & 0.9339 \end{bmatrix}$$

$$K_p = \begin{bmatrix} 0.0973 & -0.0072 & -0.4393 & 0.7065 \\ 0.5707 & 0.2004 & -1.3609 & -0.8356 \\ 1.6080 & 2.2454 & -15.8092 & 0.7703 \end{bmatrix}$$

With these gain matrices and with the dynamics of the existing servo actuators included, the responses of the aircraft to a step input in attitude controller, airspeed controller, and the flight path controller are shown in Figures 30, 31 and 32, respectively. As shown in these figures, the couplings in the response are relatively small; also, the control surface usage is not excessive. Without including the actuator dynamics, there is no coupling in the response. Similar results were obtained for the lateral-directional case.

3.4 Envelope Limiting System

Among the parameters that define the design flight envelope of the commercial transports, the angle of attack (α) and the load factor (n_z) are perhaps of paramount importance. For both safety and economical reasons, it is important to ensure satisfactory operation of the commercial transport aircraft in high angles of attack flight conditions; for safety because an inadvertent penetration of the aircraft into the stall region may precipitate a departure of the aircraft into dangerous, uncontrollable flight regimes (References 24 - 30) and for economy because the design lift performance limit may be attained. The load factor must be limited to the design value for obvious reasons of structural integrity.

These two major parameters, among others, may be used as feedback signals for designing an active control system to prevent the operation of the aircraft outside its design flight envelope and to achieve a maximum utilization of the design flight envelope.

The unique capability of the TIFS aircraft and the versatility of its variable stability system (VSS), both in the response-feedback mode and the model-following mode of operation, provides an ideal test bed for concept verification as well as generation of valid data for developing the design criteria for envelope limiting systems. Examples of system mechanization on the TIFS aircraft for in-flight investigations on the envelope limiting control systems are discussed in the following.

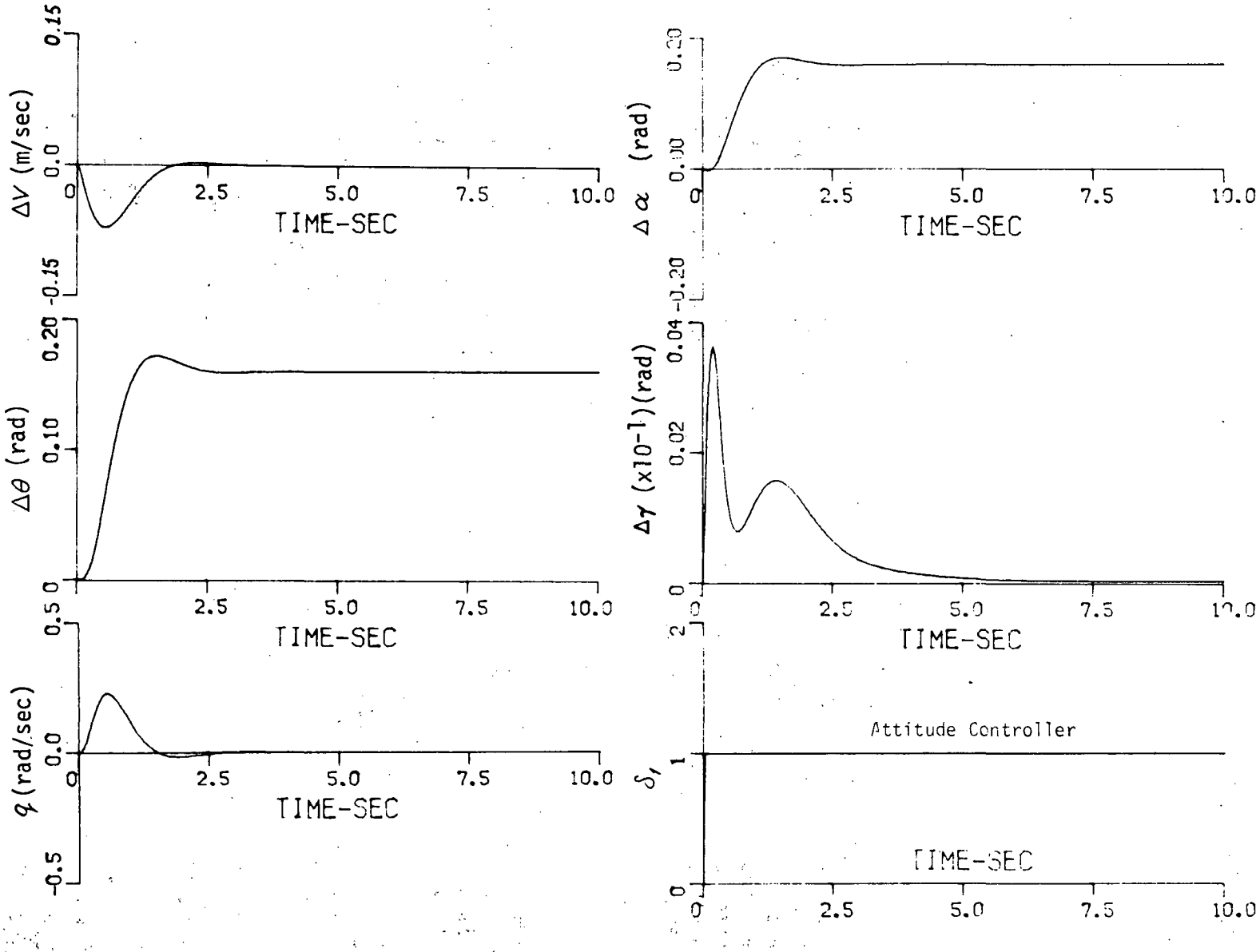

Figure 30 AIRCRAFT RESPONSE TO A STEP INPUT IN ATTITUDE CONTROLLER, ACTUATOR DYNAMICS INCLUDED

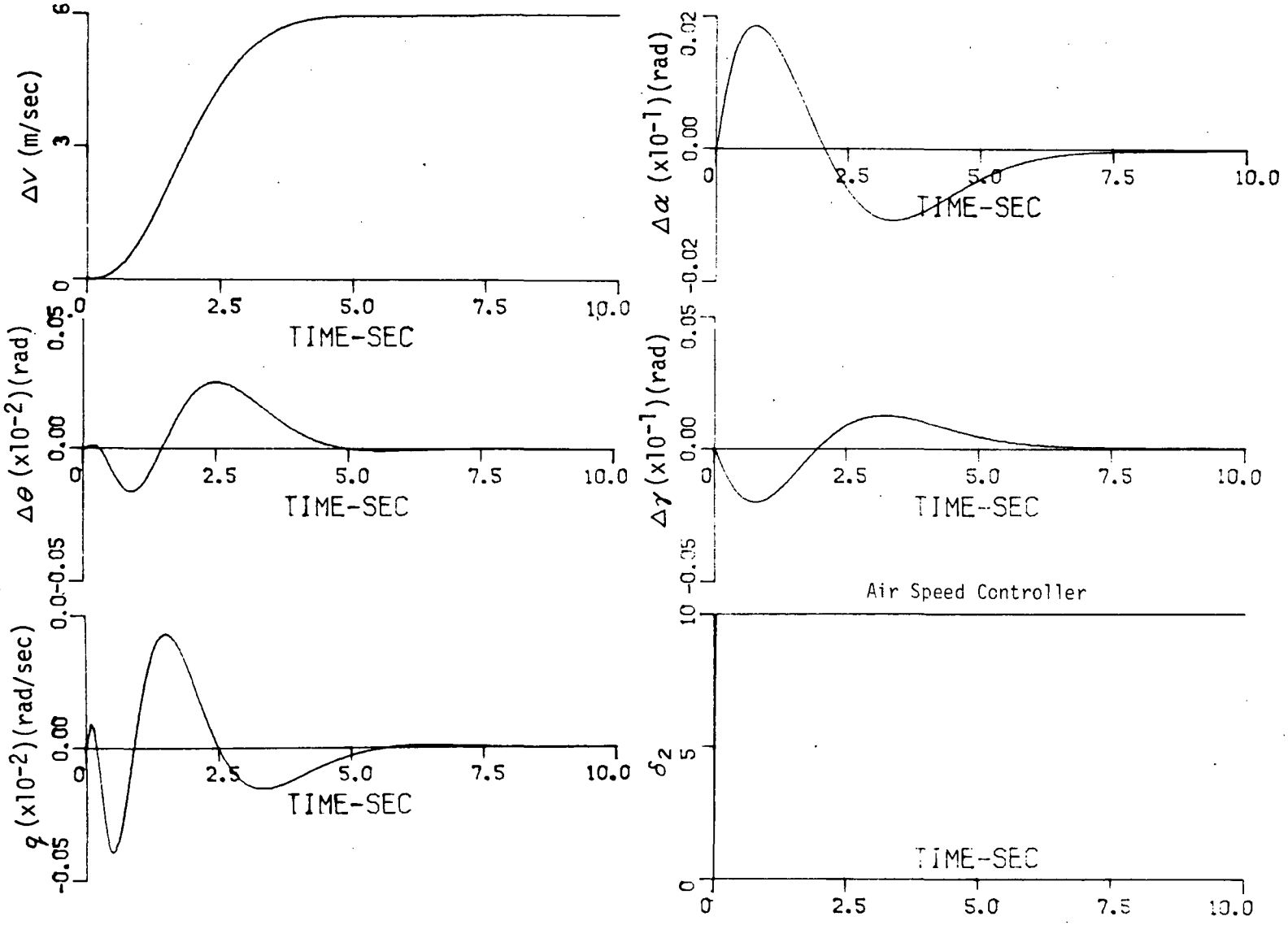

Figure 31 AIRCRAFT RESPONSE TO A STEP INPUT IN AIRSPEED CONTROLLER, ACTUATOR DYNAMICS INCLUDED

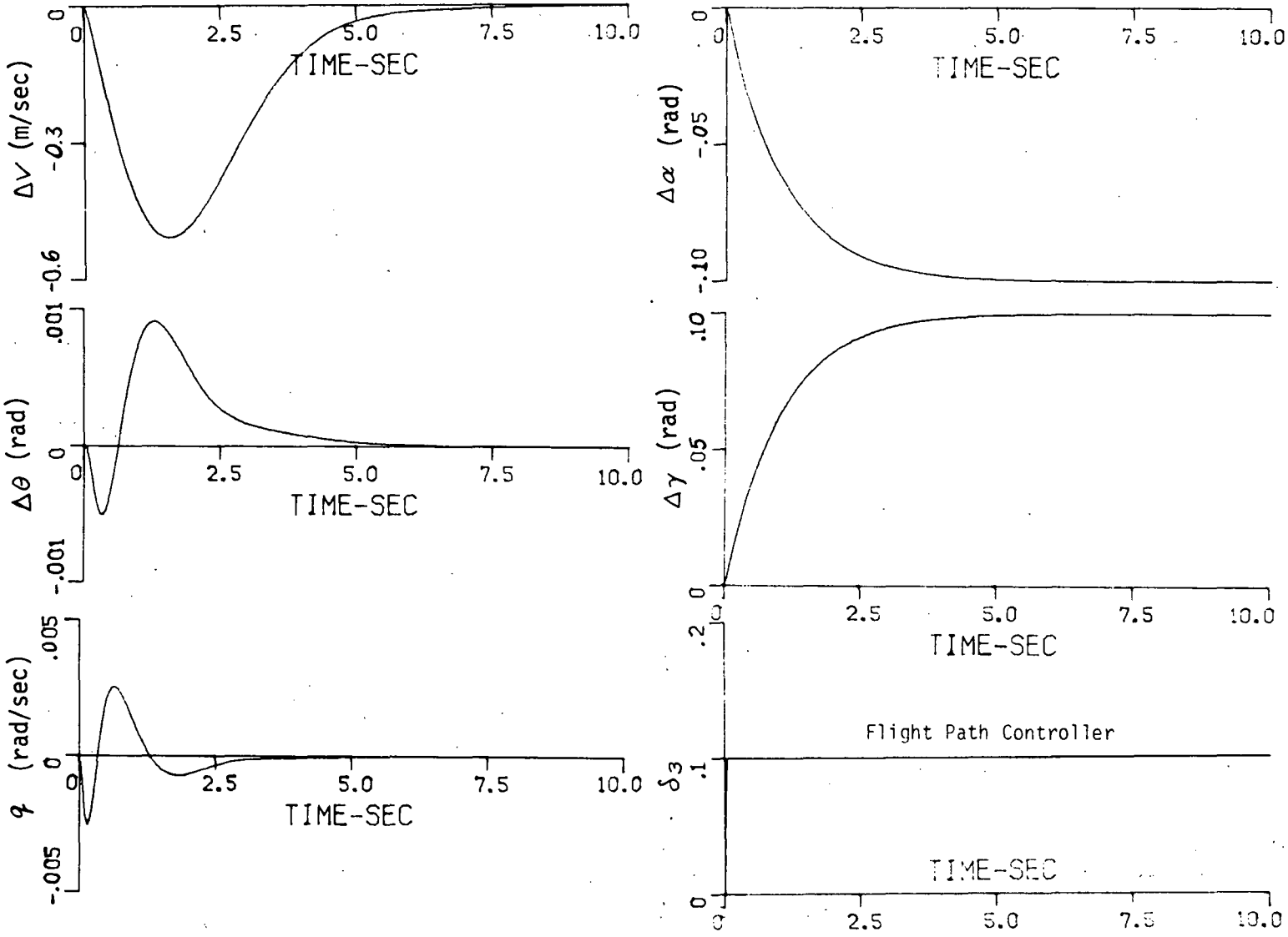

Figure 32 AIRCRAFT RESPONSE TO A STEP INPUT IN THE FLIGHT PATH CONTROLLER, ACTUATOR DYNAMICS INCLUDED

Angle of Attack Limiter

The factors that influence the stall-departure characteristics of the aircraft are many and complex. Some stall/departure characteristics may, however, be classified as being precipitated by the longitudinal problems such as pitch up, "deep stall" or lateral-directional problems such as wing rock/"nose slice" (or directional instability). Provided that the control surface remains effective in the stall region, experience has shown that it is possible to design an automatic departure prevention system to help attain the design lift performance limit of the aircraft and to ensure that in an inadvertent penetration of the aircraft into the stall region, departures into dangerous flight conditions may automatically be prevented.

Figure 33 shows an example of an α limiter that can readily be mechanized on the TIFS aircraft using its existing VSS. As shown in this figure, the α limiter is mechanized to interface with the SCAS for augmenting the relaxed longitudinal static stability. The feedback gain for the normal acceleration at the pilot station is phased out at a preselected angle of attack to prevent a rapid excursion in α at the high α conditions where $C_{L_{max}}$ is approached. At the same time, the feedback gain for the angle of attack is introduced to provide the necessary augmentation for the relaxed static stability. A nonlinear gain may be programmed to limit the α excursion by providing a high gain feedback of α beyond the preselected angle of attack.

Using the TIFS aircraft, in-flight investigation may also be made for aircraft whose stall/departure problems are of lateral-directional origin. For these aircraft, elimination of the sideslip excursion can be as critical as the reduction in the angle of attack (Reference 24). In this case, α_c in Figure 33 may be scheduled as a function of β as well as $\dot{\alpha}$. To limit the sideslip excursion, the SCAS for augmenting the relaxed directional stability may be programmed as a function of both α and β (Reference 24). To further reduce the sideslip excitation due to roll maneuver at high α regimes, the gain of the aileron to rudder crossfeed may be used and properly scheduled as a function of α .

Load Factor Limiter

Several schemes may be used to limit the load factor of the aircraft (References 31 and 32). Figure 34 shows an example of achieving the load factor limitation by limiting the pilot's command on the normal load factor. Verification of this concept as well as many others may readily be implemented on the TIFS airplane using its VSS.

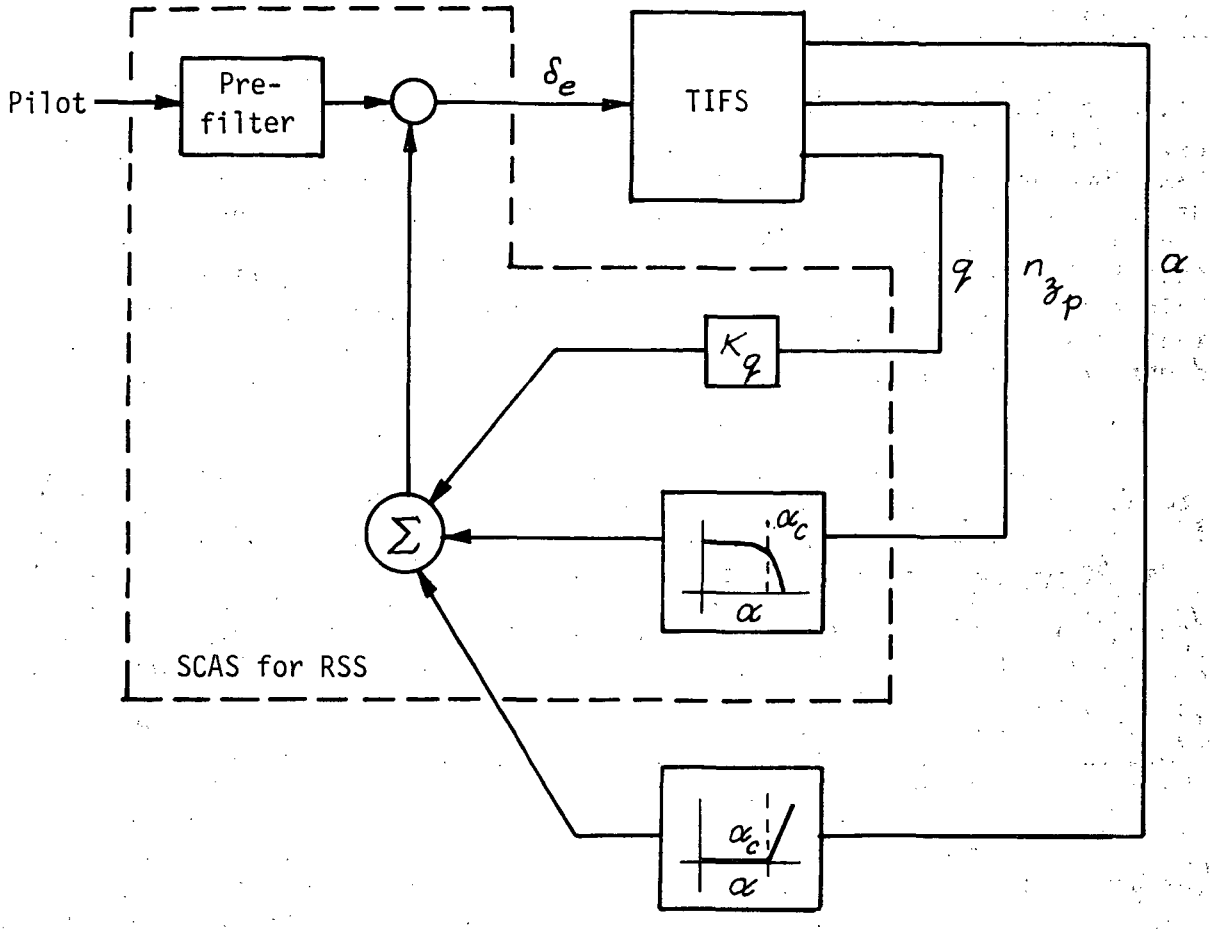

Figure 33 α LIMITER MECHANIZATION ON THE TIFS

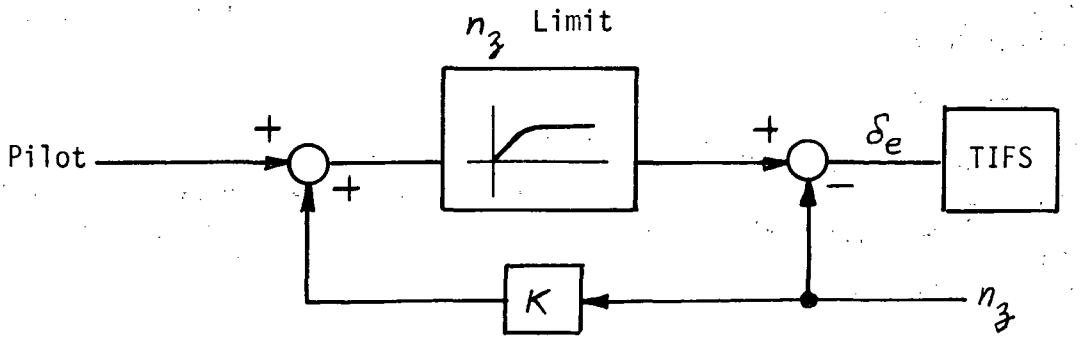

Figure 34 LOAD FACTOR LIMITER WHICH LIMITS THE PILOT COMMAND

3.5 Augmentation of Relaxed Stability

The potential benefits of relaxing the inherent static stability of the aircraft have been studied extensively in the past (References 2, 33,34). These system studies have indicated that the major potential benefits are the reduction in the tail size (and hence weight) and the trim drag, thus tending to improve the aircraft performance.

By relaxing the inherent static stability, the criteria for sizing the tail will now be based solely on the control requirements. Many control-oriented questions must be considered:

(i) Does the tail provide adequate control power for trim and for the maneuver?

(ii) Does the full time stability and control augmentation system (SCAS) saturate its control authority? What is the effect of inherent instability on the augmentation control power requirements? What is the effect of structural modes?

(iii) How reliable is the SCAS?

These questions must be adequately answered and design criteria quantitatively defined in order to fully assess the benefits that the previous system studies have indicated. Figure 35 summarizes the general trend and the trade-off parameters considered for sizing the tail in the previous studies (References 2, 33 and 34).

The TIFS aircraft can be used to verify the RSS concept in flight and to gather data for the development of design criteria. These can be accomplished by both direct and indirect ways. Indirectly, the variable stability system (VSS) of the TIFS aircraft can be used to simulate RSS conditions. Figure 36 shows an example of simulating various types of transport aircraft with RSS, with and without SCAS, using the existing VSS of the TIFS aircraft. Two modes of simulation, the model-following mode and the response-feedback mode as shown in the figure can be used in the existing VSS of the TIFS. Experience gained at Calspan indicates that much more flight time is required with the response feedback mode of simulation than the model-following mode for such necessary but unproductive purposes as in-flight calibration of the simulated aircraft. Therefore, the model-following mode of simulation is more economical in terms of data and results gathered per dollar spent on a flight program.

For direct in-flight verification of the RSS concept and gathering data for the design criteria development, limited changes in c.g. position of the TIFS can be used. Sample calculations were made using the TIFS data in Reference 3 to determine the amount of c.g. shift (and corresponding

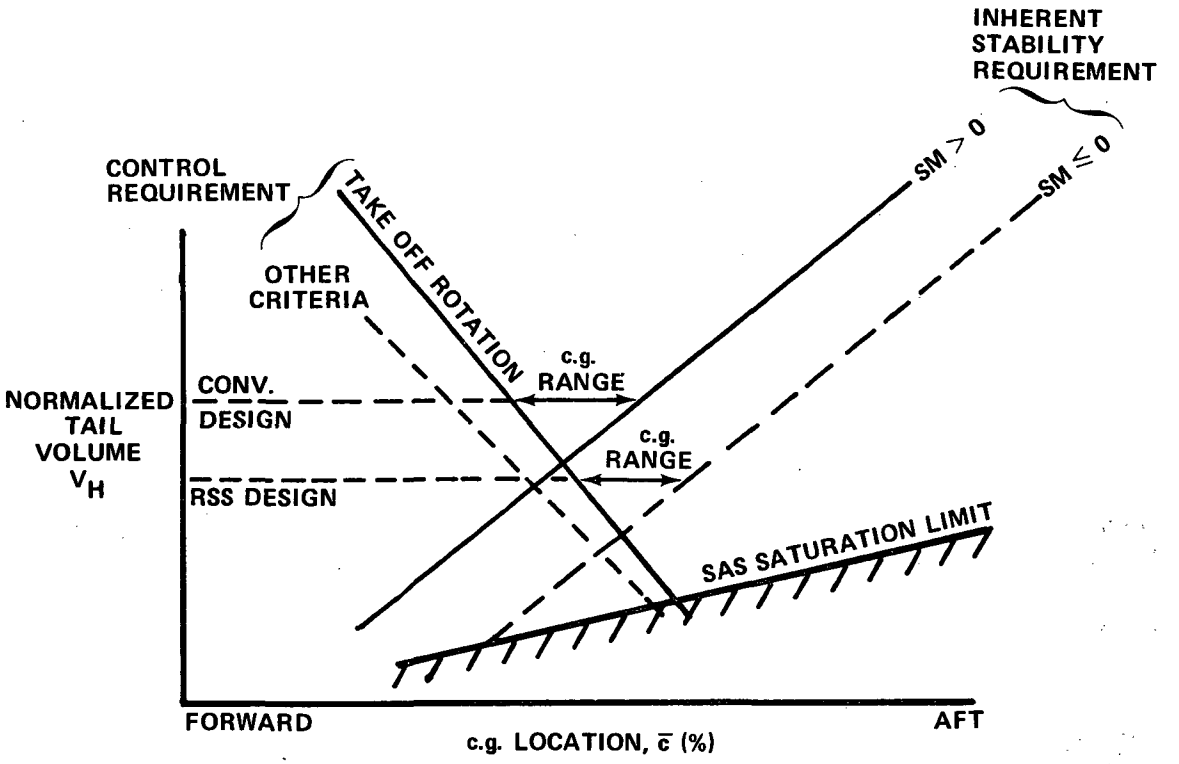

Figure 35 HORIZONTAL TAIL SIZING FACTORS

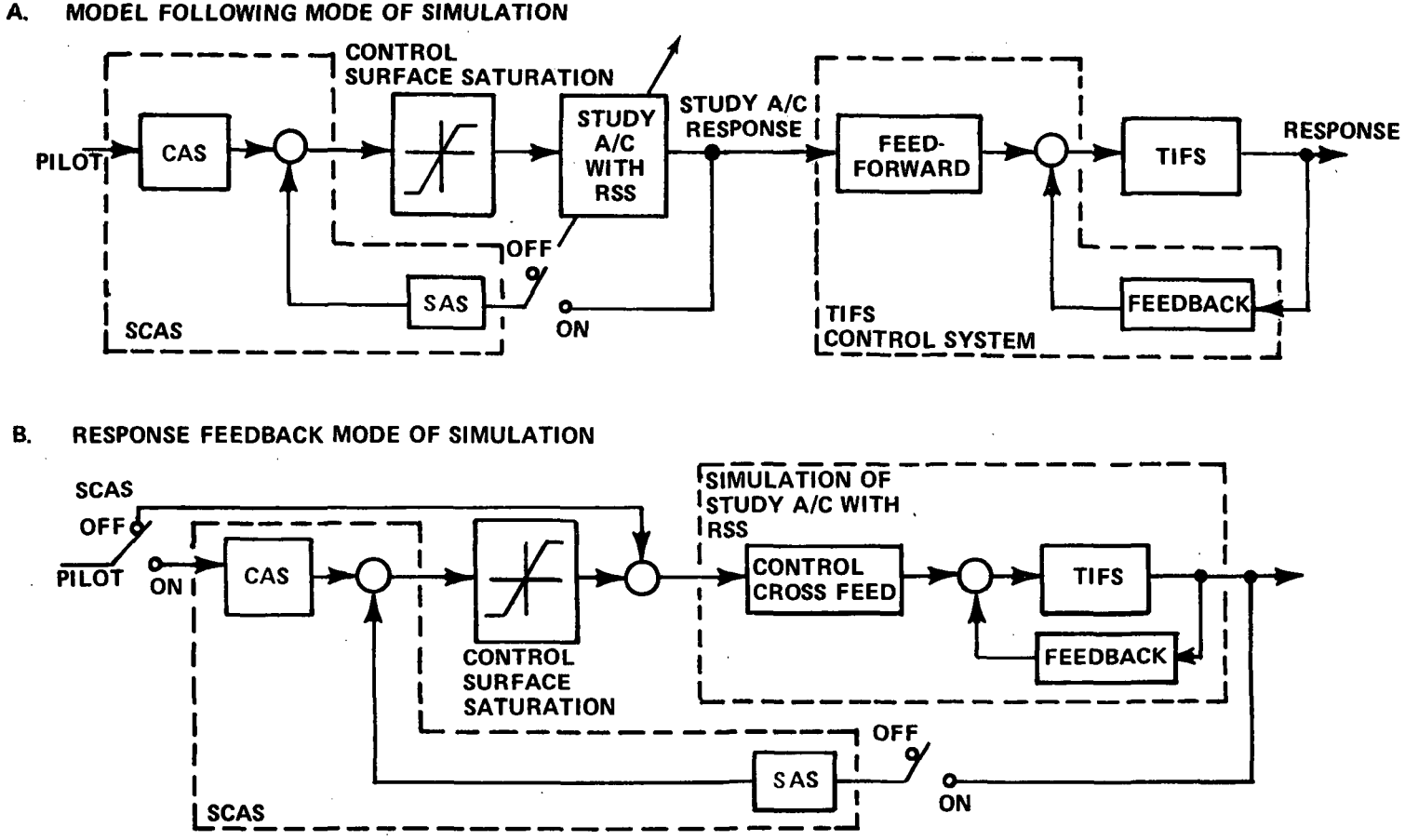

Figure 36 EXAMPLE OF TIFS MODES OF SIMULATION OF AIRCRAFT WITH RSS TO EVALUATE SAS SATURATION AND OTHER EFFECTS

ballast) that would be necessary to obtain zero static margin or maneuver margin on TIFS. At a cruise flight condition of 250 KIAS at 3048 m (10,000 ft), a c.g. shift of 0.21 m would be needed from the nominal c.g. position of 0.266 $\bar{c}$ to obtain zero static margin and 0.49 m to obtain a zero maneuver margin. These c.g. shifts would correspond to adding 4626 N (1040 lb) and 10573 N (2377 lb) ballast respectively, in the aft fuselage of the 231307 N (52,000 lb) TIFS.

An alternate method of reducing static stability is to reduce the tail size and thereby shift the neutral and maneuver points forward. To shift the neutral point forward to the nominal c.g. position of .266 $\bar{c}$ for the above flight condition, a 6.3% reduction of tail size would be necessary. To shift the maneuver point forward to the c.g., a 14.3% reduction would be needed. This approach has not been examined in sufficient detail at this time to indicate whether this degree of reduction in tail size can be accommodated safely over the complete flight regime, considering problems such as nose wheel lift-off.

The design goal of the SCAS is, of course, to satisfy the flying qualities requirements. The SCAS design philosophy and technique have been extensively discussed in the past, especially for application to modern high performance military aircraft. Although the preliminary design of the SCAS for the TIFS with relaxed static stability was not performed, a brief discussion will be given here, for sake of completeness, on a number of factors that must be considered in the design.

Consider the design of longitudinal SCAS as an example. The immediate problem caused by the relaxation of the static stability by reducing the horizontal tail size is the reduction in control power (or control derivatives) and major changes in several stability derivatives such as M_α and M_q . This implies that the SCAS requires use of multiple sensor and high gain feedback with limited control authority. With the structural weight saving as being one of the major benefits of the ACT functions, the airframe will tend to be more flexible. As a result, the low frequency structural modes must be considered to determine the limits of gains that the SCAS can use. Also, considerations must be given to the impact of the low frequency structural modes, in addition to the stabilization capability, reliability, complexity, and benefits to other ACT functions, in the selection of sensor type and location for use in the SCAS.

3.6 Maneuver Load Control (MLC)

The primary objective of MLC in transport type aircraft is to redistribute the lift generated in maneuvers to reduce the wing bending moment. The capability of the TIFS aircraft for verification of the MLC concept was assessed with and without modifications of its wing control surfaces. Some considerations for MLC system design have also been given.

3.6.1 Potential Benefits of the TIFS with MLC

The concept of shifting the maneuver load inboard can be accomplished with the existing direct lift flaps of the TIFS; however, the benefit would be small. Significant benefits may be obtained, though, if modifications are made on the ailerons to act collectively and the Fowler flaps to act as an inboard plain flap.

Calculations have been made using Reference 3 (see Appendix C) to obtain the lift effectiveness and lift distribution of the various possible MLC concepts using the TIFS airplane.

- DLF alone
- DLF with Collective Ailerons
- Inboard Plain Flap
- Inboard Plain Flap with Collective Aileron
- Inboard Plain Flap, DLF and Collective Aileron

Figure 37 and Table 5 summarize the results. It can be seen that the inboard flap with collective ailerons yields the greatest shift in the lift center from η =.44 to η =.29 with η being the normalized wing station. However, the maximum incremental maneuver capability is only .32 g. The use of all three controllers would shift the lift center from η = .44 to η =.33 with an incremental maneuver capability of 1.12 g. This latter concept appears to be the most beneficial system to investigate but does involve major modifications to the TIFS. However, just modifying the ailerons to act collectively would greatly increase the capability of TIFS to investigate MLC.

3.6.2 MLC System Design Considerations

The preliminary design of the MLC system for the TIFS must consider the following factors:

- Selection of system configuration to achieve the major functional objective of the MLC.
- Proper interface with other ACT systems
  - (i) compatibility with RSS (effect on flying qualities and control power)
  - (ii) compatibility with other ACT functions, such as gust alleviation and flutter control.

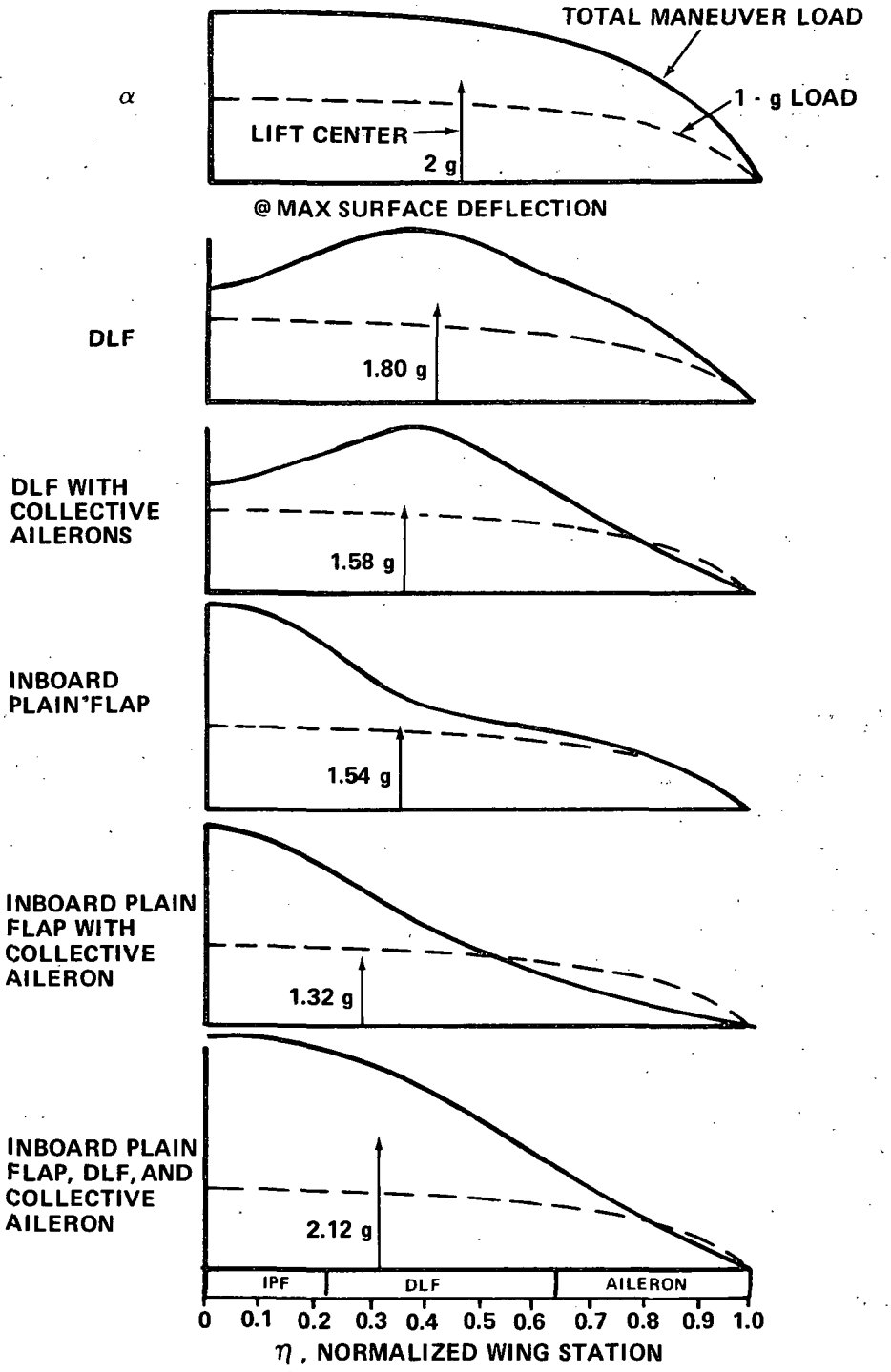

Figure 37 WING LOADING DISTRIBUTIONS(ESTIMATED)
@ V_1 = 178 KIAS; W = 222,411 N (50,000 lb)

TABLE 5

TIFS MANEUVER LOAD CAPABILITIES

Maneuvering Mechanism	Maximum Wing Load (due to max surface deflection) and Lift Center (Normalized Wing Station)	Maximum WRBM as % of WRBM due to α alone at max maneuver load
(Basic TIFS)	one-g load 1 g @ η = .44 max maneuver 1 g @ η = .44 total load 2 g @ η = .44	100% at 2 g
DLF	one-g load 1 g @ η = .44 max maneuver .8g @ η = .41 total load 1.8 g @ η = .427	97% at 1.8 g
DLF & Collective Ailerons	one-g load 1 g @ η = .44 max maneuver .58g @ η = .22 total load 1.58g @ η = .359	82% at 1.58 g
Inboard Plain Flaps	one-g load 1 g @ η = .44 max manuever .54g @ η = .18 total load 1.54g @ η = .35	79% at 1.54 g
Inboard Plain Flaps & Collective Ailerons	one-g load 1 g @ η = .44 max maneuver .32g @ η =-.17 total load 1.32g @ η = .29	66% at 1.32 g
Inboard Plain Flaps DLF and Collective Ailerons	one-g load 1 g @ η = .44 max maneuver 1.12 g @ η = .24 total load 2.12 g @ η = .33	76% at 2.12 g

Figure 38 shows some MLC system configurations which can be mechanized on the TIFS aircraft. These MLC system configurations range from a conventional open-loop mechanization by properly scheduling the control crossfeed (Reference 36) to a closed-loop mechanization using quadratic synthesis techniques. The use of quadratic synthesis techniques has been studied previously by Calspan for the UASF using the variable stability T-33 aircraft (Reference 35). The system synthesis procedure employed a quadratic performance index of the form.

$$2J = \min_{u} \int_{o}^{\infty} \left[\left\| \dot{x} - Lx \right\|_{Q}^{2} + \left\| \Delta D \right\|_{V}^{2} + \left\| \Delta WRBM \right\|_{T}^{2} + \left\| u \right\|_{R}^{2} \right] dt \qquad (30)$$

for solving the control law $u = -Kx$, subject to the constraint of the equations of motion of the TIFS

$$\dot{x} = Fx + Gu \qquad (31)$$

where L = matrix of dimensional stability derivative of a "good" flying qualities model

$\Delta D = Ex + Hu$ = linearized expression for the change in drag

$\Delta WRBM = Mx + Nu$ = linearized expression for the change in wing root bending moment

u = control deflections

x = state vector of the airplane $x^{T} = \left[\Delta V, \Delta\theta, q, \Delta\alpha \right]$

Q, V, T, R = weighting matrices

Because of both time and fund limitations, the preliminary design was not carried out. Since the techniques for designing the MLC system are in existence for interface with the RSS (References 35 and 36), future emphasis should be placed on the interface and compatibility with other ACT systems such as GA and FC.

(i) Open Loop Mechanization - Control Crossfeed Scheduling

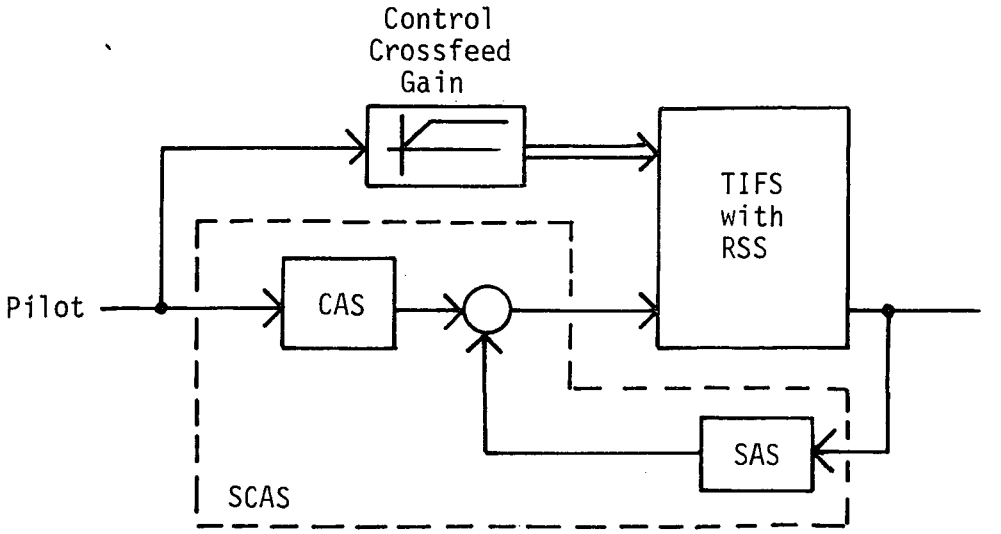

(ii) Closed-loop Mechanization

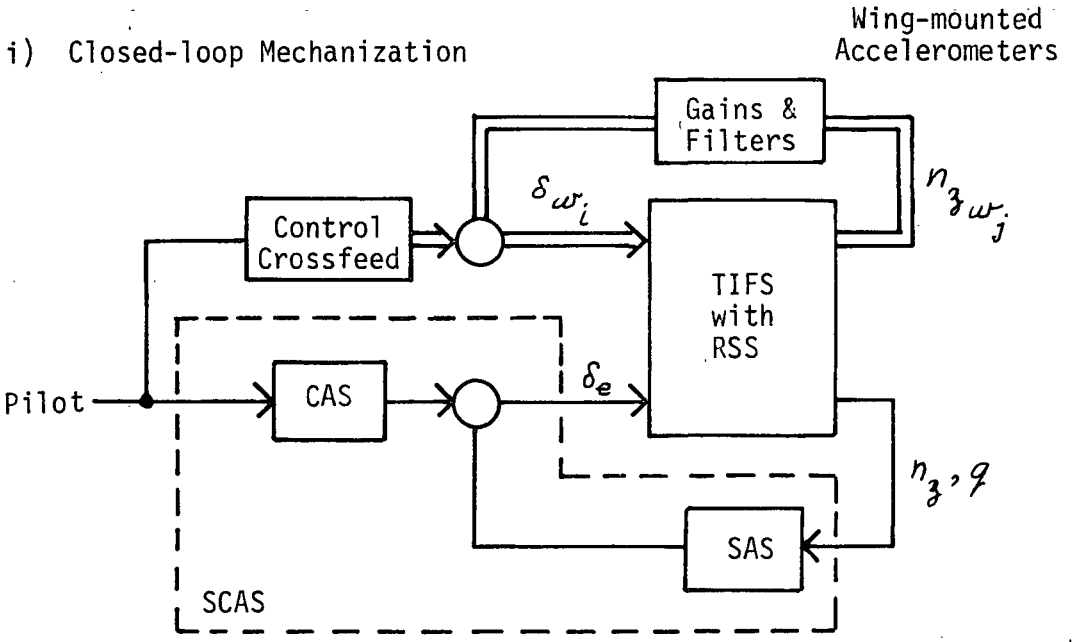

(iii) Closed-loop Mechanization Using Quadratic Synthesis Technique

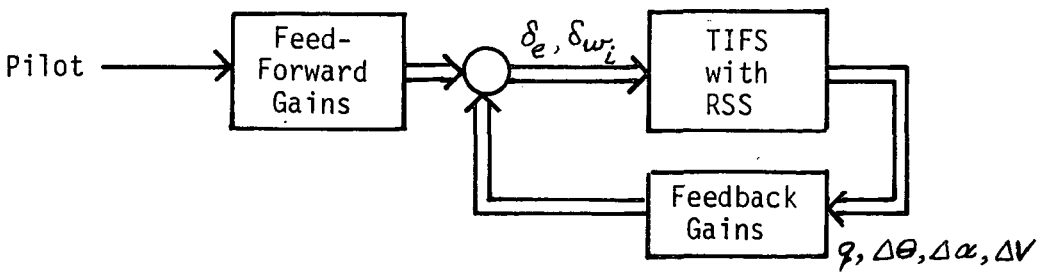

Figure 38 MLC SYSTEM CONFIGURATIONS WHICH CAN BE MECHANIZED ON THE TIFS AIRCRAFT

4. DEVELOPMENT OF FLEXIBLE EQUATIONS OF MOTION

The equations of motion of the rigid TIFS airplane were an early requirement in the TIFS control system design. Although structural properties were of concern in TIFS design from both the point of view of flutter and realizable control system gains, no attempt had been made before this program, at Calspan, to define the differential equations of even the lower order structural modes.

In order to develop the equations of motion in an expedient manner, a search of existing structural data at Calspan was performed. The existing data were of the form of uncoupled wing, tail and fuselage bending modes, and are described more fully in the section concerning flutter (Section 3.2). To produce the desired normal mode description of the TIFS, these uncoupled modes were coupled and the resulting modes were orthogonalized using modal transformation. Aerodynamic coupling of the normal structural modes is described in the following section.

4.1 Aerodynamic Coupling of Symmetric Normal Structural Modes

The symmetric flexible equations of motion of the TIFS vehicle were computed using a normal mode representation of the structural dynamics. The basic equations of motion are of the following form.

$$\left\{\left[M\right]s^2 + \left[K\right]\right\}\left[\xi\right] = \left[F\right] + \left[G\right]\left[u\right] \tag{32}$$

where $\left[M\right]$ is a diagonal matrix of generalized masses of the normal modes $\left[N \times N\right]$.

$\left[K\right]$ is a diagonal matrix of generalized stiffness for the normal modes $\left[N \times N\right]$.

$\left[F\right]$ represents, in generalized coordinates, the aerodynamic forces and moments per unit deflection of the normal mode coordinates. This matrix is a function of ξ and higher derivatives of ξ $\left[N \times 1\right]$.

$\left[G\right]$ represents, in generalized coordinates, the aerodynamic forcing terms due to deflection of control surfaces and atmospheric turbulence $\left[N \times L\right]$.

$[\xi]$ is a column of generalized coordinates $[N \times 1]$

$[u]$ the external forcing terms such as control surface deflections or atmospheric turbulence $[L \times 1]$

N the number of normal modes

L the number of control surfaces

A thorough derivation of these equations can be found in Reference 38 which also forms the basis of the development to follow.

For the symmetrical degrees of freedom of the TIFS, the generalized coordinates were defined as follows:

ξ_1 h rigid body translation (meter or feet)
ξ_2 θ rigid body rotation, (radian)
ξ_3 deflection of the second fuselage bending mode, 2FB (meter or feet)
ξ_4 deflection of the second wing bending mode, 2 WB, (meter or feet)
ξ_5 deflection of the first wing bending mode, 1WB, (meter or feet)
ξ_6 deflection of the first fuselage bending mode, 1FB (meter or feet)
ξ_7 angular rotation of the first wing torsion mode, 1WT, (radians)
ξ_8 deflection of the first horizontal tail bending mode, 1HTB, (meter or feet)

Sign conventions for all coordinates involving deflections (i.e., those units of meter or feet) are positive down and for all coordinates involving rotations (i.e., units of radians) are positive nose up.

Matrices $[M]$ and $[K]$ are properties of the mormal modes in vacuo and were computed as described above. Note that

$$[M]^{-1}[K] = [\omega^2] \tag{33}$$

where $[\omega^2]$ is the diagonal matrix of structural mode natural frequencies in vacuo.

The identification of the structural modes above as 1WB, 1FB, etc. describe the primary motion of the mode. In general, any normal structural mode includes some bending of the wing fuselage and tail as well as torsion of wing and tail.

Matrices F and G describe the aerodynamic forcing terms in the equations of motion and were computed using the aerodynamic strip theory. This technique involves dividing the aircraft into small aerodynamic lifting surfaces or strips and describing the forces and moments on the strips by average stability derivatives across the strip. The angle of attack and pitch rate of

each strip can be obtained by combining the structural deflection of each mode in an appropriate manner. The forces and moments of each strip can then be determined and appropriately summed to determine the generalized forces affecting each mode.

The assumptions and simplifications employed in this strip theory are listed below

- Unsteady aerodynamics, wing bending in the x-y plane, and interference between strips were neglected.
- The center of pressure for each strip was assumed to be fixed at the local quarter chord of the strip.
- Modal truncation was employed to include structural modes with natural frequencies in the range of 1 to 100 radians per second.
- Angle of attack change due to atmospheric turbulence was constant across the entire vehicle.
- The TIFS fuselage was divided into 67 strips of approximately 1 meter (40 inches) in width (32 in wing, 12 in tail, 23 in fuselage). Only one half of the wing and tail strips were actually utilized due to the symmetry of the vehicle.
- Downwash including downwash lag ($\dot{\alpha}$) effects on the tail were included.
- The angle of attack of the wing and tail strips was assumed to be the angle of attack at the local 3/4 chord of the strip in accordance with theoretical aerodynamics, Reference 39.
- The angle of attack of fuselage strips was the geometric center of the strip viewed from above.

For simplicity, the forces on the various strips were calculated at the center of pressure (1/4 chord of wing or tail strips, geometric center for fuselage strips) and were assumed to act in the Z direction.

For the i^{th} strip the Z-force can be written as

$$Z_{1/4_i} = -\frac{\rho u_o^2}{2} S_i C_{L_{\alpha_i}} \alpha_{3/4_i} \tag{34}$$

where $\alpha_{3/4_i}$ is the angle of attack of the 3/4 chord point of strip i (rad)

$C_{L_{\alpha_i}}, S_i$ are the lift curve slope and area of strip i (nondimensional, m^2 or ft^2)

ρ atmospheric density (Kg/m^3 or slug/ft^3)

u_o reference velocity (m/sec or ft/sec)

The angle of attack can be written in terms of pitch angle and translation of each strip as follows (Note h is positive downward)

$$\alpha_{3/4_i} = \theta_{3/4_i} + \frac{\dot{h}_{3/4_i}}{u_o} \tag{35}$$

where $\theta_{3/4_i}$ is the angle at the 3/4 chord of the i^{th} strip (rad)
$\dot{h}_{3/4_i}$ is the rate of change of translation of the i^{th} strip (m/sec or ft/sec)

In general, the pitch angle and translational of each strip will result from motion of each of the generalized coordinates, ξ. For strip i, this relationship can be expressed as

$$\theta_{3/4_i} = \sum_{j=1}^{N} \phi'_{3/4_{ij}} \xi_j \tag{36}$$

$$\dot{h}_{3/4_i} = \sum_{j=1}^{N} \phi_{3/4_{ij}} \dot{\xi}_j \tag{37}$$

$\phi_{3/4}$ is the mode shape matrix which defines the mode shape of each mode at the local 3/4 chord point of each strip. This matrix describes the translation of the 3/4 chord point for unit deflection of the generalized coordinates ($M \times N$)

$\phi'_{3/4}$ is the partial derivative with respect to the x-direction of the mode shapes at the 3/4 chord point. This matrix describes the rotation at the 3/4 chord point for a unit deflection of the generalized coordinates ($M \times N$)

N is the number of generalized coordinates

M is the number of strips

Figure 39a shows sign conventions for mode shapes and slopes and gives insight into the equations above.

In the special case of strips which experience downwash generated by strips elsewhere on the aircraft, the expressions for $\alpha_{3/4_i}$ must be modified. Such is the case for tail surfaces located in the downwash field of the wing. Figure 39b describes the physical situation. The angle of attack at the tail is reduced by an angle ϵ, the downwash

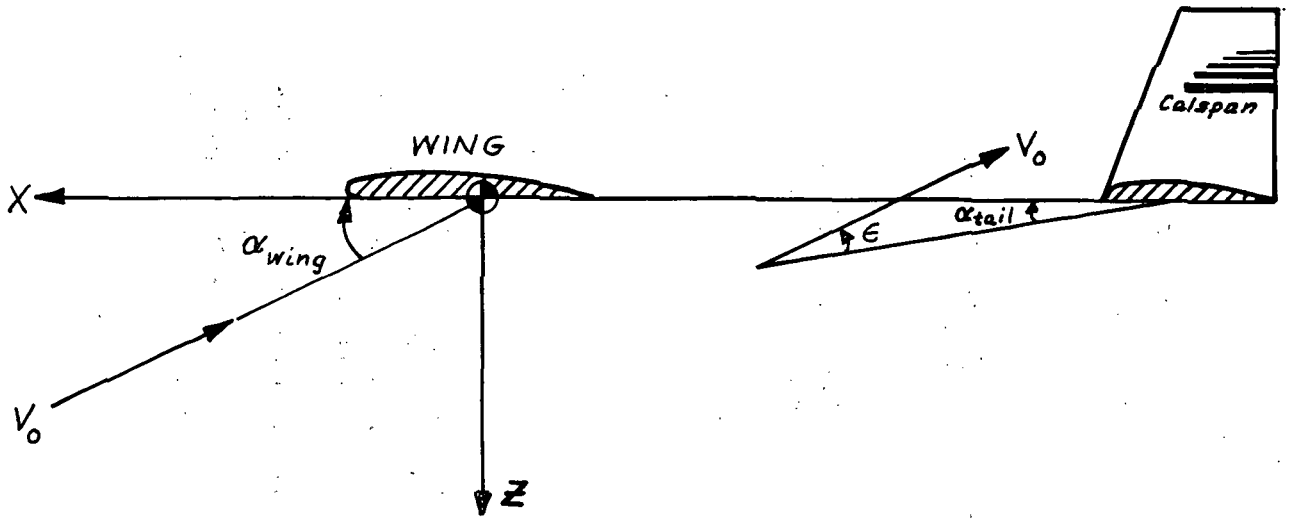

Figure 39b Downwash Effects

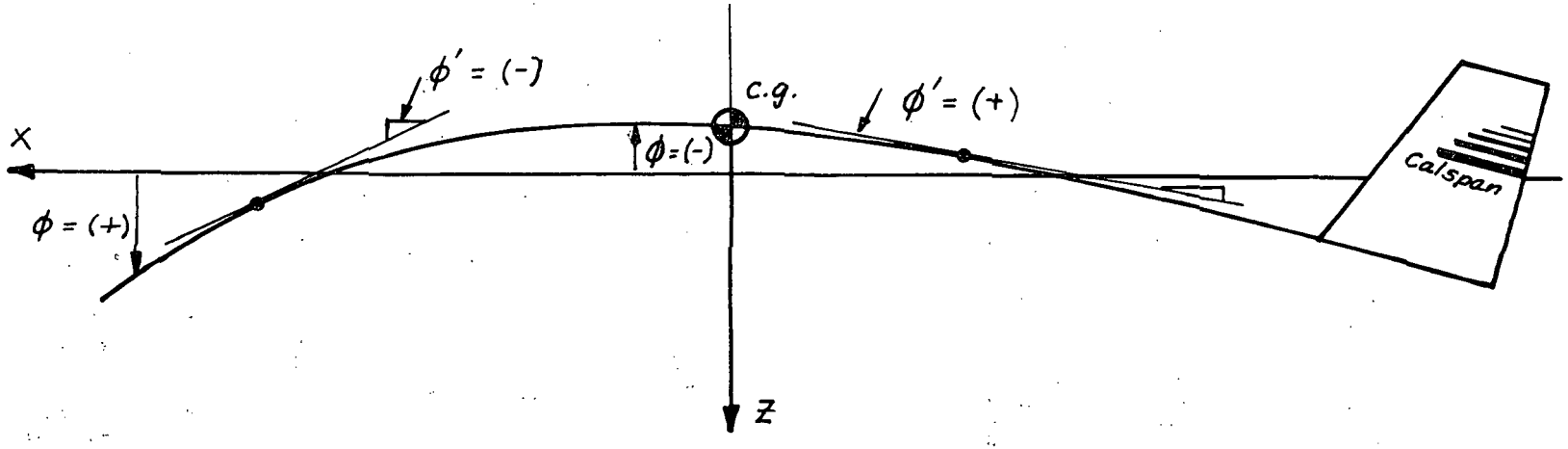

Figure 39a Mode Shape Sign Convention

angle. The downwash angle can be written as a function of the wing angle of attack as follows (Reference 40).

$$\epsilon = \frac{d\epsilon}{d\alpha}\left(\alpha_w - \frac{\ell_d}{u_o}\,\dot{\alpha}_w\right) \tag{38}$$

where α_w is the angle of attack of the wing(rad)

ℓ_d is the distance from the center of pressure of the wing to the center of pressure of the tail (meter or feet)

$d\epsilon/d\alpha$ is the steady state change in downwash angle per unit change in α_w (nondimensional)

The second term in the above expression results because a finite time is required for the downwash disturbance to travel from the wing to the tail ($\Delta t = \ell_d/u_o$). For the case where the wing is flexible, there is no single angle of attack of the wing but for this study the angle of attack of the inner-most wing strip was assumed to generate the downwash.

If strip p of the tail experiences downwash generated by strip q of the wing, then the angle of attack on strip p is given by

$$\hat{\alpha}_p = \alpha_p - \frac{d\epsilon}{d\alpha}\,\alpha_q + \frac{d\epsilon}{d\alpha}\,\frac{\ell_d}{u_o}\,\dot{\alpha}_q \tag{39}$$

Expresssing this in terms of the generalized coordinates yields

$$\hat{\alpha}_p = \sum_{j=1}^{N} \phi'_{\substack{3/4 \\ pj}}\,\xi_j + \frac{1}{u_o}\sum_{j=1}^{N} \phi_{\substack{3/4 \\ pj}}\,\xi_j$$

$$- \frac{d\epsilon}{d\alpha}\left[\sum_{j=1}^{N} \phi'_{\substack{3/4 \\ qj}}\,\xi_j + \frac{1}{u_o}\sum_{j=1}^{N} \phi_{\substack{3/4 \\ qj}}\,\xi_j\right]$$

$$+ \frac{d\epsilon}{d\alpha}\,\frac{\ell_d}{u_o}\left[\sum_{j=1}^{N} \phi'_{\substack{3/4 \\ qj}}\,\dot{\xi}_j + \frac{1}{u_o}\sum_{j=1}^{N} \phi_{\substack{3/4 \\ qj}}\,\ddot{\xi}_j\right] \tag{40}$$

The only moment (pure) considered resulted from pitching velocity. For the i^{th} strip this is given by

$$M_i = \frac{\rho u_o}{4} S_i C_i^2 C_{m_{q_i}} \dot{\theta}_i \tag{41}$$

where C_i is the local mean aerodynamic chord of the i^{th} strip (meter or feet)
C_{m_q} is the nondimensional coefficient describing the variation of pitching moment with pitch rate

Once again, downwash of the wing (section q) on the tail (section p) will modify this as follows

$$M_p = \frac{\rho u_o}{4} S_p C_p^2 C_{m_q} \left(\dot{\theta}_p - \dot{\epsilon}_q\right) \tag{42}$$

where ϵ_q is the downwash off the q^{th} wing surface.

The forces, Z, and moments, M, represent the entire aerodynamic properties of the vehicle. A second transformation (Reference 38) is required to describe the influences of each of these elements into the equations of motion of the generalized coordinates. Let Z be an $M \times 1$ vector of generalized forces and M be an $M \times 1$ vector of moments on each of the M strips. Then aerodynamic matrix, F, for the generalized coordinates is given by

$$F = \overset{N \times 1}{\left[\phi_{1/4}^T\right.} \vdots \overset{N \times M}{\left.\phi_{1/4}'^T\right]} \overset{N \times M}{\begin{bmatrix} Z \\ \hline M \end{bmatrix}} \begin{matrix} M \times 1 \\ M \times 1 \end{matrix} \tag{43}$$

where the subscript T denotes matrix transpose
$\phi_{1/4}$ is the matrix of mode shapes at the 1/4 chord point
$\phi'_{1/4}$ is the matrix of slopes of mode shapes at the 1/4 chord point

Insight into the reason for this transformation can be gained with some additional explanation of the nature of the mode shape matrices. Figure 40 shows mode shapes and slopes of mode shapes for an idealized missile with translation, rotation and symmetric fuselage bending modes. For the translation mode the mode shape indicates that the translation degree of freedom departs equal translation to the entire aircraft and the slope of the mode shape indicates this mode contributes no rotation. For the rigid rotation degree of freedom the mode shape indicates that the translation of any point on the fuselage is proportional to the distance from the point of rotation (c.g. in this case) and the slope of the mode shape indicates that an equal rotation angle is imparted everywhere. For the fuselage bending mode the translation and rotation are nonlinear functions of fuselage station.

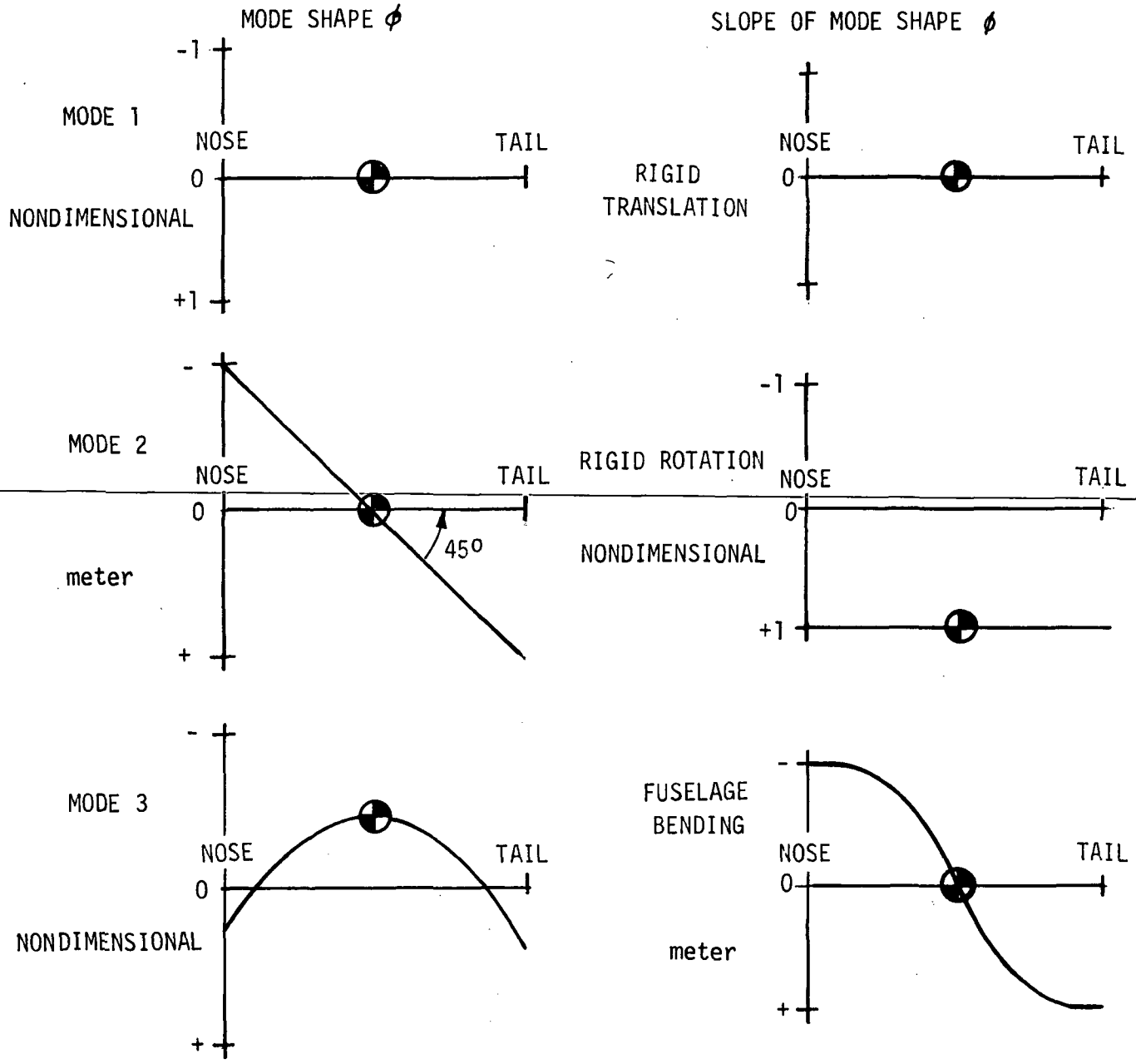

Figure 40 Mode Shapes and Slopes for Idealized Missile

The first element of the F matrix (corresponding to the translation mode) will consist of the following

$$F_1 = \sum_{i=1}^{M} \phi_{\substack{1/4 \\ i1}} Z_i + \sum_{i=1}^{M} \phi'_{i1} M = \sum_{i=1}^{M} Z_i \tag{44}$$

or, for translation, the generalized force is the sum over the entire aircraft of all the forces.

For the rotation degree of freedom

$$F_2 = \sum_{i=1}^{M} \phi_{\substack{1/4 \\ i2}} Z_i + \sum_{i=1}^{M} \phi'_{i2} M_i = \sum_{i=1}^{M} \ell_i Z_i + \sum_{i=1}^{M} M_i \tag{45}$$

where ℓ_i is the distance of the 1/4 chord point of the strip to the cg (positive aft)

For this mode the generalized force is the sum of all the distributed forces times their moment arm plus the sum of all moments due to pitching velocity.

For the bending mode the physical significance is less obvious. However, forces located at nodes of mode shapes contribute nothing to the generalized force while those located at antinodes will add to the generalized force.

The matrix F is a linear function of ξ, $\dot{\xi}$ and $\ddot{\xi}$ through the forces and moments Z and M which can be represented in the following way

$$\underset{(N\times 1)}{F} = \underset{(N\times N)(N\times 1)}{F_0 \xi} + \underset{(N\times N)(N\times 1)}{F_1 \dot{\xi}} + \underset{(N\times N)(N\times 1)}{F_2 \ddot{\xi}} \tag{46}$$

The functions F_0, F_1, and F_2 are described fully in Appendix D.

The control matrix G is evaluated in the following way

$$\left[G\right] = \left[\phi_c\right]^T \left[Q\right] \tag{47}$$

where $\left[Q\right]$ is a diagonal matrix whose elements are the Z force per unit deflection of each control surface ($L \times L$).

$$Q_i = \frac{-\rho u_0}{2} S_{\delta_i} C_{L_{\delta_i}} \tag{48}$$

S_{δ_i} is the reference area associated with the i^{th} control

$C_{L_{\delta_i}}$ is the lift force effectiveness of the i^{th} control

ϕ_c is the mode shape matrix for the N modes and L controllers ($L \times N$) and describes the mode shape of each mode averaged over each controller location

For the elevator control surface, δ_e , and assuming two modes of motion the G matrix would take the following form

$$[G] = \begin{bmatrix} g_1 \\ g_2 \end{bmatrix} = \begin{bmatrix} \phi_{\delta_e 1} \\ \phi_{\delta_e 2} \end{bmatrix} \left(-\frac{\rho u_o}{2} S_{\delta_e} C_{L_{\delta_e}} \right)$$

The generalized input of the elevator into the mode i equation would be $g_i = \left(-\frac{\rho u_o}{2} S_{\delta_e} C_{L_{\delta_e}}\right)$ where $\phi_{\delta_e i}$ is the mode shape of the i^{th} mode at the elevator location. For atmospheric turbulence, the corresponding column(s) of G are computed from the matrices F_o , F_1 , and F_2 .

The equations of motion can now be written in Laplace transform form as

$$\left\{ M s^2 + K \right\} \xi = F_o \xi + F_1 s \xi + F_2 s^2 \xi + G u \qquad (49)$$

where s is the Laplace operator

Multiplying through by M^{-1} yields

$$\left\{ s^2 I + M^{-1} K \right\} \xi = M^{-1} F_o \xi + M^{-1} F_1 s \xi + M^{-1} F_2 s^2 \xi + M^{-1} G u \qquad (50)$$

Note that $M^{-1}K = [\omega^2]$ which is the matrix of structural mode natural frequencies. Solving for $s^2\xi$ yields

$$s^2 \xi = \left[I - M^{-1} F_2 \right]^{-1} \left\{ \left[M^{-1} F_o - [\omega^2] \right] \xi + \left[M^{-1} F_1 - [D] \right] \xi + M^{-1} G u \right\} \qquad (51)$$

The diagonal matrix $[D]$ has been added at this point to include the inherent damping of physical structurals in vacuo.

The equations of motion in this form can be easily implemented on many linear system computer programs. Transformations to first-order form are straightforward and if desired the rigid variables h , θ can be substituted by the more familiar w , θ through the transformation below.

$$\xi = W \xi' \qquad (52)$$

where

$$[\xi']^T = \left[\frac{w}{s}, \theta, \xi_3 \ldots \right]$$

$$W = \begin{bmatrix} 1 & -\frac{u_o}{s} & 0 & \\ 0 & 1 & 0 & 0 \\ 0 & 0 & 1 & \ddots \\ & 0 & & 1 \end{bmatrix}$$

w is the component of velocity (m/sec or ft/sec) in the z direction related to θ and h as follows

$$w = u_o \sin\theta + \dot{h}\cos\theta \cong u_o\theta + \dot{h} \tag{53}$$

The above transformation also allows for the elimination of the variable θ since stability derivatives multiplying θ will be identically zero. The state vector can now be written in the more familiar form

$$\xi^T = [w, q, \xi_3, \xi_4, \cdots, \xi_n] \tag{54}$$

where q is pitch rate (rad/sec).

4.2 Computation of Geometric and Aerodynamic Characteristics for a Flexible Vehicle

In order to compute the flexible equations of motion, the aircraft was divided into 67 strips, 32 in the wing, 12 in the tail and 23 in the fuselage. However, because of symmetry, only one half of the wing and tail surfaces were utilized. To account for this, the generalized masses for each mode of motion and the areas of the fuselage strips were reduced by one half of their respective values for the complete vehicle.

Geometric properties of each strip were computed from three-view drawings of the aircraft and are summarized in Table 6 The C_{m_q} for each strip was estimated at the theoretical value (Reference 38) to be $-\pi/4$ for wing and tail strips and zero for fuselage strips.

The computation for C_{l_α} for the fuselage strips was based on DATCOM Section 4.2.2.1, Reference 37. DATCOM provides a method for computing ΔC_{m_α} due to the fuselage for a rigid aircraft in which the flow across the fuselage is strongly influenced statically by both upwash in front of the wing and downwash behind the wing. The individual contributions of each fuselage strip to ΔC_{m_α} were then related to a strip C_{l_α} by an appropriate nondimensional length. The results are shown in Table 6.

Lift distribution across the wing and tail was computed from DATCOM Section 6.1.5.1. The following TIFS wing data were used in these computations.

$C_{l_{\alpha_w}}$ = 6.65/rad = two dimensional lift curve slope of wing
β = 1 = Mach number parameter = $\sqrt{1 - (\text{Mach No.})^2}$
AR_w = 12 = aspect ratio of the wing
S_w = 280.4 m (920 ft) = wing area
b_w = 23.1 m (105.3 ft) = wing span
λ_w $\cong$ taper ratio = tip chord/root chord

TABLE 6

TIFS STRIP AERODYNAMIC AND GEOMETRIC PROPERTIES

Strip	Location	S m^2	S (ft^2)	c m	c (ft)	C_{L_α} (ND)	C_{m_q} (ND)
1	Wing (Root)	2.07	(22.3)	4.07	(13.35)	5.09	$-\pi/4$
2	Wing	3.98	(42.8)	3.92	(12.85)	5.3	
3		3.76	(40.5)	3.71	(12.18)	5.6	
4		3.56	(38.3)	3.51	(11.5)	5.83	
5		3.35	(3.61)	3.31	(10.85)	5.91	
6		3.17	(34.1)	3.12	(10.25)	5.96	
7		3.02	(32.5)	2.97	(9.75)	5.96	
8		2.83	(30.5)	2.79	(9.15)	6.0	
9		2.66	(28.6)	2.62	(8.58)	6.06	
10		2.50	(26.9)	2.46	(8.08)	5.94	
11		2.34	(25.2)	2.31	(7.58)	5.82	
12		2.16	(23.3)	2.14	(7.01)	5.87	
13		1.99	(21.4)	1.96	(6.42)	5.76	
14		1.83	(19.7)	1.80	(5.92)	5.25	
15		1.65	(17.8)	1.63	(5.34)	4.67	
16	Wing (Tip)	1.77	(19.0)	1.45	(4.75)	2.32	
17	Fuselage (Fwd)	0.197	(2.12)	NR		.206	0
18	Fuselage	0.506	(5.45)			.287	
19		0.557	(6.0)			.344	
20		0.624	(6.72)			.43	
21		0.627	(6.75)			.481	
22		0.627	(6.75)			.544	
23		0.689	(7.42)			.682	
24		0.729	(7.85)			.866	
25		0.729	(7.85)			1.1	
26		0.729	(7.85)			1.49	
27						2.14	
28						8.07	
29						- .046	

TABLE 6 CONT.

TIFS STRIP AERODYNAMIC AND GEOMETRIC PROPERTIES

Strip	Location	S m^2 (ft^2)	c m (ft)	C_{L_α} (ND)	C_{m_q} (ND)
30	Fuselage	0.729 (7.85)	NR	- .097	0
31				- .132	
32				- .155	
33				- .166	
34				- .178	
35		0.697 (7.5)		- .178	
36		0.627 (6.75)		- .166	
37		0.527 (5.675)		- .143	
38		0.402 (5.325)		- .115	
39	Fuselage (Aft)	0.262 (2/825)		- .074	
40	Tail (Root)	2.819 (30.34)	2.78 (9.11)	2.0	$-\pi/4$
41	Tail	2.488 (26.78)	2.45 (8.05)	2.12	
42		2.160 (23.25)	2.13 (6.99)	2.2	
43		1.830 (19.7)	1.81 (5.93)	2.2	
44		1.501 (16.16)	1.48 (4.87)	2.26	
45	Tail (Tip)	1.172 (12.61)	1.16 (3.81)	1.12	

NR = Not Required

The two-dimensional lift curve slope is an average theoretical value since the TIFS wing has various different sections. The taper ratio can be deceiving since the wing actually has two distinct tapers.

TIFS tail data is shown below

$c_{l_{\alpha_t}}$ = 6.60
β = 1
AR_t = 6.32
S_t = 23.51 m^2 (253.1 ft^2)
b_t = 12.19 m (40 ft)
λ_t = 1/3

The DATCOM method gives a loading function G/δ as a function of spanwise location for a wing with no flap (or equivalently, a full chord flapped wing). The lift curve slope for the i^{th} strip is related to the average value of this function over the i^{th} strip by the following relationship

$$C_{L_{\alpha_i}} = \frac{2b^2}{S_i} \left.\frac{G}{\delta}\right|_{ave_i} \Delta\eta_i \quad \text{(nondimensional)} \tag{55}$$

where $\Delta\eta_i$ is the nondimensional width of strip i
S_i is area of strip i
b is wing or tail span
$G/\delta|_{ave_i}$ is the average value over the i^{th} strip of the loading function G/δ given by DATCOM.

Using these techniques, the lift curve slope for the entire wing was computed to be $C_{l_{\alpha_w}}$ =5.67 and for the entire tail $C_{L_{\alpha_t}}$ =4.46. When combined the C_{L_α} for the wing-tail combination was computed to be

$$C_{L_{\alpha_{WT}}} = C_{L_{\alpha_W}} + \frac{S_t}{S_W} C_{L_{\alpha_t}} \left(1 - \frac{d\epsilon}{d\alpha}\right) = 6.28 \tag{56}$$

where $d\epsilon/d\alpha$ = variation of downwash angle with angle of attack = .5 from wind tunnel and flight tests ($C_{L_{\alpha_{TIFS}}}$ =6.11). Despite this reasonable agreement in C_{L_α}, the pitching moment change with angle of attack was substantially too negative (too stable) when compared to prior estimates based on both wind-tunnel and flight tests. The pitching moment due to angle of attack results through the distribution or moment arms of forces (which vary with angle of attack) across the aircraft. The destabilizing effects of the wing and fuselage were small compared to the large stabilizing effect of the tail. Since the geometry of the TIFS is accurately known, the problem is believed to be the result of an aerodynamic source not modeled. The destabilizing effects of the rather large engine nacelles forward of the center of gravity and of the engines themselves are believed to be responsible for this problem. More study into this area is warranted but was not attempted. As an expedient solution the lift curve slope of the tail was reduced to 2.05.

4.3 Flexible Model Verification

Two bodies of existing TIFS data facilitated the verification of the equations of motion computed in this study. The first consisted of a power spectrum of the normal acceleration at the TIFS pilot station measured in flight (h = 1402 m, V_T = 95.1 m/sec) in actual atmospheric turbulence. Since the gust input, α_g , was measured during this record, it was possible to normalize the measured TIFS response to a nominal condition (σ_{α_g} = 0.3048 m/sec or 1 ft/sec).

In Figure 41 this flight data is plotted along with the computed power spectrum of normal acceleration at the pilot's station (h = 1524 m, V_T = 106 m/sec) given by the analytical model developed in Section 4.1. It should be noted that the flight conditions between flight and computer data are slightly different, that the flight data reflects the response of the TIFS airplane to actual atmospheric turbulence ($\dot{\alpha}_g$, $\dot{q}$, α_g, etc.) and that the computed spectrum is based on the von Karman spectrum (L = 762 m, V_T = 106 m/sec for a α_g only.

The figure shows two significant trends. The first is that in the flexible region (ω > 10 rad/sec) the amplitudes of the resonant peaks are computed to be higher than were actually measured in flight. This may be the result of unsteady aerodynamics effects which have been ignored in the derivation of the equations. The second trend is that the frequency at the resonant peaks is computed to be lower than was observed in flight.

The second experimental result consists of ground vibration tests (Reference 41) of the TIFS airplane. These tests determined resonant frequencies and the primary motion of each mode and these results are shown in Table 7. Also shown in the table are the computed resonant frequencies and the resonances found in the flight test results. As before, the mode frequencies are consistently higher in the ground vibration tests than were computed.

The mass of the TIFS (maximum gross weight) in the ground vibration test and that used in the computation of structural mode properties were the same. However, the mass of the TIFS during the flight test was less because of fuel usage. The fact that the resonant frequencies from the ground vibration tests and flight tests agree well suggest that the stiffness data rather than the mass data used to compute the structural mode frequencies may be in error.

As a result of these experimental tests, considerable justification exists for increasing the computed mode frequencies to those measured in flight. This, however, was not performed.

TABLE 7

STRUCTURAL RESONANCE FREQUENCIES (rad/sec)

Primary Motion	Computed*	Flight Test**	Ground Vibration Test
First Wing Bending	17.8	19.6	20.1
First Wing Torsion	29.0	31.4	30.8
First Fuselage Bending	35.1	44.8	41.5
First Horizontal Tail Bending	43.1	NA	47.6
Second Wing Bending	51.8	62.8	60.9
Second Fuselage Bending	104.3	107.6	NA

* V_T = 106 m/sec (348 ft/sec) h = 1524 m (5000 ft)

** V_T = 95.1 m/sec (312 ft/sec) h = 1402 m (4600 ft)

NA = Not available

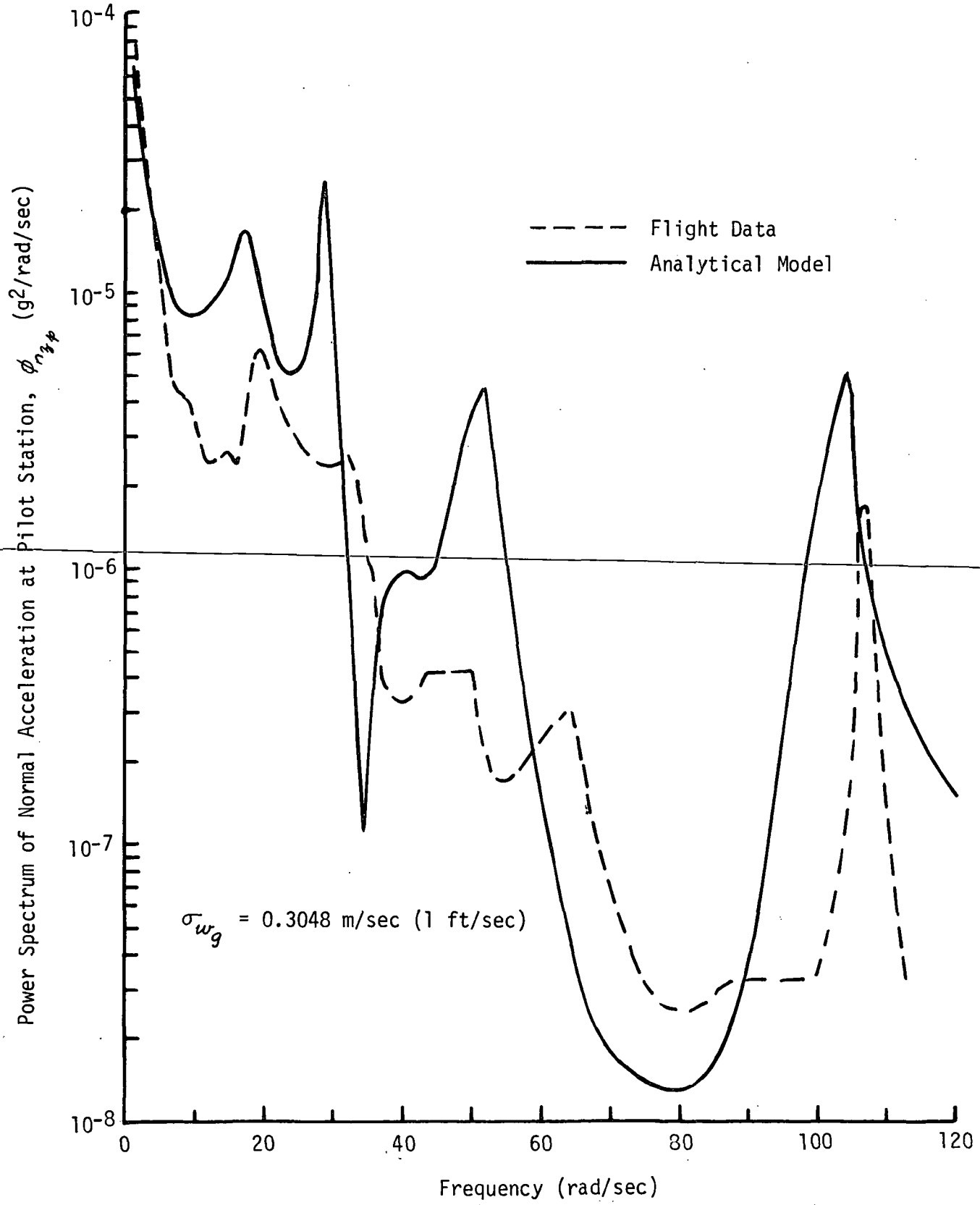

Figure 41 COMPARISON OF TIFS FLIGHT DATA TO ANALYTICAL MODEL, TIFS FLEXIBLE MODEL

5. AVAILABILITY AND COST OF TIFS AS AN ACT TESTBED FOR CONCEPT VERIFICATION

TIFS I

Air Force TIFS, designated in this report as TIFS I, has been developed by the Calspan Corporation for the Air Force Flight Dynamics Laboratory (AFFDL), Wright-Patterson Air Force Base, Ohio.

TIFS I has been operated by Calspan Corporation since its completion in 1971 under the direction and administration of the AFFDL and has been engaged in various research experiments since that time.

The aircraft in its present state of development is suitable to engage in ACT programs as outlined in Section 5.4 of this report.

TIFS II

The AT/TIFS aircraft, designated TIFS II in this report is owned by Aero Spacelines, Inc. (ASI) of Galeta, Calif. and is presently stored in hangar space provided by ASI in Santa Barbara, Calif. The effort required to complete this aircraft as a VS (variable stability) and ACT flying testbed is outlined in Section 5.1 of this report. The aircraft in its present configuration is for sale subject to negotiation with ASI. Based on actual costs to prepare the aircraft for a ferry flight to California in May 1974 it is estimated the aircraft could be prepared and ferried to Calspan Corporation in Buffalo, New York for completion as outlined in Section 5.1 for approximately $25,000. There are outstanding technical orders on this airplane which were waived by the FAA when the ferry permit was issued in May of 1974. This cost estimate assumes a waiver will be available to ferry it back. The outstanding work is included in subsequent cost estimates.

5.1 Cost Estimate for Outfitting the TIFS II as an ACT Flight Demonstration Vehicle Limited to 190 Knots Flight Envelope

Work on the TIFS II airplane under Contract CC139 was terminated as of January 5, 1970. During the hiatus, the development of the similar Air Force TIFS was completed and its operation demonstrated over a large portion of the flight envelope. The original objective of the TIFS II was to simulate a Boeing 707 series airplane with sufficient fidelity that pilot training might be effectively accomplished and credit granted by the FAA for such training time in the TIFS II aircraft. Calspan's specific objective in the program was to provide and install in the sponsor-supplied airframe a variable stability system that would demonstrate responses to the 707 controls that satisfactorily corresponded to those computed from the aerodynamic data utilized in the design.

The completion of the TIFS II airplane to a state suitable for demonstrating Active Control Technology, but not necessarily as a Boeing 707 simulator, involves not only completion of the original Calspan effort on the design, development, checkout, calibration and flight test demonstration of the variable stability system, but also finishing those portions of the work that were handled by other organizations: that effort associated with the completion and checkout of the modifications to the basic airplane to provide hydraulic and electrical power, avionics, environmental control and other systems as required to accept and support the variable stability system including the minimum completion required of the simulation cockpit, aircraft inspection as well as other work involved in the reactivation of the program.

Those tasks associated with the variable stability system per se and the ground/flight checkout of the airplane are summarized in Reference 42. The estimate of the cost of the other work (including completion and checkout of the APU installation, the electrical and hydraulic power systems, completion of the airplane interior and other unfinished tasks that are less well defined) has been based on available information in inspection records, individual notes and correspondence, and References 43 and 44.

Neither the ferry flight costs for pickup and delivery of the aircraft nor training of the sponsor's personnel have been included in this budgetary estimate. It is anticipated all work would begin after July 1975 with a subsequent labor rate increase of 7% which is included in the estimate. It is assumed the contract would be a cost plus fixed fee contract with a fee of 9%. It is assumed that missing NAVCOMM equipment worth approximately $19,000 will be supplied by Aerospace Lines, Inc. or the sponsor.

1. Aft Cabin

The aft cabin requires the fabrication and installation of a latch to hold the tunnel door open, installation of handles along the computer ceiling mount, installation of fire extinguishers near the auxiliary power unit (APU) compartment, the fabrication and installation of a storage container to hold the computer patch panels and soundproofing trim in the aft cabin.

2. Complete Card Reader Design and Installation

The card reader system has never been functionally tested. The cabling must be completed in the aircraft and the NCR card reader requires readjustment as there are apparent skew and timing problems in the data pulses. An elaborate bench setup may be required to isolate individual problems with the system.

3. Update Variable Stability System Compatible with TIFS I

During the hiatus since 1970, TIFS II has remained unchanged while numerous improvements have been incorporated in TIFS I. Some of these modifications are necessary while others provide improved system efficiency and operation.

Electrical modifications have been added to the flap and side force surfaces to aid in monitoring and troubleshooting system malfunctions, and the control logic was modified to eliminate sensitivity to moisture.

The complementary filters in the air data packages have been modified to eliminate vertical sink rate offset.

Component changes have been incorporated in the address system to improve system performance.

The feel system electronics rack has been shielded to reduce electromagnetic interference.

Teflon seals were added to the elevator hydraulic servo actuator to reduce piston leakage.

Multipliers on the MF-RF and model computers have been replaced with a different type to eliminate interaction between multipliers.

An indicating light system has been added to the VSS safety trip system to determine the signal causing the trip.

The synchro converter cards that are used to drive the simulator attitude director indicators and the compass heading indicators have been modified to eliminate a design deficiency.

The direct lift flap Marrotta bypass and shutoff switch actuating plunger was reworked to reduce sensitivity to vibration.

The side force surface position switch was remounted to prevent a possible operational malfunction.

A four channel FM tape recorder has been installed to provide "canned" turbulence.

4. Calibration and Checkout of VS System

This includes the calibration of the sensors, checkout of the MF-RF and simulation computers, checkout of Go - No Go system, completion of the design and checkout of the VS system and recording system, checkout of the 580 and VSS control surfaces procurement, fluid power control system design and patching of the model and MF-RF boards. This also includes correcting

the system malfunctions observed in the 24 May 1974 checkout and recorded in Reference 44.

5. Replate Propellers

This includes removal of the propellers, shipping them to Hamilton Standard Division of United Aircraft Corporation, stripping the propellers and hubs of plating and checking for corrosion, replating the propellers and shipping them to Calspan for mounting on the TIFS aircraft.

6. Hydraulic Modifications and Repair

This includes the addition of a cooler to the VSS hydraulic system, additional valves and quick disconnects, completion of installation drawings, and procurement and installation of a VSS hydraulic system pressure transducer.

Modifications are required to the 580 hydraulic system to rectify hydraulic starter problems and the DC hydraulic pump cavitation problems.

7. Complete APU Installation and Checkout

Further checkout and modifications are required to rectify the problems associated with the auxiliary power units (APU's). The units shut down in flight during zero "g" maneuvers.

One of the gas turbines has a cracked weld at the combustor drain and must be reworked. Additional mechanical modifications and drawing updating is required.

8. Complete Unfinished ASI Projects

This includes reworking the side force surface locking pins to provide better seating and rework of the skirt seals on the side force surfaces.

It is necessary to complete changes in the intercom and to rectify problem areas in that system.

The design documentation and test of the environmental control system is incomplete.

The documentation and installation of the oxygen system is incomplete. The engineering orders and documentation of the airspeed tubing installation, nose pressure survey installation and other engineering orders are incomplete.

It is necessary to complete the pertinent open items on the ASI planning schedule and to rectify the inspection squawks as listed in Reference 43.

All material such as multipliers, FM recorders, direct charges such as computer time and flight pay are included under this category.

9. Ground and Flight Test

This includes the flight test of the APU systems and the flight test of the control surfaces. A minimum ground and flight test program is included to check the TIFS II aircraft as an active control demonstration vehicle in the response feedback mode. It is assumed that aviation fuel will be supplied by the sponsor. The checkout and simulation of a linear or nonlinear Boeing 707 model is not included in the ground and flight test program.

10. Program Administration and Miscellaneous Charges

This includes the services of a full time program manager, administration of other personnel as required, secretarial service, program reorganization and other miscellaneous items and services not included in the listed task categories.

11. Documentation and Reports

This includes the documentation and reports to complete the TIFS aircraft as an ACT demonstration vehicle in the form of program memos. It does not include a final report or operational manual.

5.2 Expansion of TIFS II Flight Envelope to 240 Knots

This section includes the tasks necessary to expand the TIFS flight envelope from 190 knots to 240 knots. It includes ground vibration tests, flight flutter tests and a propeller survey required for expansion of the TIFS flight envelope. The tasks versus cost and time are outlined in Figure 42.

5.2.1 Ground Vibration Tests

The ground vibration tests will be performed like a survey run on TIFS I by Rochester Applied Science Associates (RASA) to substantiate the similarity of the two airplanes.

5.2.2 Propeller Stress Survey

On the basis of a successful program conducted by Detroit Diesel Allison Division (DDAD) of General Motors on TIFS I and the physical similarity of the two TIFS aircraft, no actual flight testing will be required. A report would be issued by DDAD similar to their report 71D71 dated 10 August 1971 to verify the flight envelope commensurate with the TIFS I vehicle.

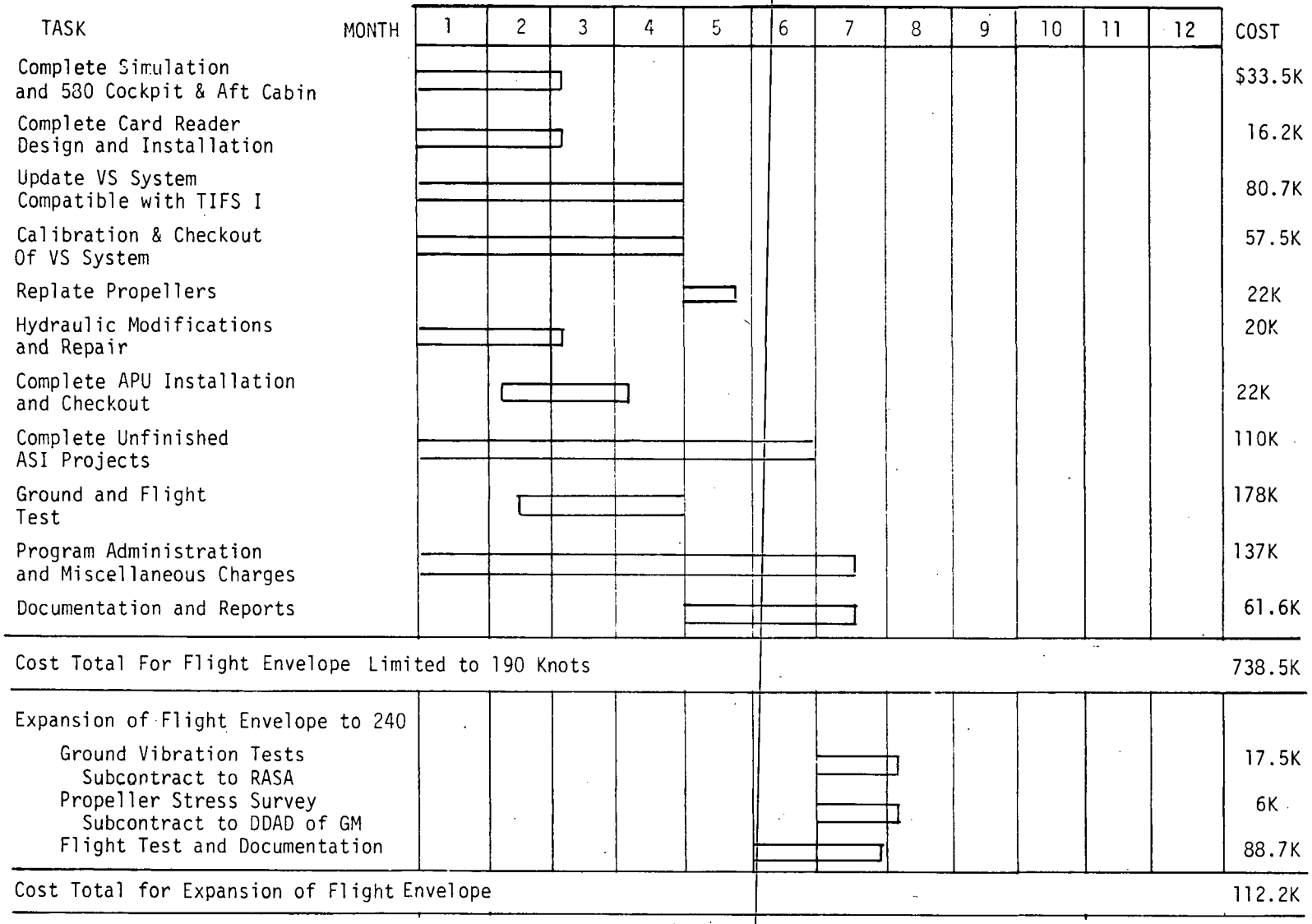

Figure 42 COMPLETION SCHEDULE FOR TIFS II

5.2.3 Flight Test and Documentation

On assuming satisfactory results are obtained on the ground vibration tests, and in view of past experience with TIFS I flight flutter tests, the flight test program can probably be accomplished in two to three flights.

The Calspan effort will be directed toward preparing the aircraft for the ground and flight tests, material costs and submission of a report.

5.3 Recommended Improvements for the TIFS Aircraft

The recommended improvements of the TIFS aircraft to expand the capabilities as an ACT test vehicle are listed and described in this section. Tasks, cost and completion schedules are presented in Figure 43. The improvements are applicable to both TIFS aircraft. Not included in these costs is the cost of a full time program manager or project engineer. The additional cost to the program for each would be approximately $6,500/month.

5.3.1 Elevator Servo Improvement

The VSS elevator frequency response of the TIFS I aircraft can be represented by a linear second order system with a frequency response of 2 hertz.

The flexure of the elevator torque tube is responsible for the low dynamic frequency response of the elevator servo. The frequency response of the elevator servo can be raised by increasing the stiffness of the elevator torque tube and mounting structure. The costs involved are for the design, fabrication and modification of the elevator torque tube and mounting structure.

Due to the similarity of both aircraft, the frequency response of the TIFS II aircraft should be similar to that of TIFS I.

5.3.2 Rudder Servo Improvement

The VSS rudder frequency response of the TIFS I aircraft can be represented by a linear second order system with a frequency response of 3 hertz. The flexure of the rudder torque tube and mounting structure is responsible for the low dynamic frequency response of the rudder servo. A similar modification as described to improve the elevator frequency response is proposed as a technique to improve the rudder frequency response.

5.3.3 Collective Aileron Modification

The prime requirement of collective aileron control is for maneuver load control studies where requirements dictate shifting the maneuver load further inboard. Full authority of the ailerons in the collective mode is required.

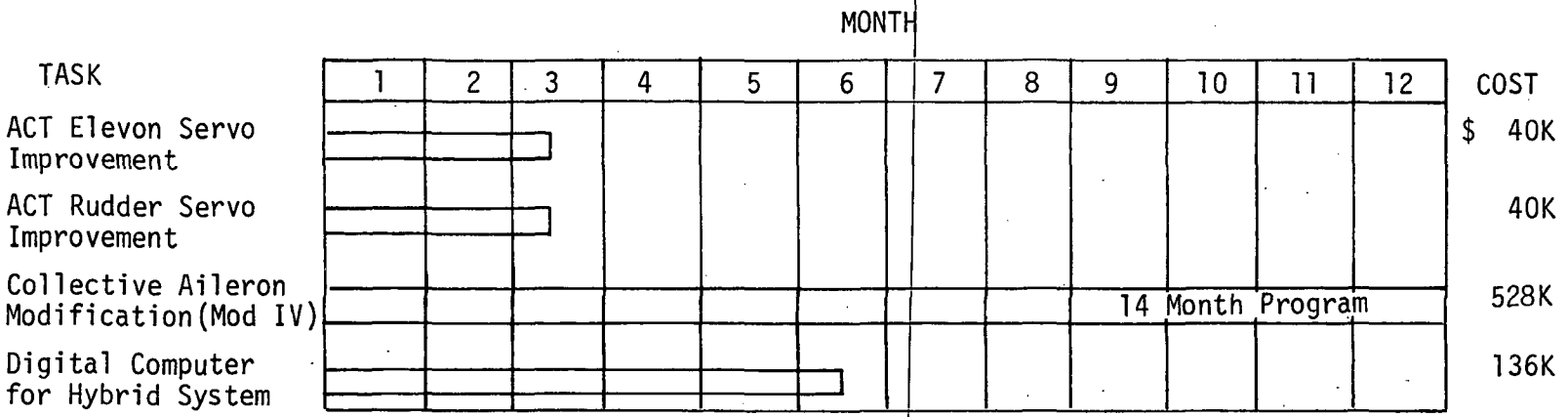

Figure 43 COMPLETION SCHEDULE FOR IMPROVEMENTS TO TIFS

Flight safety is of prime importance in any aircraft modification. In the past, Calspan Corporation VS systems have permitted the safety pilot to override the servo actuators controlling the surface under VSS operation providing full control of the surfaces through mechanical cables and links.

The only exception to this have been the TIFS aircraft where mechanical linkages to the direct lift flap (DLF) and side force surfaces (SFS) were not installed, but the systems were designed with either a dual redundant electrohydraulic system as in the DLF system, or a means of aerodynamically forcing the surface to a null as was provided in the SFS and mechanical locks were provided for a third back-up system.

At present, the ailerons are the only effective means of producing and controlling rolling moments on the TIFS aircraft. Any modification to the aileron control system must not compromise the safety and integrity of the aircraft.

Several schemes to provide collective aileron control are summarized in Table 8 and described in further detail in Reference 47. This does not imply that these methods are the optimum design or will be the final selection for collective aileron control but are presented as a comparison of system cost versus improved "design reliability".

The present aileron cabling and control system arrangement is shown in Appendix E, Figures 44 through 46. A schematic representation of a modification (Mod IV) to the present aileron control scheme is outlined in Figure 47. The basic philosophy of the modification described in Figure 47 is to disconnect the present control cables from each wheel in the 580 cockpit and to install separate cabling and aileron cable drums to each aileron from each control wheel. A mechanical or hydraulic disconnect would be provided to revert the ailerons to normal differential operation upon disengagement of the electrohydraulic differential-collective control system. If space limitations permit mounting the electrohydraulic actuators near each surface, excellent static and dynamic performance can be expected of the collective-differential control installation. The only new device required would be a mechanical or electrohydraulic interconnect between each aileron. This modification permits individual control of each aileron should an actuator or the aileron interconnect fail.

5.3.4 Digital Computer for Hybrid System

The simulation and computation capability of the TIFS aircraft can be enhanced with the addition of a digital computer system. Additional details concerning the computer selection are described in Reference 46.

The Rolm Model 1602 Rugged Nova computer was selected as a candidate computer on the basis of its airworthiness, reliability, process speed, microprogram capability and manufacturer's support capability.

TABLE 8

COLLECTIVE AILERON CONTROL SCHEMES

Modification			
Mod I	(Full authority)	$261,428	One aileron mechanically disconnected and driven electrohydraulically for normal control. Both ailerons driven hydraulically for VSS control.
Mod II	(Full authority)	318,396	Same as Mod I except dual electrohydraulic system provided for mechanically disconnected aileron.
Mod III	(Full authority)	911,724	Ailerons modified to operate like direct lift flaps. Spoiler surfaces added for aileron control.
Mod IV	(Full authority)	527,635	Disconnect wheel cable interconnects, tie pilot wheel to left aileron and co-pilot wheel to right aileron and add dual electrohydraulic servo system for both ailerons with wheel mechanical connect/disconnect system.
Mod V	(Limited authority)	$381,448	Add mechanical summers with special designed electrohydraulic servo actuator with centering spring and lock and limited authority (20%) electrical and hydraulic redundancy not provided.

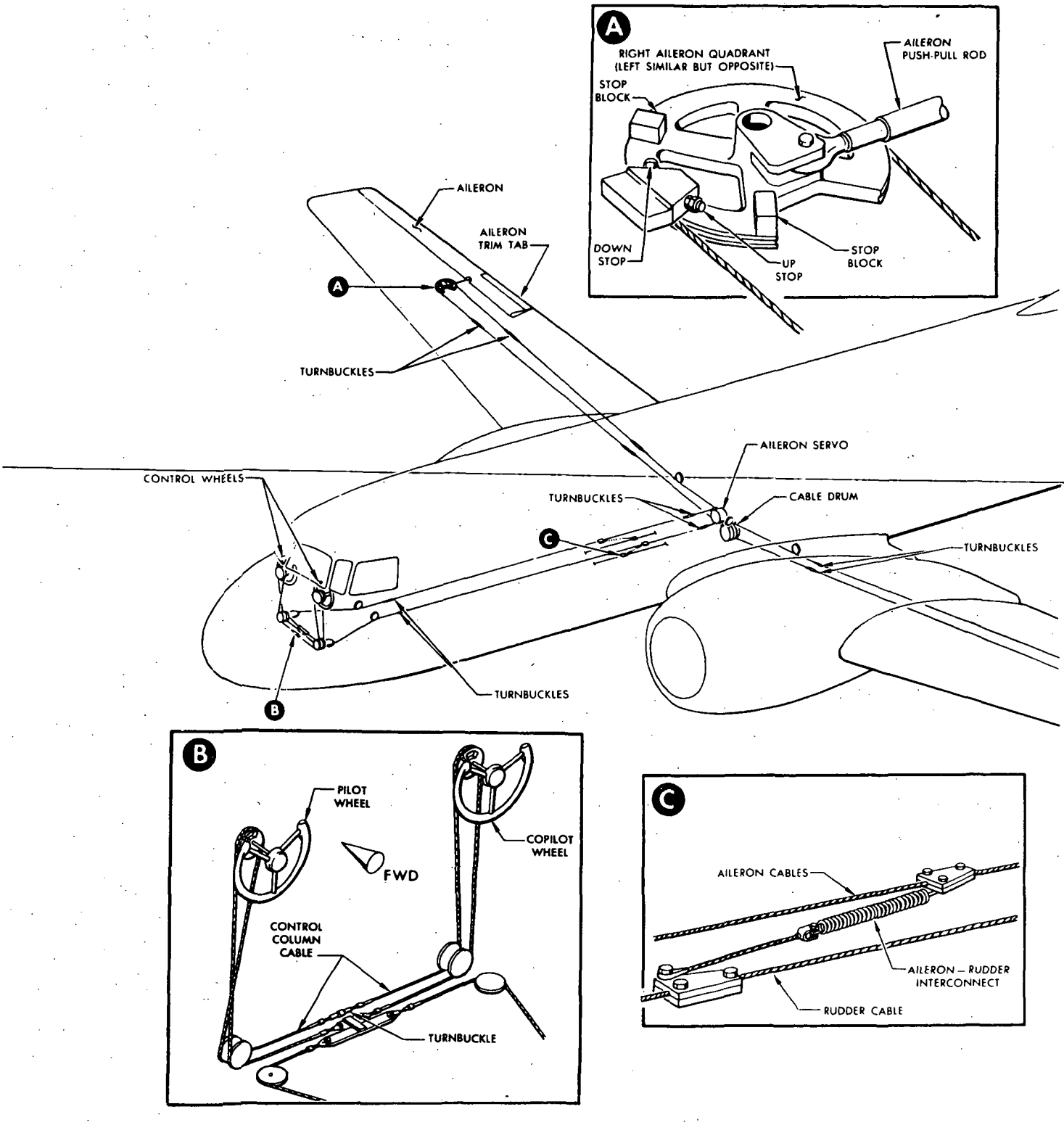

Figure 44 AILERON CABLING ARRANGEMENT

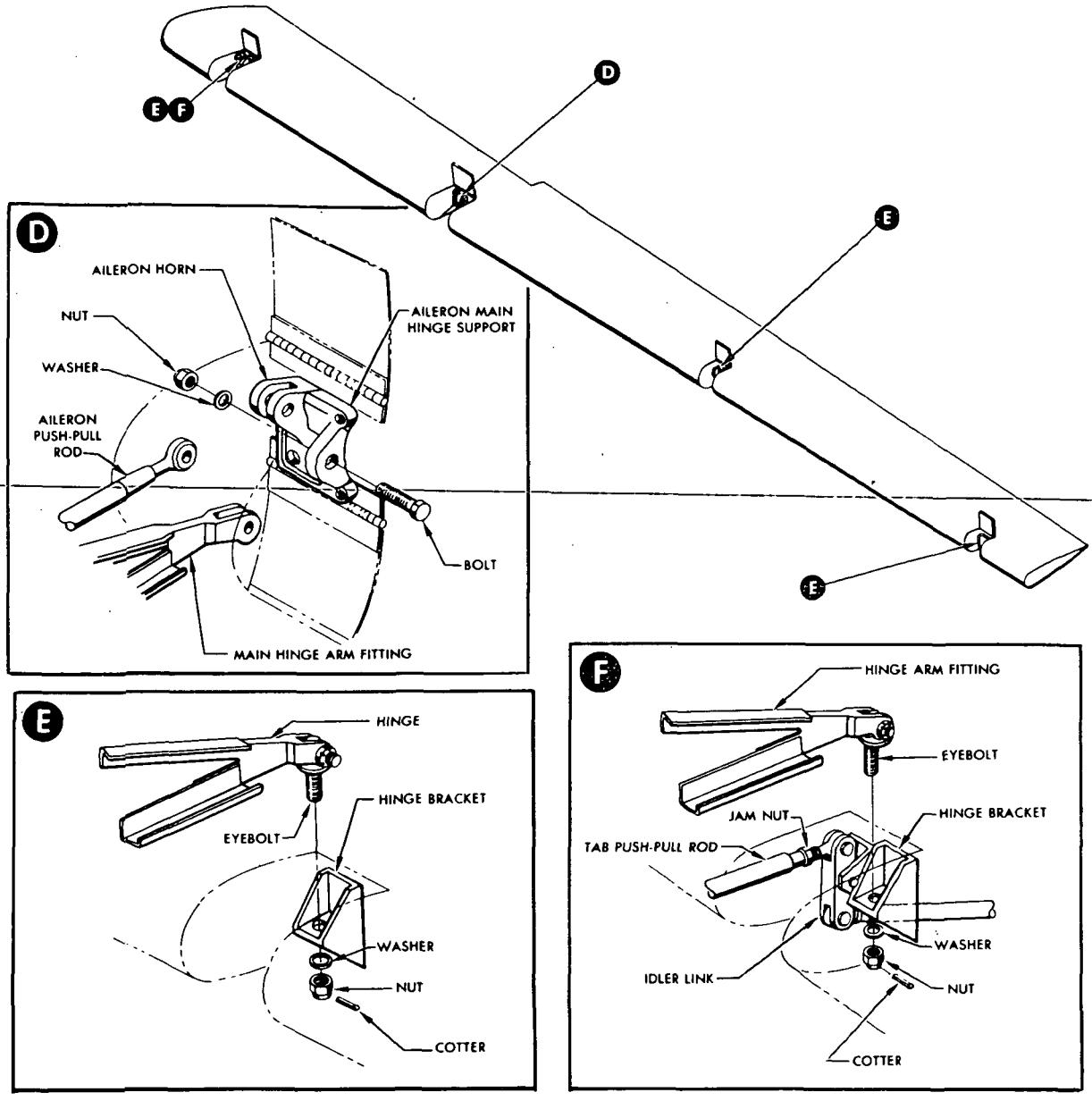

Figure 45 AILERON MECHANICAL ARRANGEMENT

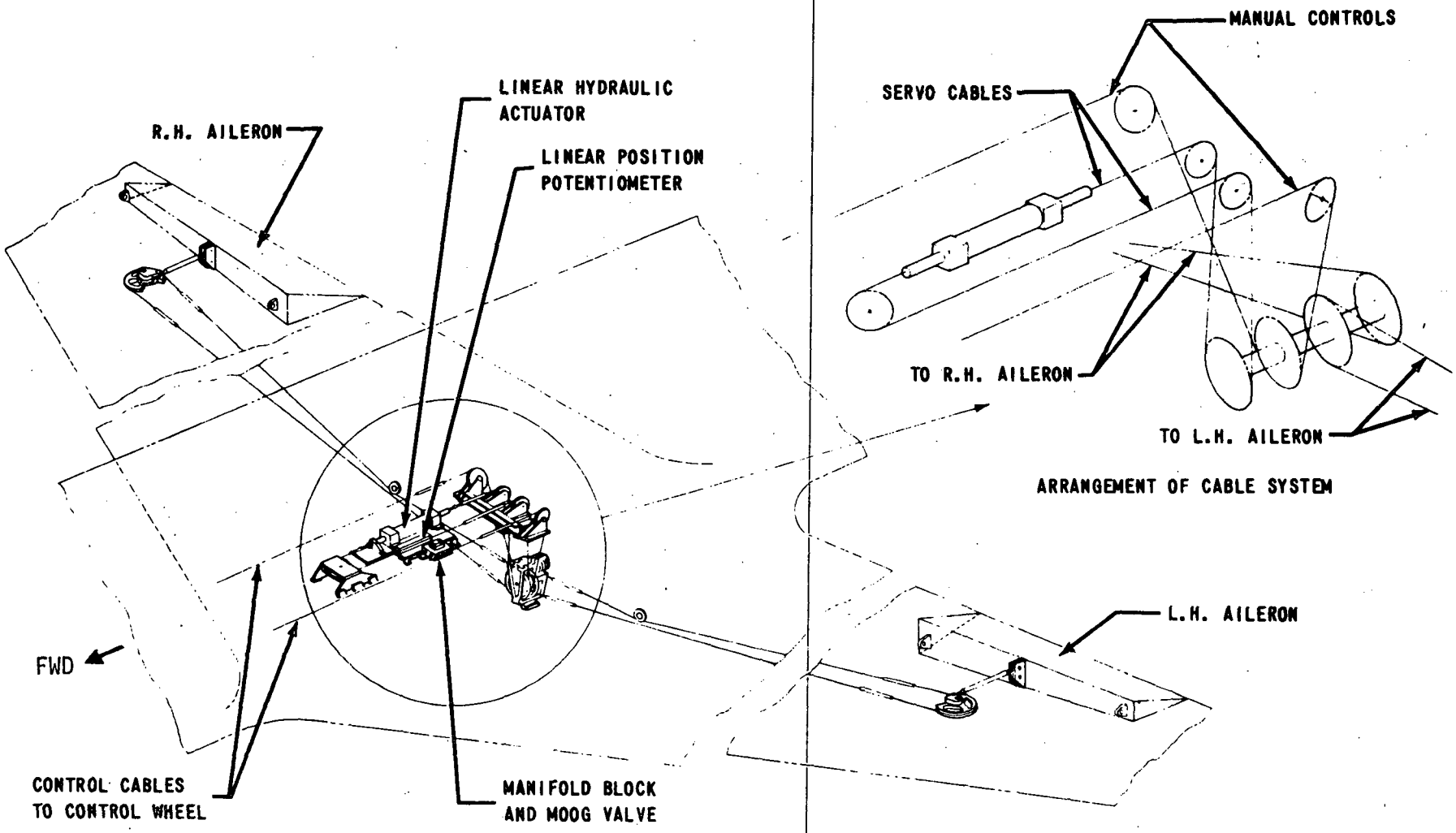

Figure 46 PRESENT VSS AILERON POSITION SERVO

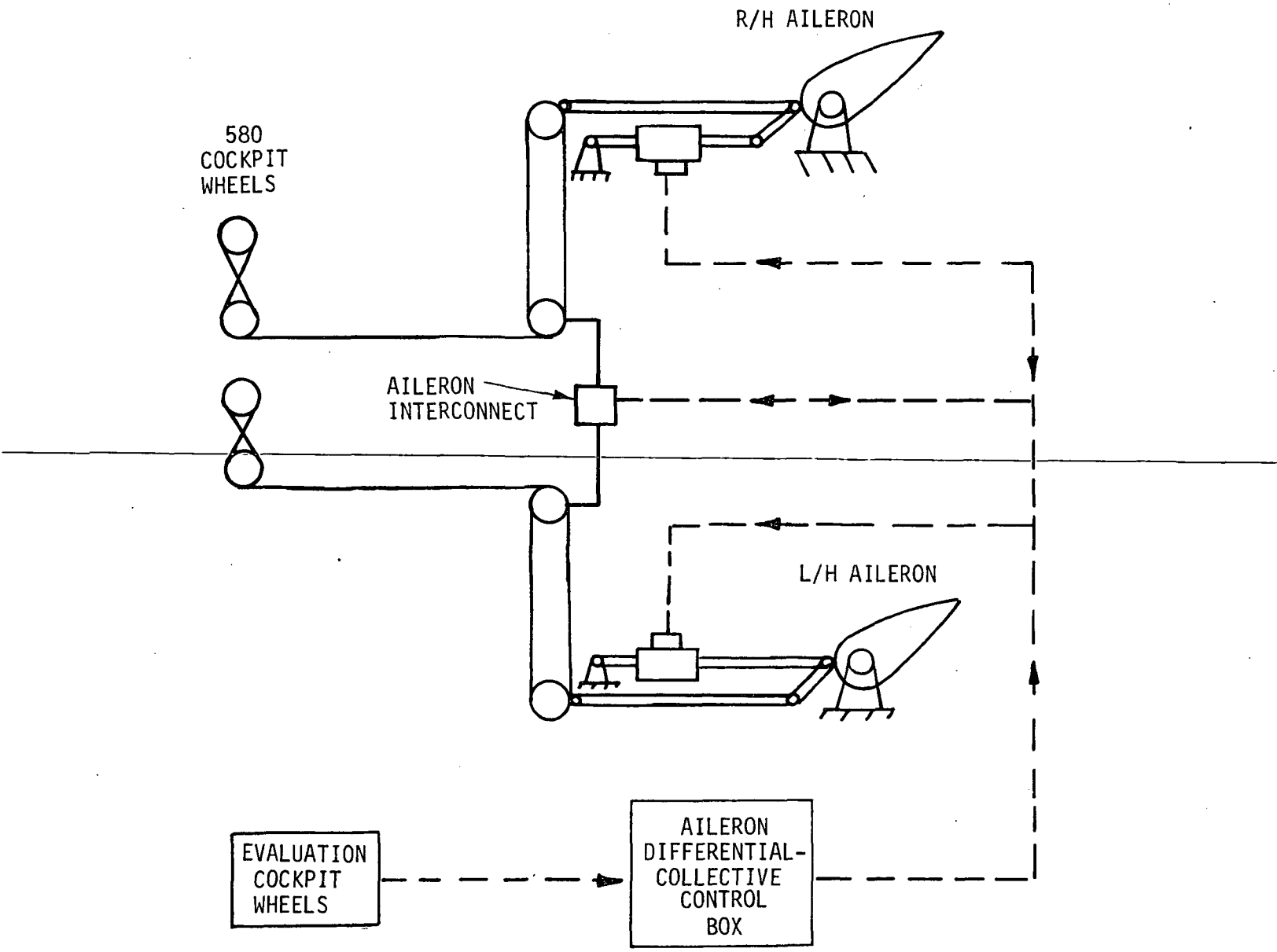

Figure 47 COLLECTIVE AILERON CONTROL SCHEME

The Model 1602 computer has a microprogrammed central processor with a 5 megacycle internal clock offering high speed execution of an extensive instruction set. Wide temperature range components (-25 C^{o} to -75 C^{o} case temperature) have been specified for the computer wherever practical.

The computer has been selected with an expanded memory capacity (4 memory slots) for inclusion of microprogram modules. The only microprogram module available, floating point instruction repertoire, has been included as a memory module.

A memory expansion chassis capable of containing 24K of memory is mounted on the back of the Model 1602 CPU, however, only 16K of memory has been specified.

Both data in analog to digital (A to D) and data out of the computer, digital to analog (D to A) have been selected to provide maximum thru-put rates for 32 data channels each. Direct memory access (DMA) will be provided for both the input and output data. The computer manufacturer provides A to D, DMA capability, however, the D to A capability provided by the computer manufacturer is prohibitively expensive and wasteful of space and weight. By utilizing the logic modules provided by Rolm, a D to A interface can be designed by Calspan Corporation and mounted in a data acquisition system purchased from Datel Systems, Inc. which includes 32 D to A converters.

The computer has been specified to operate from either a 60 Hz or a 400 Hz power supply. The intent is to provide the capability to remove the computer from the aircraft when extensive programming is necessary. A Texas Instrument "Silent 700" teletype which is three times faster than the normally used ASR-33 teletype has been selected for use when the computer is used remotely from the aircraft. A termiflex hand-held terminal has been selected for use within the aircraft because of its small size, light weight (approximately 1-1/2 lb) and ruggedness.

An ECCO paper tape reader has been selected to input programs into the computer. This paper tape reader has been chosen because of its ruggedness, permitting programs to be changed in flight.

Included in the budgetary cost estimate is installation and checkout of the computer, two man weeks of training at Rolm headquarters at Cupertino, Calif., the cost to interface the D to A converters to the computer, and its peripheral equipment. A completion schedule is depicted in Figure 43.

6. CONCLUSIONS AND RECOMMENDATIONS

6.1 Conclusions

This study program has indicated the following:

(i) The TIFS aircraft are suitable test beds for in-flight research and validation of many ACT concepts. With the existing capability of the TIFS I, first phase flight programs can be initiated in a relatively short period of time for in-flight verification of potential benefits of such ACT functions as gust alleviation, precise flight path control, augmentation of relaxed static stability and envelope limiting systems. With internal modifications on the mechanization of the ailerons to operate collectively as well as differentially (as they presently operate), first phase flight research programs for the maneuver load control and flutter control could then be initiated. These first phase programs would yield preliminary in-flight assessment of the predicted benefits and identification of potential problem areas for a more comprehensive follow-on flight research program using the TIFS aircraft.

(ii) Preliminary design study of the gust alleviation system for the TIFS aircraft has shown that the low frequency structural modes can essentially nullify the effectiveness of the gust alleviation system designed using the rigid body dynamic representation. Several avenues as indicated in Section 3.1 may be approached to achieve higher bandwidth gust alleviation capability.

(iii) Preliminary design study of the precise flight path control (PFPC) system, applying decoupling control theory has shown that the TIFS aircraft as presently equipped is capable of flight research work in PFPC to investigate reduction in pilot workload in precisely flying approach paths designed for the purposes of noise abatement and for reducing the congestion in the terminal operations.

(iv) With the versatility of the variable stability system of the TIFS aircraft, a relatively safe and cost effective flight research program can be conducted for verification of several envelope limiting (EL) concepts, such as angle of attack limiter, normal load factor limiter, etc., and for gathering flight test data for development of EL system design criteria.

(v) Preliminary calculations have indicated that the stimulation and suppression of the flutter mode could be realized using active control of separate control surfaces, the DLF and collective ailerons of the TIFS aircraft. Also, a procedure for in-flight verification of the FC concept using the TIFS aircraft has been discussed in Section 3.2.

(vi) Limited benefits can be achieved for the TIFS aircraft using its direct lift flaps and elevator for maneuver load control; however, more significant benefits could be realized, if the ailerons are mechanized for collective operation and/or the Fowler flaps are replaced by simple plain flaps.

(vii) Limited direct verification of the relaxed static stability (RSS) concept can be realized using the TIFS aircraft by changing the c.g. of the TIFS for relaxation of static stability; augmentation of the stability and control characteristics can be realized using its VSS. Indirect verification of RSS concept and gathering of valid flight test data for the development of design criteria can be achieved using the model following mode of the simulation capability of the TIFS aircraft.

(viii) If NASA wishes access to a dedicated near full time ACT research airplane, it is feasible to complete the TIFS II airplane within the cost estimate presented in Section 5. Also, some suggested improvements common to both TIFS I and TIFS II have been discussed in Section 5.

6.2 Recommendations

Experimental results and analyses indicate a significant potential for active control technology as a means of improving the aerodynamic and structural efficiency of future commercial aircraft. Intelligent application of ACT can result in lighter, lower drag aircraft with improved ride qualities which also use much less of the world's dwindling fuel reserves.

However, the developer of a new commercial aircraft invests hundreds of millions of dollars in his venture. No matter what its potential, he cannot take advantage of a new design concept unless he has confidence that it will not interfere with the safety, reliability and overall economic and schedule constraints of his program. Therefore, if the air transportation system is to reap the benefits of active control technology, a flight demonstration program which clearly verifies the safe, reliable application of active controls and generates the technical information required to support the aircraft designer is an important national need.

To assist NASA in developing the emerging active control technology to a level of maturity ready for use in the next generation commercial transport aircraft, Calspan recommends a comprehensive 2-phase flight research program using the TIFS aircraft.

Using the TIFS I as the test bed, the recommended Phase I programs would provide a means for early assessments of some promising ACT concepts, both individually and in combinations in the actual operational environment. In an order of priority and readiness, four flight programs are recommended in Phase I:

- Gust alleviation and ride control (GA/RC)
- Precise flight path control and envelope limiting (PFPC/EL)
- Maneuver load control and augmentation of relaxed static stability (MLC/RSS)
- Integration of the above ACT functions

An estimated time schedule for these programs is shown in Table 9. The time schedule includes the three internal modifications that will be involved in this phase, i.e., the improvement of bandwidth of the elevator and rudder servos and the mechanization of the ailerons for collective as well as for the existing differential operations.

Logical inclusion of two ACT functions in each of the first three programs would facilitate the integration program - the fourth program in Phase I - for the final assessment of the results of all the six ACT systems functioning simultaneously. These first phase programs would not only provide an early in-flight verification of the predicted potential benefits of these ACT systems, but also identify the problem areas and limitations that the presently configured TIFS I aircraft might have. The flight test data gathered in the first phase will be of vital importance for definitive and effective planning for the Phase II flight programs.

The recommended Phase II flight research program for ACT development, as presently envisioned, consists of the following three programs:

- Advanced Gust Alleviation, Ride Control and Flutter Control
- Advanced Maneuver Load Control
- Advanced Integration Program

These Phase II programs are designed to further validate such ACT functions as the MLC and GA/RC in a more complete manner as well as the concept of active flutter control (FC) using the TIFS aircraft. An estimated time schedule of the Phase II programs is shown in the lower portion of Table 9. Of course

TABLE 9

ACTIVE CONTROL TECHNOLOGY DEVELOPMENT AND DEMONSTRATION PROGRAM

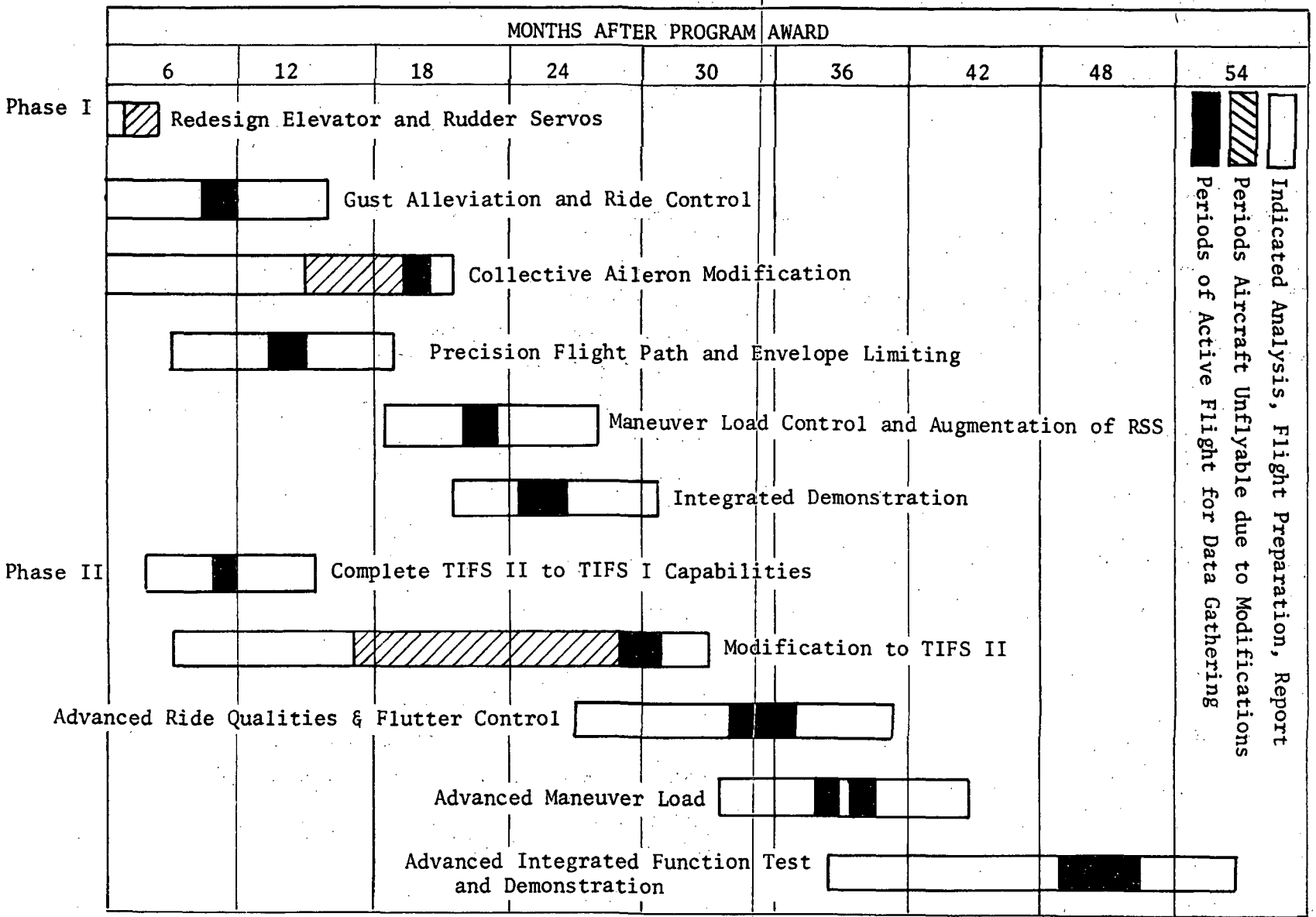

these programs are subject to changes and/or deletions that may be found desirable as a result of the Phase I investigations. The Phase II programs may involve extensive structural modifications of the TIFS such as replacement of the Fowler flaps by plain flaps, addition of canard surfaces, etc. The need for these modifications will have been established in the Phase I program, so only the most desirable and necessary modifications need be made.

The fact that two TIFS aircraft are in existence permits planning a most efficient and effective flight program for the ACT development. As the need for modifications becomes evident by a Phase I flight program on the TIFS I aircraft, the TIFS II could be brought to completion and modified in the most cost-effective manner with minimum lost time. The TIFS II aircraft is available for purchase by NASA and could be modified extensively without concern for conflicts with Air Force plans.

APPENDIX A

TIFS DATA USED IN THE PRELIMINARY DESIGN OF GUST ALLEVIATION AND PRECISE FLIGHT PATH CONTROL SYSTEMS

Analytical expressions of the aerodynamic coefficients of the TIFS aircraft, which are suitable for preliminary design purposes, have been given in Reference 3. They are

$$C_L = .15 + .105\alpha + .012\delta_e + .34\left(\frac{\delta_z + 3.5}{30.}\right)\left[\frac{.3 + \left(\frac{\delta_z + 3.5}{30.}\right)^2}{.1 + \left(\frac{\delta_z + 3.5}{30.}\right)^2}\right] + .25\left(\frac{\delta_F}{40.}\right)$$

and

$$C_D = C_{D_o} + kC_L^2$$

where

$$C_{D_o} = .028 + .023\left(\frac{\delta_z}{30.}\right)^2 + .037\left(\frac{\delta_F}{30.}\right)^2 + .027G + .045\left(\frac{\delta_y}{30.}\right)^2$$

$$k = .037 + .034\left(\frac{\delta_z}{30.}\right)^2 - .011\left(\frac{\delta_z}{30.}\right)^3$$

$G = 0$ or 1 depending on whether the landing gear is up or down, and all angles are in degrees.

$$C_Y = -.017\beta + \left(1. - .23\frac{\alpha}{10}\right)\left[.075\left(\frac{\delta_y - .73\beta}{10}\right) - .0056\left(\frac{\delta_y - .72\beta}{10}\right)^3\right] + .005\delta_r + .367\frac{r}{V}$$

$$T = (\delta_x - 34.)\left[320. + \frac{V}{100}\left(8.88\frac{h_p}{10^4} - 36.4\right) - 63.2\frac{h_p}{10^4}\right]$$

where T is in pounds

δ_x is in degrees, $34.^o \leq \delta \leq 90^o$

V is in ft/sec

and h_p is in ft

$$C_\ell = (-.0018 + .00005\alpha)\beta + .0005\delta_r + (-.0017 + .00001|\delta_a|)\delta_a$$

$$-.00005\delta_y + .14\frac{r}{V} - .48\frac{p}{V}$$

$$C_n = (.0019 - .00007\alpha)\beta - .0019\delta_r + (-.00017\delta_a + .00017\delta_y)$$
$$-.127\frac{r}{V} + (-.015 - .0045\alpha)\frac{p}{V} - .027\ \frac{T \times 10^{-3}}{\bar{q}}$$

$$C_{m_{CG}} = \left(\frac{x_{CG}}{9.52} - .266\right)C_L + .103 - .092C_{L_{\substack{\delta_F=0\\ \delta_e=0}}} + .081C^2_{L_{\substack{\delta_F=0\\ \delta_e=0}}} - .104C^3_{L_{\substack{\delta_F=0\\ \delta_e=0}}} - .015G$$
$$+ \left(.086 - .070C_{L_{\substack{\delta_F=0\\ \delta_e=0}}}\right)\left(\frac{\delta_z}{30}\right) + \left(.018 + .006G_{\substack{\delta_F=0\\ \delta_e=0}}\right)\left(\frac{\delta_z}{30}\right)^2$$
$$+ \left(.023 + .016C_{L_{\substack{\delta_F=0\\ \delta_e=0}}}\right)\left(\frac{\delta_z}{30}\right)^3 + \left\{.15 + .005\alpha + \left(-.68 + .030\alpha\right)\frac{T \times 10^{-3}}{q}\right\}\left(\frac{\delta_z}{40}\right)$$
$$+ .74\ \frac{T \times 10^{-3}}{q} - .035\delta_e - 1.41\frac{\dot{\alpha}}{V} - 3.74\frac{q}{V}$$

In the above expressions, all angles are in degrees and V in ft/sec. Using these expressions and the following geometrical parameters of the TIFS,

S	= 85.47 m^2 (920 sq ft)
$\bar{c}$	= 2.90 m (9.52 ft)
b	= 32.09 m (105.3 ft)
I_{xx}	= 324,040 Kg-m^2 (239,000 slug-ft^2)
I_{yy}	= 721,295 Kg-m^2 (532,000 slug-ft^2)
I_{zz}	= 1,035,844 Kg-m^2 (764,000 slug-ft^2)
I_{xz}	= negligible

the stability and control derivatives in the three-degree-of-freedom longitudinal and lateral-directional small perturbation equations of motion

$$\dot{x} = Fx + Gu$$

were calculated at the three selected flight conditions (gross weight W = 52,000 lb)

	Landing	Climb	Cruise
Altitude m (ft)	60.96 (200)	1524 (5000)	3048 (10,000)
True Speed m/sec (ft/sec)	67.97 (223)	106.07 (348)	149.66 (491)

The state x and the control u are defined as follows:

$$
\begin{aligned}
x &= (q,\ \Delta\theta,\ \Delta V,\ \Delta\alpha)^T && \text{longitudinal motion} \\
&= (p,\ \phi,\ r,\ \beta)^T && \text{lateral-directional motion} \\
u &= (\delta_e,\ \delta_x,\ \delta_z)^T && \text{longitudinal controls} \\
&= (\delta_a,\ \delta_r,\ \delta_y)^T && \text{lateral-directional controls}
\end{aligned}
$$

The stability and control derivatives for the flexible equations of motion are given in Appendix D.

In the random gust response study discussed in Section 3.1, both the von Karman form and the Dryden form of the gust spectrum were used. They are

$$
\Phi_{w_g}(\Omega) = \begin{cases} \dfrac{L}{\pi} \dfrac{1 + \frac{8}{3}(1.339 L\Omega)^2}{\left[1 + (1.339 L\Omega)^2\right]^{11/6}} \sigma_{w_g}^2 & \text{- von Karman form} \\ \dfrac{L}{\pi} \dfrac{1 + 3L^2\Omega^2}{\left[1 + L^2\Omega^2\right]^2} \sigma_{w_g}^2 & \text{- Dryden form} \end{cases}
$$

In converting the spatial frequency Ω to the temporal frequency $\omega = \Omega V$ (rad/sec), the following transformation was applied

$$
\Phi_{w_g}(\omega) = \frac{1}{V} \Phi_{w_g}\left(\Omega = \frac{\omega}{V}\right)
$$

The scale L depends on the flight condition as shown in Table A.2.

TABLE A.1
STABILITY AND CONTROL MATRICES
(unit in rad and ft/sec)

	Flt. Cond.	Landing (h = 60.96 m or 200 ft) (V_T = 67.97 m/sec or 223 ft/sec)	Climb (h = 1,524 m or 5,000 ft) (V_T = 106.07 m/sec or 348 ft/sec)	Cruise (h = 3,048 m or 10,000 ft) (V_T = 149.66 m/sec or 491 ft/sec)
Longitudinal equations	F	$\begin{bmatrix} -1.259 & 0.000027 & 0.0042 & -0.997 \\ 1. & 0. & 0. & 0. \\ 0. & -32.170 & -0.0171 & 17.808 \\ 1. & -0.00002 & -0.0013 & -0.917 \end{bmatrix}$	$\begin{bmatrix} -1.686 & 0.000035 & 0.000231 & -0.486 \\ 1. & 0. & 0. & 0. \\ 0. & -32.17 & -0.0143 & 18.027 \\ 1. & -0.000013 & -0.000531 & -1.223 \end{bmatrix}$	$\begin{bmatrix} -2.062 & 0. & 0.000142 & -0.7155 \\ 1. & 0. & 0. & 0. \\ 0. & -32.17 & -0.0151 & 17.610 \\ 1. & 0. & -0.00027 & -1.495 \end{bmatrix}$
	G	$\begin{bmatrix} -2.091 & 0.00116 & -0.0863 \\ 0. & 0. & 0. \\ 0. & 6.5577 & -3.1286 \\ -0.095 & -0.00358 & -0.1991 \end{bmatrix}$	$\begin{bmatrix} -4.3778 & 0.000218 & -0.19948 \\ 0. & 0. & 0. \\ 0. & 5.4442 & -3.0933 \\ -0.1273 & -0.000514 & -0.2667 \end{bmatrix}$	$\begin{bmatrix} -7.5685 & 0. & -0.3709 \\ 0. & 0. & 0. \\ 0. & 3.7738 & -3.1547 \\ -0.1557 & 0. & -0.3262 \end{bmatrix}$
Lateral-directional equations	F	$\begin{bmatrix} -3.001 & 0. & 1.1756 & -2.166 \\ 1. & 0. & 0. & 0. \\ -0.356 & 0. & -0.1887 & 0.6549 \\ 0.122 & -.1443 & -1.0135 & -0.1901 \end{bmatrix}$	$\begin{bmatrix} -3.977 & 0. & 1.2429 & -4.6482 \\ 1. & 0. & 0. & 0. \\ -0.476 & 0. & -0.2951 & 1.3687 \\ 0.033 & 0.0924 & -0.9999 & -0.2545 \end{bmatrix}$	$\begin{bmatrix} -4.845 & 0. & 1.3724 & -8.100 \\ 1. & 0. & 0. & 0. \\ -0.5828 & 0. & -0.3802 & 2.362 \\ 0. & 0.0655 & -0.999 & -0.311 \end{bmatrix}$
	G	$\begin{bmatrix} -2.342 & 0.5591 & -0.0574 \\ 0. & 0. & 0. \\ -0.1062 & -0.8075 & 0.07175 \\ 0. & 0.04375 & 0.0603 \end{bmatrix}$	$\begin{bmatrix} -4.874 & 1.3186 & -0.1334 \\ 0. & 0. & 0. \\ -0.222 & -1.6874 & 0.16874 \\ 0. & 0.0586 & 0.0808 \end{bmatrix}$	$\begin{bmatrix} -8.399 & 2.372 & -0.238 \\ 0. & 0. & 0. \\ -0.383 & -2.912 & 0.259 \\ 0. & 0.0717 & 0.0988 \end{bmatrix}$

TABLE A.2

Flight Conditions	Scale L m (ft)	
	Dryden form	von Karman form
Landing h = 60.96 m V = 67.97 m/sec	60.96 (200)	60.96 (200)
Climb h = 1,524 m V = 106.07 m/sec	533.4 (1,750)	762 (2,500)
Cruise h = 3,048 m V = 149.66 m/sec	533.4 (1,750)	762 (2,500)

APPENDIX B

PARAMETERS USED IN FLUTTER ANALYSIS

Generalized Masses

Generalized masses and mass coupling terms which were used in the flutter computations of Section 3.2 are listed in Table B.1.

Determination of Generalized Oscillating Aerodynamic Forces

The generalized oscillating aerodynamic forces used in the flutter computations were based on sectional coefficients for incompressible flow as given in the classical treatment of Reference 15. Values of the following wing parameters are listed in Table B.2 as a function of spanwise station

- s = spanwise station
- b = wing semichord
- a = distance of elastic axis aft of midchord (fraction of semichord)
- c = distance of aileron or DLF hinge line aft of midchord (fraction of semichord)
- e = distance of aileron or DLF leading edge aft of midchord (fraction of semichord)
- Δs_h = aileron spanwise interval
- Δs_{fl} = DLF spanwise interval

Tables B.3 and B.4 list printouts of values of $p = -\frac{1}{3}(1-e^2)^{3/2}$, Theodorsen T-functions, and Kussner Φ-functions corresponding to these parameters which were used in computing sectional aerodynamic forces.

The shapes of the following uncoupled modes which were used as degrees of freedom in analyzing wing flutter are listed in Table B.2.

- $f_w^{(1)}$ = first symmetric wing bending mode shape
- $f_w^{(2)}$ = second symmetric wing bending mode shape
- F_w = first symmetric wing torsion mode shape

No listings are given for aileron and DLF rotations about their respective hinge lines because these rotations were assumed constant along the span. These modes were used in computing generalized aerodynamic forces from the sectional aerodynamic data.

The numerical procedure for computing generalized aerodynamic forces involved dividing the wing span into a number of segments and using a trapezoidal rule integration technique. Table B.2 lists spanwise intervals used in treating the aileron and DLF.

TABLE B.1
GENERALIZED MASSES USED IN FLUTTER CALCULATIONS
(All values are per side)

$gM_{1,1}$	=	4.04829E	02	lbs.	(1800.8 N)
$gM_{1,2}$	=	0.0			
$gM_{1,3}$	=	9.58632E	03	lbs. in.	(1083.1 N.m)
$gM_{1,4}$	=	0.0			
$gM_{1,5}$	=	4.31387E	01	lbs. in.	(4.874 N.m)
$gM_{2,1}$	=	0.0			
$gM_{2,2}$	=	2.42372E	02	lbs.	(1078.1 N)
$gM_{2,3}$	=	1.14736E	04	lbs. in.	(1296.3 N.m)
$gM_{2,4}$	=	0.0			
$gM_{2,5}$	=	2.41963E	00	lbs. in.	(0.273 N.m)
$gM_{3,1}$	=	9.58632E	03	lbs. in.	(1083.1 N.m)
$gM_{3,2}$	=	1.14736E	04	lbs. in.	(1296.3 N.m)
$gM_{3,3}$	=	5.57775E	07	lbs. in.^{2}	(160071 N.m^2)
$gM_{3,4}$	=	2.79523E	03	lbs. in.^{2}	(8.022 N.m^2)
$gM_{3,5}$	=	3.19679E	04	lbs. in.^{2}	(91.742 N.m^2)
$gM_{4,1}$	=	0.0			
$gM_{4,2}$	=	0.0			
$gM_{4,3}$	=	2.79523E	03	lbs. in.^{2}	(8.022 N.m^2)
$gM_{4,5}$	=	2.89500E	03	lbs. in.^{2}	(8.308 N.m^2)
$gM_{4,5}$	=	0.0			
$gM_{5,1}$	=	4.31387E	01	lbs. in.	(4.874 N.m)
$gM_{5,2}$	=	2.41963E	00	lbs. in.	(0.273 N.m)
$gM_{5,3}$	=	3.19679E	04	lbs. in.^{2}	(91.742 N.m^2)
$gM_{5,4}$	=	0.0			
$gM_{5,5}$	=	3.66560E	04	lbs. in.^{2}	(105.2 N.m^2)

Subscript	Generalized Coordinate
1	$h_w^{(1)}$ = 1st sym. wing bending (m)
2	$h_w^{(2)}$ = 2nd sym. wing bending (m)
3	α_w = 1st sym. wing torsion (rad.)
4	δ_a = aileron rotation (rad.)
5	δ_z = DLF rotation (rad.)

TABLE B.2 BASIC PARAMETERS USED IN OSCILLATING AERODYNAMIC FORCE COMPUTATIONS

(distance in inches)

s (in)	b (in)	a	$f_w^{(1)}$	$f_w^{(2)}$	F_w
0.0	8.092999E 01	-2.700000E-01	-6.699997E-02	5.515000E-02	0.0
2.837999E 01	7.812000E 01		-6.527995E-02	5.198000E-02	1.456000E-01
8.837999E 01	7.217000E 01		-4.925000E-02	2.388000E-02	4.709000E-01
1.495000E 02	6.517999E 01		-1.446000E-02	-2.812000E-02	8.832999E-01
2.057500E 02	6.117999E 01		3.566000E-02	-8.504999E-02	8.987000E-01
2.595298E 02	5.584000E 01		1.009000E-01	-1.327000E-01	9.134000E-01
3.085298E 02	5.287000E 01		1.756000E-01	-1.542000E-01	9.270000E-01
3.470298E 02	4.975000E 01		2.470000E-01	-1.429999E-01	9.380000E-01
3.745298E 02	4.750999E 01		3.000000E-01	-1.170000E-01	9.439999E-01
4.012500E 02	4.526999E 01		3.530000E-01	-7.450998E-02	9.484000E-01
4.350000E 02	4.245000E 01		4.407000E-01	1.098000E-02	9.543999E-01
4.780698E 02	3.912000E 01		5.506000E-01	1.610000E-01	9.525000E-01
5.311599E 02	3.481999E 01		7.025999E-01	4.179000E-01	9.737000E-01
5.943699E 02	2.968999E 01		8.963000E-01	7.919000E-01	9.902000E-01
6.275498E 02	2.700000E 01		1.000000E 00	1.000000E 00	1.000000E 00

	AILERON			DLF	
s	Δs_a	e	c	Δs_{fl}	$e = c$
0.0	0.0			0.0	
2.837999E 01	0.0			0.0	
8.837999E 01	0.0			0.0	
1.495000E 02	0.0			0.0	
2.057500E 02	0.0			5.353000E 01	4.432000E-01
2.595298E 02	0.0			5.400000E 01	4.694999E-01
3.085298E 02	0.0			4.400000E 01	4.972000E-01
3.470298E 02	0.0			3.300000E 01	5.221000E-01
3.745298E 02	0.0			2.200000E 01	5.420000E-01
4.012500E 02	0.0			3.146999E 01	5.639000E-01
4.350000E 02	3.800000E 01	4.400000E-01	6.000000E-01	0.0	
4.780698E 02	4.612999E 01	4.400000E-01		0.0	
5.311599E 02	6.006000E 01	4.400000E-01		0.0	
5.943699E 02	6.635999E 01	4.400000E-01		0.0	
6.275498E 02	0.0	4.400000E-01		0.0	

TABLE B.3 COMPUTER PRINTOUT OF SECTIONAL VALUES OF p AND THEODORSEN T-FUNCTIONS
(distance in inches)

S(in)	p	T_1	T_3	T_4
0.0	0.0	0.0	0.0	0.0
2.837999E 01	0.0	0.0	0.0	0.0
8.837999E 01	0.0	0.0	0.0	0.0
1.495000E 02	0.0	0.0	0.0	0.0
2.057500E 02	-2.401000E-01	-1.537000E-01	-8.149999E-02	-7.140999E-01
2.595298E 02	-2.294000E-01	-1.452000E-01	-6.750000E-02	-6.576000E-01
3.085298E 02	-2.176999E-01	-1.277000E-01	-5.480000E-02	-6.188999E-01
3.470298E 02	-2.068000E-01	-1.127999E-01	-4.390000E-02	-5.761999E-01
3.745298E 02	-2.004000E-01	-1.016000E-01	-3.730000E-02	-5.425000E-01
4.012500E 02	-1.877000E-01	-9.029995E-02	-3.110000E-02	-5.059000E-01
4.360000E 02	-2.413999E-01	-1.659000E-01	-8.309996E-02,	-7.201000E-01
4.780698E 02	-2.413999E-01	-1.659000E-01	-8.309996E-02	-7.201000E-01
5.311599E 02	-2.413999E-01	-1.659000E-01	-8.309996E-02	-7.201000E-01
5.943699E 02	-2.413999E-01	-1.659000E-01	-8.309996E-02	-7.201000E-01
6.275498E 02	-2.413999E-01	-1.659000E-01	-8.309996E-02	-7.201000E-01

T_5	T_7	T_{10}	T_{11}	T_{12}
0.0	0.0	0.0	0.0	0.0
0.0	0.0	0.0	0.0	0.0
0.0	0.0	0.0	0.0	0.0
0.0	0.0	0.0	0.0	0.0
-1.155700E 00	9.900000E-03	2.007799E 00	1.521700E 00	9.359998E-02
-1.053399E 00	1.180000E-02	1.964999E 00	1.417299E 00	8.209997E-02
-9.357000E-01	1.320000E-02	1.917899E 00	1.309699E 00	7.189995E-02
-8.494999E-01	1.380000E-02	1.874399E 00	1.215300E 00	6.299996E-02
-7.931000E-01	1.420000E-02	1.838400E 00	1.166699E 00	5.650000E-02
-7.211000E-01	1.400000E-02	1.797400E 00	1.061700E 00	4.990000E-02
-1.168799E 00	9.599999E-03	2.013200E 00	1.534599E 00	9.449995E-02
-1.168799E 00	9.599999E-03	2.013200E 00	1.534699E 00	9.449995E-02
-1.168799E 00	9.599999E-03	2.013200E 00	1.534699E 00	9.449995E-02
-1.168799E 00	9.599999E-03	2.013200E 00	1.534699E 00	9.449995E-02
-1.168799E 00	9.599999E-03	2.013200E 00	1.534699E 00	9.449995E-02

TABLE B.4 COMPUTER PRINTOUT OF SECTIONAL VALUES OF KÜSSNER Φ -FUNCTIONS
(distance in inches)

S (in)	Φ_1	Φ_2	Φ_3	Φ
0.0	0.0	0.0	0.0	0.0
2.837999E 01	0.0	0.0	0.0	0.0
8.837999E 01	0.0	0.0	0.0	0.0
1.495000E 02	0.0	0.0	0.0	0.0
2.057500E 02	2.007700E 00	1.521299E 00	7.140000E-01	1.293699E 00
2.595298E 02	1.964999E 00	1.417450E 00	5.675700E-01	1.297400E 00
3.085298E 02	1.917899E 00	1.362009E 00	6.188800E-01	1.299000E 00
3.470298E 02	1.874399E 00	1.215710E 00	5.762500E-01	1.298200E 00
3.745298E 02	1.838400E 00	1.141629E 00	5.405300E-01	1.295899E 00
4.012500E 02	1.797400E 00	1.061419E 00	5.058399E-01	1.291499E 00
4.360000E 02	2.013200E 00	1.534699E 00	7.201000E-01	1.293099E 00
4.780698E 02	2.013200E 00	1.534699E 00	7.201000E-01	1.293099E 00
5.311599E 02	2.013200E 00	1.534699E 00	7.201000E-01	1.293099E 00
5.943699E 02	2.013200E 00	1.534699E 00	7.201000E-01	1.293099E 00
6.275498E 02	2.013200E 00	1.534699E 00	7.201000E-01	1.293099E 00

Φ_6	Φ_8	Φ_{10}	Φ_{17}	Φ_{31}
0.0	0.0	0.0	0.0	0.0
0.0	0.0	0.0	0.0	0.0
0.0	0.0	0.0	0.0	0.0
0.0	0.0	0.0	0.0	0.0
2.388300E 00	9.328997E-02	2.781799E-01	1.155299E 00	2.150300E-01
2.252899E 00	8.230996E-02	2.583600E-01	1.053399E 00	1.991400E-01
2.108600E 00	7.187998E-02	2.372900E-01	9.496700E-01	1.826700E-01
1.979899E 00	6.318998E-02	2.188100E-01	8.513300E-01	1.685500E-01
1.875999E 00	5.657000E-02	2.042100E-01	7.910200E-01	1.575800E-01
1.762500E 00	4.972000E-02	1.883200E-01	7.208500E-01	1.458200E-01
2.405700E 00	9.454000E-02	2.808599E-01	1.168799E 00	2.172000E-01
2.405700E 00	9.454000E-02	2.808599E-01	1.168799E 00	2.172000E-01
2.405700E 00	9.454000E-02	2.808599E-01	1.168799E 00	2.172000E-01
2.405700E 00	9.454000E-02	2.808599E-01	1.168799E 00	2.172000E-01
2.405700E 00	9.454000E-02	2.808599E-01	1.168799E 00	2.172000E-01

Φ_{32}	Φ_{35}	Φ_{36}	Φ_{37}
0.0	0.0	0.0	0.0
0.0	0.0	0.0	0.0
0.0	0.0	0.0	0.0
0.0	0.0	0.0	0.0
1.212999E 00	1.606899E 00	2.157200E 00	5.764100E-01
1.136000E 00	1.559199E 00	1.973900E 00	5.006000E-01
1.055099E 00	1.505500E 00	1.786300E 00	4.599100E-01
9.839600E-01	1.455000E 00	1.625500E 00	3.684900E-01
9.274800E-01	1.412600E 00	1.499000E 00	3.249100E-01
8.658700E-01	1.363799E 00	1.367900E 00	2.810300E-01
1.223000E 00	1.612800E 00	2.181199E 00	5.865900E-01
1.223000E 00	1.612800E 00	2.181199E 00	5.865900E-01
1.223000E 00	1.612800E 00	2.181199E 00	5.865900E-01
1.223000E 00	1.612800E 00	2.181199E 00	5.865900E-01
1.223000E 00	1.612800E 00	2.181199E 00	5.865900E-01

APPENDIX C

MANEUVER LOAD CONTROL CALCULATIONS

To obtain the effectiveness of the various control devices for maneuver load control (MLC) the lift effectiveness and lift distributions of each control surface had to be calculated. Standard DATCOM (Reference 37) methods were used.

The surfaces investigated were the ailerons (operated collectively), the DLF, and inboard plain flaps (replacing the present Fowlers). The location of each is (η = normalized span location)

ailerons, η = 1.0 to .64, 21% chord

DLF, η = .64 to .22, 26% chord

inboard flap, η = .22 to 0.0, 26% chord

The lift effectiveness was first obtained from DATCOM Section 6.1.4.1-1

$$C_{L_{\delta_i}} = \frac{\Delta C_\ell}{\delta_i}\left(\frac{C_{L_\alpha}}{C_{\ell_\alpha}}\right)\left[\frac{(\alpha_\delta)_{C_L}}{(\alpha_\delta)_{C_\ell}}\right] K_b$$

where

$$\frac{\Delta C_\ell}{\delta_i} = \left[\frac{C_{\ell_\delta}}{(C_{\ell_\delta})_{theory}}\right](C_{\ell_\delta})_{theory}\ K'$$

(see DATCOM for definitions)

$$\frac{\Delta C_\ell}{\delta_i} = [.83](3.7)(.95) = 2.92 \qquad \text{(aileron)}$$

$$= [.84](4.2)(.95) = 3.35 \qquad \text{(DLF)}$$

$$= [.84](4.2)(.95) = 3.35 \qquad \text{(inboard flap)}$$

$$C_{L_{\delta_i}} = (2.92)\left(\frac{5.4}{6.5}\right)[1.04](.21) = .53\ \frac{1}{rad} \quad \text{(ailerons)}$$

$$= (3.35)\left(\frac{5.4}{6.5}\right)[1.04](.47) = 1.36^{*}\ \frac{1}{rad} \quad \text{(DLF)}$$

$$= (3.35)\left(\frac{5.4}{6.5}\right)[1.04](.32) = .90\ \frac{1}{rad} \quad \text{(inboard flaps)}$$

* this value of $C_{L_{\delta_{DLF}}}$ agrees with the value given in Reference 3 for $C_{L_{\delta_{DLF}}}$ linearized about $C_{L_{\delta_{DLF}}}$ = 5 degrees. Therefore, it is believed that this DATCOM method yields reasonable results.

The incremental lift distribution due to deflections of the individual controllers was then determined. Using graphical techniques from DATCOM Section 6.1.5, Figure C.1 shows the full lift distribution for the entire wing (due to α) and the portion of the whole that would be due to each surface. A planimeter was used to measure equal areas to determine the center of lift at η = .44 for the lift due to α . Figure C.2 shows the lift distributions for the individual control surfaces. Again a planimeter was used to find the lift centers at

η = .71 (aileron)
η = .41 (DLF)
η = .18 (inboard flaps)

The wing root bending moment due to each controller is then calculated from the lift effectiveness times the moment arm:

$$WRBM_i = C_{L_{\delta_i}} \cdot \eta_{\substack{Lift \\ Center}} \cdot \bar{q} S \frac{b}{2} \cdot \delta_i$$

WRBM	= (.53) (34 ft)	(aileron)
	= (1.36) (19.6 ft)	(DLF)
	= (.90) (8.6 ft)	(inboard flap)

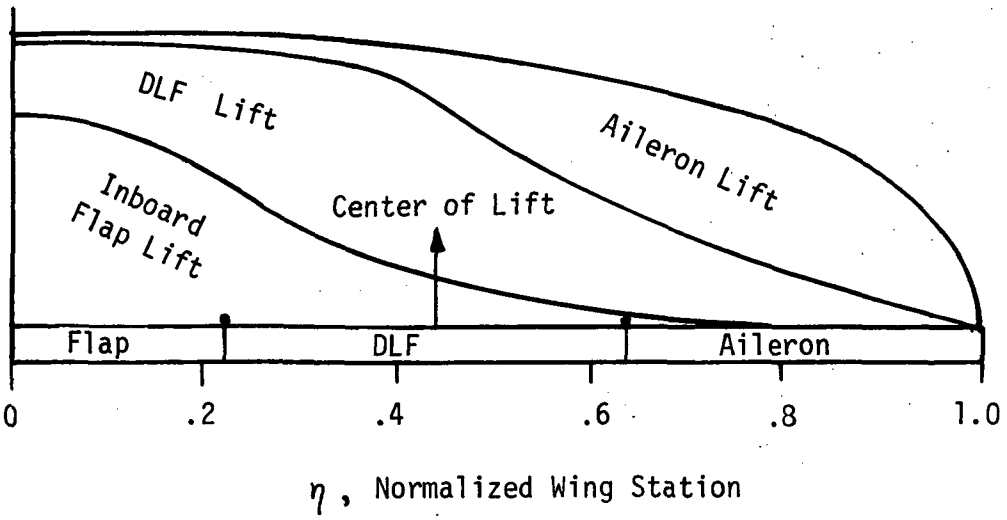

Figure C.1 LIFT DISTRIBUTION FOR WHOLE WING

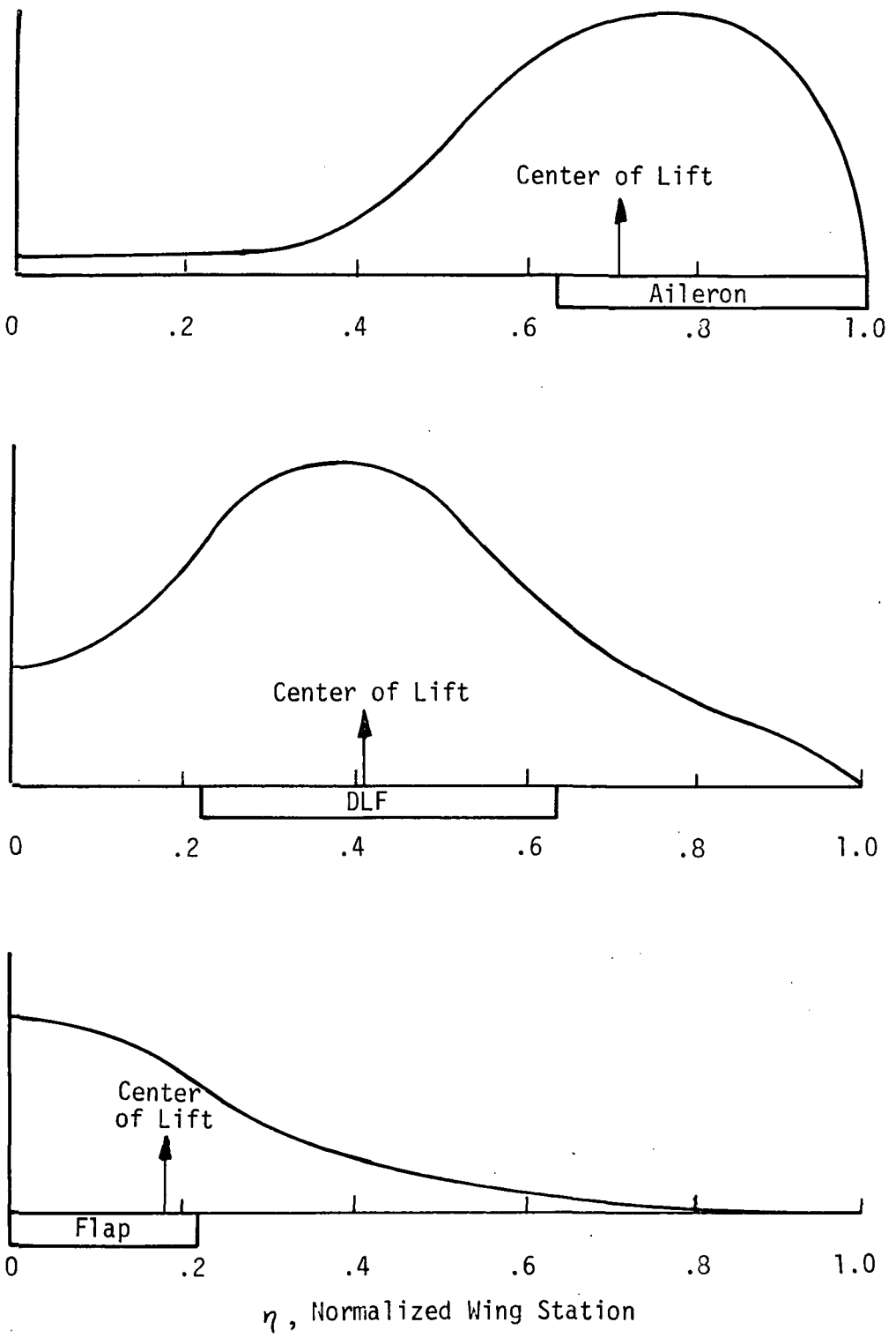

Figure C.2 LIFT DISTRIBUTIONS FOR SEPARATE SURFACES

APPENDIX D

CALCULATION OF AERODYNAMIC MATRIX F

The description and assumptions applicable to the structural mode equations are contained in Section 4.1 and will not be repeated here. This appendix will document in detail the calculation of the aerodynamic matrix F in the structural mode equations.

As outlined in Section 4.1 the matrix F can be written in the following way

$$\overset{N\times 1}{F} = \left[\overset{N\times M}{\phi^{T}_{1/4}} \;\vdots\; \overset{N\times M}{\phi'^{T}}\right]\left[\begin{array}{c}\overset{M\times 1}{Z}\\ \hdashline M\end{array}\right]_{M\times 1} = \overset{N\times N}{F_0}\;\overset{N\times 1}{\xi} + F_1\dot{\xi} + F_2\ddot{\xi}$$

where M = Number of strips

N = Number of normal modes

In the development to follow, the expressions for Z, M, α first introduced in Section 4.1 in subscript notation are generalized to matrix notation. Evaluation of F_0, F_1 and F_2 is accomplished by expressing Z and M in terms of ξ, $\dot{\xi}$ and $\ddot{\xi}$ by making the substitutions for $\alpha_{3/4}$ and θ. Expressing Z and M in matrix form yields the following representation

$$\overset{M\times 1}{\left[Z\right]} = -\frac{1}{2}\rho u_0^2 \overset{M\times M}{\left[SCL\right]}\overset{M\times 1}{\left[\alpha_{3/4}\right]}$$

$$\left[M\right] = \frac{1}{4}\rho u_0 \overset{M\times M}{\left[SCQ\right]}\overset{M\times 1}{\left[\dot{\theta}\right]}$$

where

$\left[\alpha_{3/4}\right]$ is the matrix of angles of attack at each strip $[M\times 1]$

$\left[\theta\right]$ is the matrix of total pitch angles at each strip $[M\times 1]$ and should not be confused with the rigid body pitch angle $\xi_2 = \theta$

$\left[SCL\right]$ is a diagonal matrix whose elements are defined as $SCL_{ii} = S_i C_{L_{\alpha_i}}$, $i = 1, M$, $[M\times M]$

$[SCQ]$ is a diagonal matrix whose elements are

defined as $SCQ_{ii} = S_i C_i C_{m_q}$, $M \times M$, $[M \times M]$

For the case of no downwash the pitch angle matrix, translation matrix and angle of attack matrix can be written as follows

$$[\theta] = [\phi'][\xi]$$

$$[h_{3/4}] = [\phi_{3/4}][\xi]$$

$$[\alpha_{3/4}] = [\theta] + \frac{1}{u_o}[\dot{h}_{3/4}] = [\phi'][\xi] + \frac{1}{u_o}[\phi_{3/4}][\dot{\xi}]$$

Since we have assumed there is no bending of the local chord lines, the slope of the mode shapes will be equal everywhere on a strip chord. Therefore

$$[\phi'_{3/4}] = [\phi'_{1/4}] = [\phi']$$

For the case of strips p_i (i = 1, 2....number of strips experiencing downwash) experiencing downwash from generating surface q , the expressions for the angle of attack of strip p_i must be modified as indicated in Section 4.1.

$$\alpha_{p_i} = \sum_{j=1}^{N} \underset{p_i j}{\phi'} \xi_j + \frac{1}{u_o} \sum_{j=1}^{N} \underset{p_i j}{\phi_{3/4}} \dot{\xi}_j$$

$$- \frac{d\epsilon}{d\alpha}\left[\sum_{j=1}^{N} \underset{qj}{\phi'} \xi_j + \frac{1}{u_o} \sum_{j=1}^{N} \underset{qj}{\phi_{3/4}} \dot{\xi}_j\right]$$

$$+ \frac{d\epsilon}{d\alpha} \frac{l_d}{u_o}\left[\sum_{j=1}^{N} \underset{qj}{\phi'} \dot{\xi}_j + \frac{1}{u_o} \sum_{j=1}^{N} \underset{qj}{\phi_{3/4}} \ddot{\xi}_j\right]$$

Note that the differences between this representation and the representation for strips not experiencing downwash are the last four terms. In the general expression for $[\alpha_{3/4}]$ only rows p_i are affected by downwash and they will have terms which describe the mode shapes at the downwash generating surface q. In matrix notation $[\alpha_{3/4}]$ can be written

$$\underset{M\times 1}{[\alpha_{3/4}]} = \underset{M\times N}{[\phi']}\underset{N\times 1}{[\xi]} + \frac{1}{u_o}\underset{M\times N}{[\phi_{3/4}]}\underset{N\times 1}{[\dot{\xi}]}$$

$$- \frac{d\epsilon}{d\alpha}\underset{M\times M}{[\delta_{p_i q}]}\underset{M\times N}{[\phi']}\underset{N\times 1}{[\xi]} - \frac{d\epsilon}{d\alpha}\frac{1}{u_o}\underset{M\times M}{[\delta_{p_i q}]}\underset{M\times N}{[\phi_{3/4}]}\underset{N\times 1}{[\dot{\xi}]}$$

$$+ \frac{d\epsilon}{d\alpha}\frac{\ell_d}{u_o}\underset{M\times M}{[\delta_{p_i q}]}\underset{M\times N}{[\phi']}\underset{N\times 1}{[\dot{\xi}]} + \frac{d\epsilon}{d\alpha}\frac{\ell_d}{u_o^2}\underset{M\times M}{[\delta_{p_i q}]}\underset{M\times N}{[\phi_{3/4}]}\underset{N\times 1}{[\ddot{\xi}]}$$

where $[\delta_{p_i q}]$ is an $M \times M$ matrix whose elements are defined as follows

$$\delta_{jk} = 1 \quad \text{if} \quad j = p_i \quad \text{and} \quad k = q$$

otherwise $\delta_{jk} = 0$

Using the relations for F, Z and M

$$F = -\frac{1}{2}\rho u_o^2 [\phi_{1/4}]^T [SCL][\phi'][\xi] + \frac{1}{2}\rho u_o^2 \frac{d\epsilon}{d\alpha}[\phi_{1/4}]^T [SCL][\delta_{p_i q}][\phi']\xi$$

$$- \frac{1}{2}\rho u_o [\phi_{1/4}]^T [SCL][\phi_{3/4}]\dot{\xi} + \frac{1}{2}\rho u_o \frac{d\epsilon}{d\alpha}[\phi_{1/4}]^T [SCL][\delta_{p_i q}][\phi_{3/4}][\dot{\xi}]$$

$$- \frac{1}{2}\rho u_o \frac{d\epsilon}{d\alpha}\ell_d [\phi_{1/4}]^T [SCL][\delta_{p_i q}][\phi'][\dot{\xi}] + \frac{1}{4}\rho u_o [\phi']^T [SCQ][\phi'][\dot{\xi}]$$

$$- \frac{1}{2}\rho \frac{d\epsilon}{d\alpha}\ell_d [\phi_{1/4}]^T [SCL][\delta_{p_i q}][\phi_{3/4}][\ddot{\xi}]$$

by collecting similar derivatives of ξ it is possible to write

$$F = F_0 \xi + F_1 \dot{\xi} + F_2 \ddot{\xi}$$

where

$$F_0 = -\frac{1}{2}\rho u_o^2 \left[\phi_{1/4}\right]^T \left[SCL\right]\left[\phi'\right] + \frac{1}{2}\rho u_o^2 \frac{d\epsilon}{d\alpha}\left[\phi_{1/4}\right]^T \left[\quad\right]\left[\delta_{p_i q}\right]\left[\phi'\right]$$

$$F_1 = -\frac{1}{2}\rho u_o^2 \left[\phi_{1/4}\right]^T \left[SCL\right]\left[\phi_{3/4}\right] + \frac{1}{2}\rho u_o \frac{d\epsilon}{d\alpha}\left[\phi_{1/4}\right]^T \left[\quad\right]\left[\delta_{p_i q}\right]\left[\phi_{3/4}\right]$$

$$-\frac{1}{2}\rho u_o \frac{d\epsilon}{d\alpha} l_d \left[\phi_{1/4}\right]^T \left[SCL\right]\left[\delta_{p_i q}\right]\left[\phi'\right] + \frac{1}{4}\rho u_o \left[\phi'\right]^T \left[SCQ\right]\left[\phi'\right]$$

$$F_2 = -\frac{1}{2}\rho \frac{d\epsilon}{d\alpha} l_d \left[\phi_{1/4}\right]^T \left[SCL\right]\left[\delta_{p_i q}\right]\left[\phi_{3/4}\right]$$

In the derivation of the equations of motion the structural mode frequencies, structural damping generalized masses and additional constants are listed in Table D.1. The six tail strips were influenced by downwash generated by the innermost wing strip. The equations of motion for the three flight conditions are listed in Table D.2. The form of these equations is as shown in Section 4.1.

$$\ddot{\xi} = A\dot{\xi} + B\xi + Cu$$

where

$$A = \left[I - M^{-1}F_2\right]^{-1}\left[M^{-1}F_0 - \left[\omega^2\right]\right]$$

$$B = \left[I - M^{-1}F_2\right]^{-1}\left[M^{-1}F_1 - \left[D\right]\right]$$

$$C = \left[I - M^{-1}F_2\right]^{-1}\left[M^{-1}Gu\right]$$

$$\xi^T = \left[\int w, \theta, \xi_3, \xi_4, \xi_5, \xi_6, \xi_7\right]$$

$$u^T = \left[\delta_y, \delta_{a_R}, \delta_e, w_g\right]$$

δ_{γ} = Direct lift flap deflection, (rad)

δ_{a_R} = Right aileron deflection, (rad)

δ_e = Elevator deflection, (rad)

w_g = $\hat{z}$ axis gust velocity, (m/sec or ft/sec)

TABLE D.1

Primary Motion	$[M]$ Generalized Mass (Per One Half Aircraft)	$[\omega^2]$ Structural Frequency rad/sec	$[D]$ Structural Damping
Rigid Translation	11,784.6 Kg (807.5 slug	0	0
Rigid Rotation	360,647.5 Kg-m^2 (266,000 slug ft^2)	0	0
2FB	1,391.24 Kg (95.33 slug)	104.2	.03
2WB	31,779.68 Kg (2,177.6 slug)	51.9	.03
1WB	62,323.25 Kg (4,270.5 slug)	17.62	.03
1FB	59,268.75 Kg (4,061.2 slug)	34.93	.03
1WT	190,537.96 Kg (13,056.0 slug)	28.80	.03
1HTB	14,164.84 Kg (970 6 slug)	43.32	.03

Note structural damping is given in a form defined for the following homogeneous second order system $\ddot{x} + g\omega\dot{x} + \omega^2 = 0$

Miscellaneous Constants

ℓ_d = 11.61 m (38.1 ft) $\quad d\epsilon/d\alpha$ = .5

Control Surface Lift Effectiveness and Corresponding Reference Area.

δ	C_{L_δ}	S_δ
Direct Lift Flap	1.32	460.
Right Aileron	.4855	460.
Elevator	1.988	126.

Configuration	Velocity m/sec (ft/sec)	Atmospheric Density Kg/m^3 (slug/ft^3)	Scale Length for Atmospheric Turbulence m (ft)	Altitude m (ft)
LANDING	67.97 (223)	1.2256 (0.002378)	60.96 (200)	60.96 (200)
CLIMB	106.07 (348)	1.0560 (0.002049)	762 (2500)	1524 (5000)
CRUISE	149.66 (491)	0.9045 (0.001755)	762 (2500)	3048 (10000)

TABLE D.2

FLEXIBLE EQUATIONS OF MOTION, CLIMB

(Unit in rad and ft/sec)

A =

-1.28189E+00	3.37040E+02	-2.32954E-02	-7.70317E-01	3.30960E+00	1.27599E+00	3.90884E+00	-6.52183E-01
-2.12281E-03	-9.07569E-01	-6.49039E-03	1.51232E-02	4.14232E-03	-8.31541E-02	6.50229E-02	-6.37902E-02
6.31078E-01	9.29409E+00	-3.39911E+00	-1.76368E-01	1.10259E+00	-9.61386E-01	-2.98242E-01	-1.09445E+00
-2.52323E-01	-1.76917E+00	-6.00805E-02	-5.21999E+00	2.77770E+00	-2.46996E+00	3.22254E+00	-6.42844E-02
6.15836E-01	1.05742E+00	-3.91024E-02	1.59218E+00	-6.57280E+00	1.06911E+00	-4.52968E+00	-6.14406E-01
-5.32408E-02	-6.49562E+00	-6.94717E-02	-1.15186E+00	2.39684E+00	-4.01999E+00	2.43415E+00	-6.88623E-01
7.03373E-02	1.75300E+00	1.14687E-02	5.08642E-01	-1.00580E+00	7.33461E-01	-2.03551E+00	6.14284E-02
-1.69256E-01	-2.71186E+01	-4.35191E-01	4.70475E-01	-2.90196E+00	-3.21710E+00	9.64140E-01	-8.77995E+00

B =

0.0	0.0	2.13363E+01	2.09315E+01	8.93344E+00	1.28975E+02	1.97412E+02	-1.22341E+01
0.0	0.0	2.69930E+00	5.30053E+00	-1.08387E-01	-3.32582E+00	1.91853E+00	1.38602E-01
0.0	0.0	-1.08826E+04	-5.03150E+01	-3.25248E+00	1.91351E+01	-2.07552E+00	-1.46896E+00
0.0	0.0	6.18326E-01	-2.69108E+03	1.54216E+00	1.45803E+01	1.72840E+01	-9.79415E-01
0.0	0.0	4.82871E+00	2.75963E+01	-3.15655E+02	-1.23210E+02	-1.53597E+02	1.10603E+01
0.0	0.0	2.57653E+01	4.35355E+01	-3.07217E-01	-1.23520E+03	3.45034E+01	-3.59127E-01
0.0	0.0	-6.23457E+00	-8.89028E+00	-4.62870E-01	-3.38903E+00	-8.44280E+02	6.99416E-01
0.0	0.0	8.98278E+01	1.73785E+02	-2.77424E+00	-1.23359E+02	2.76880E+01	-1.87044E+03

C =

-9.34488E+01	-3.39744E+01	-3.86750E+01	-1.28189E+00
-3.35005E-01	4.06614E-02	-4.45757E+00	-2.12281E-03
1.10396E+01	-2.79397E+00	5.82901E+01	6.31078E-01
6.91698E+01	-4.80501E+01	-1.04737E+01	-2.52323E-01
4.42220E+01	8.20317E-01	-1.49157E+01	6.15836E-01
2.87810E+01	-3.19920E+01	-4.62605E+01	-5.32408E-02
-1.79785E+00	1.50924E+01	1.03286E+01	7.03373E-02
-3.70138E+01	4.27473E+01	-2.01191E+02	-1.69256E-01

TABLE D.2 (Cont'd)

FLEXIBLE EQUATIONS OF MOTION, CRUISE

(Unit in rad and ft/sec)

A =

-1.55024E+00	4.77755E+02	-3.00908E-02	-9.43068E-01	3.99701E+00	1.55107E+00	4.72362E+00	-7.88476E-01
-2.69774E-03	-1.09684E+00	-8.07542E-03	1.68213E-02	4.70023E-03	-9.94052E-02	7.85649E-02	-7.71284E-02
7.64178E-01	1.12324E+01	-3.45336E+00	-1.96262E-01	1.33600E+00	-1.17439E+00	-3.60258E-01	-1.32216E+00
-3.05083E-01	-2.13807E+00	-7.28811E-02	-5.98537E+00	3.35642E+00	-2.98361E+00	3.89435E+00	-7.77334E-02
7.43812E-01	1.27766E+00	-4.79734E-02	1.91960E+00	-7.83381E+00	1.29535E+00	-5.47404E+00	-7.42616E-01
-6.54731E-02	-7.85036E+00	-8.59405E-02	-1.40445E+00	2.89390E+00	-4.63031E+00	2.94149E+00	-8.32522E-01
8.52683E-02	2.11859E+00	1.43280E-02	6.17618E-01	-1.21487E+00	8.84182E-01	-2.27972E+00	7.43145E-02
-2.08946E-01	-3.27743E+01	-5.33633E-01	5.20161E-01	-3.51711E+00	-3.85170E+00	1.16468E+00	-1.03407E+01

B =

0.0	0.0	2.12357E+01	4.67384E+00	1.38890E+01	2.34929E+02	3.33608E+02	-2.08496E+01
0.0	0.0	2.79072E+00	5.32715E+00	-3.45489E-01	-3.87411E+00	2.91327E+00	2.37555E-01
0.0	0.0	-1.08792E+04	-4.27550E+01	-3.68207E+00	1.17893E+01	6.12519E-01	-2.51893E+00
0.0	0.0	-1.09739E+00	-2.69371E+03	2.43863E+00	2.69938E+01	2.90450E+01	-1.66847E+00
0.0	0.0	2.61651E+00	3.55498E+01	-3.19812E+02	-2.04511E+02	-2.62998E+02	1.89620E+01
0.0	0.0	2.84214E+01	4.24653E+01	-1.89940E+00	-1.23046E+03	5.57661E+01	-6.01803E-01
0.0	0.0	-5.97336E+00	-7.66882E+00	-4.64891E-01	-9.40497E+00	-3.54021E+02	1.19007E+00
0.0	0.0	9.28912E+01	1.72876E+02	-1.00756E+01	-1.50567E+02	3.53022E+01	-1.86604E+03

C =

-1.59298E+02	-5.80118E+01	-6.58971E+01	-1.55024E+00
-5.66696E-01	5.93504E-02	-7.59491E+00	-2.69774E-03
1.87709E+01	-4.64815E+00	9.93241E+01	7.64178E-01
1.17944E+02	-8.19403E+01	-1.78517E+01	-3.05083E-01
7.54151E+01	1.36775E+00	-2.54150E+01	7.43812E-01
4.91119E+01	-5.46337E+01	-7.88296E+01	-6.54731E-02
-3.07454E+00	2.57535E+01	1.75998E+01	8.52683E-02
-6.29608E+01	7.25548E+01	-3.42859E+02	-2.08946E-01

TABLE D.2 (Concl'd)

FLEXIBLE EQUATIONS OF MOTION, LANDING
(Unit in rad and ft/sec)

A =

-9.52575E-01	2.14849E+02	-1.50928E-02	-5.60814E-01	2.46357E+00	9.40067E-01	2.90772E+00	-4.84799E-01
-1.48745E-03	-6.74909E-01	-4.55987E-03	1.26907E-02	3.34817E-03	-6.29039E-02	4.84448E-02	-4.74135E-02
4.66272E-01	6.91145E+00	-3.33221E+00	-1.47907E-01	8.16888E-01	-7.02654E-01	-2.22816E-01	-8.14252E-01
-1.87543E-01	-1.31567E+00	-4.43645E-02	-4.27943E+00	2.06607E+00	-1.83818E+00	2.39669E+00	-4.77764E-02
4.58277E-01	7.86534E-01	-2.82525E-02	1.18857E+00	-5.02281E+00	7.91793E-01	-3.36843E+00	-4.56847E-01
-3.88136E-02	-4.83037E+00	-4.93801E-02	-8.44285E-01	1.78480E+00	-3.26732E+00	1.81101E+00	-5.11895E-01
5.21254E-02	1.30360E+00	7.99035E-03	3.75360E-01	-7.48549E-01	5.47616E-01	-1.73542E+00	4.56296E-02
-1.22839E-01	-2.01664E+01	-3.14767E-01	3.97913E-01	-2.14927E+00	-2.42789E+00	7.19936E-01	-6.86180E+00

B =

0.0	0.0	2.23681E+01	3.49743E+01	5.34666E+00	4.94072E+01	9.65180E+01	-5.84145E+00
0.0	0.0	2.74593E+00	5.51679E+00	7.86614E-02	-3.02755E+00	1.20611E+00	6.47156E-02
0.0	0.0	-1.08664E+04	-5.86651E+01	-3.06141E+00	2.58502E+01	-4.37355E+00	-6.84545E-01
0.0	0.0	2.02802E+00	-2.68885E+03	8.89701E-01	5.23519E+00	8.58347E+00	-4.68339E-01
0.0	0.0	6.82601E+00	2.24232E+01	-3.12533E+02	-6.31896E+01	-7.22938E+01	5.26676E+00
0.0	0.0	2.47737E+01	4.63507E+01	9.69187E-01	-1.23965E+03	1.89413E+01	-1.82597E-01
0.0	0.0	-5.91720E+00	-1.02735E+01	-4.83624E-01	1.29668E+00	-8.37101E+02	3.36013E-01
0.0	0.0	9.13626E+01	1.82311E+02	3.01301E+00	-1.06778E+02	2.29026E+01	-1.87372E+03

C =

-4.45461E+01	-1.61648E+01	-1.84456E+01	-9.52575E-01
-1.61063E-01	2.25027E-02	-2.12604E+00	-1.48745E-03
5.27747E+00	-1.36775E+00	2.77990E+01	4.66272E-01
3.29621E+01	-2.28952E+01	-4.99342E+00	-1.87543E-01
2.10702E+01	4.00621E-01	-7.11363E+00	4.58277E-01
1.37039E+01	-1.52195E+01	-2.20609E+01	-3.88136E-02
-8.53942E-01	7.18617E+00	4.92575E+00	5.21254E-02
-1.76864E+01	2.04758E+01	-9.59379E+01	-1.22839E-01

REFERENCES

1. NASA Symposium on Advanced Control and Its Potential for Future Transport Aircraft, July 1974.

2. Hood, R.V. : A Summary of the Application of Active Controls Technology in the ATT System Studies. Paper presented at the NASA Symposium on Advanced Control and Its Potential for Future Transport Aircraft, July 1974.

3. Reynolds, P.A., et al. : Capability of the Total In-Flight Simulator (TIFS). AFFDL TR-72-39, July 1972.

4. Notess, C.B. : The Effects of Atmospheric Turbulence Upon Flight at Low Altitude and High Speed. Cornell Aeronautical Laboratory FDM No. 325, October 1961.

5. Davis, H.M. and Swaim, R.L. : Controlling Dynamic Response in Rough Air. AIAA Paper No. 66-997, November 1966.

6. Wykes, J.H. : Structural Dynamic Stability Augmentation and Gust Alleviation of Flexible Aircraft. AIAA Paper No. 68-1067, October 1968.

7. Chalk, C.R., et al. : Background Information and User Guide for MIL-F-8785B(ASG). AFFDL TR-69-72, August 1969.

8. Swaim, R.L. : Aircraft Elastic Mode Control. J. of Aircraft, pp 65-71, Vol. 8, No. 2, February 1971.

9. Conner, D.W. and Thompson, G.O. : Active Controls for Ride Smoothing. Paper presented at the Symposium on Advanced Control Technology and Its Potential for Future Transport Aircraft, Los Angeles, California, July 9-11, 1974.

10. Reynolds, P.A. and Pruner, J.R. : The Total In-Flight Simulator (TIFS) - A New Aircraft Design Tool. AIAA Paper No. 71-794, July 1971.

11. Hodges, Garold, E. : Active Flutter Suppression....B-52 Controls Configured Vehicle AIAA Paper No. 73-322.

12. Beals, V. and Targott, W.P. : Control Surface Oscillatory and Stationary Aerodynamics Coefficients Measured on Rectangular Wings of Low Aspect Ratio. WADC TR 53-64, April 1953.

13. DeSanto, D.F. and Grace, J.M. : Three-Dimensional Flutter Analysis of Wing/DLF/Aileron System Reciprocating-Engine TIFS. TIFS Memo No. 212, 17 August 1968.

14. DeSanto, D.F. : Three-Dimensional Flutter Analysis of Wing/DLF/SFS/ Aileron System - Air Transport TIFS. CTIFS Memo No. 157, 2 April 1969.

15. Smilg, B. and Wasserman, L.S. : Application of Three-Dimensional Flutter Theory to Aircraft Structures. Army Air Force Technical Report No. 4798, July 9, 1942.

16. Scanlon, R.H. and Rosenbaum, K. : Introduction to the Study of Aircraft Vibration and Flutter. MacMillen, New York, 1951.

17. Oral Briefing at NASA, November 19, 1974.

18. Nissim, E. : Flutter Suppression Using Active Controls Based on the Concept of Aerodynamic Energy. NASA TN D-6199, 1971.

19. Doggett, Robert V., Jr., Abel, Irving, and Ruhlin, Charles L. : Some Experiences Using Wind-Tunnel Models in Active Control Studies. Presented at the Symposium on Advanced Control Technology and Its Potential for Future Transport Aircraft, July 1974.

20. Morse, A.S., and Wonham, W.M. : Status of Non-Integrating Control. IEEE Trans. on AC, pp 568-581, Vol. A.C. -16, No. 6, December 1971.

21. Falb, P.L. and Wolovich, W.A. : Decoupling in the Design and Synthesis of Multivariable Control Systems. IEEE Trans., Vol. A.C. -12, pp 651-659, No. 6, December 1967.

22. Chen, R.T.N. and Mesiah, C.L. : Preliminary Design of a Direct Velocity Control System for the X-22A Aircraft in Hover and in Transition. X-22A T.M. No. 73, 8 April 1974.

23. Chalk, C.R., et al. : Revisions to MIL-F-8785B(ASG) proposed by Cornell Aeronautical Laboratory, Inc. Under Contract No. F33615-71-C-1254. AFFDL-TR-72-41, April 1973.

24. Chen, R.T.N. , Newell, F.D. and Schelhorn, A.E.: Development of an Automatic Departure Prevention System and Stall Inhibitor for Fighter Aircraft. AFFDL-TR-73-29, April 1973.

25. Stall/Post Stall/Spin Symposium. Sponsored by ASD/AFFDL, Wright Patterson AFB, Ohio, 15-17 December 1971.

26. Bull, G. : Investigation of Lateral Stability at Stall. Final Report No. TB-679-F-12, WADC TR 54-498, 18 February 1954.

27. Schuler, J.M. : Theoretical Development of an Automatic Control System for Stabilizing the Large Uncontrolled Motions of Airplanes. CAL Report No. TB-1132-F-1, April 1958.

28. Rubertus, D.P. : Twead Control Augmentation System. Paper presented at the National Aerospace Electronics Conference, Dayton, Ohio, 15-17 May 1972.

29. Thomas, H.H.B.M. : On Problems of Flight Over an Extended Angle of Attack Range. Aeronautical Journal, pp 412-423, August 1973.

30. Lamers, J.P. : Design for Departure Prevention in the YF-16. AIAA Paper No. 74-794, August 1974.

31. Deazley, W.R. : The Development and Flight Evaluation of a Mechanically Implemented Normal Acceleration Limiting System. WADC TR-58-504, November 1958.

32. Vehicle Design Considerations for Active Control Application to Subsonic Transport Aircraft. NASA CR-2408.

33. Hood, R.V. : Active Controls Changing the Rules of Structural Design. Astronautics and Aeronautics pp 50-55, August 1972.

34. Holloway, R.B. and Burris, P.M. : Aircraft Performance Benefits from Modern Control System Technology. J. Aircraft, Vol. 7, No. 6, pp 550-553, December 1970.

35. Rynaski, E.G. and Weingarten, N.C. : Flight Control Principles for Control Configured Vehicles. AFFDL TR-71-154, January 1972.

36. Rohling, W.J. et al. : Compatibility of Maneuver Load Control and Relaxed Static Stability. AFFDL TR-71-183, January 1972.

37. Hoak, D.E. and Finck, R.D. : USAF Stability and Control DATCOM. AFFDL, October 1960.

38. Pearce, B.F., Johnson, W.A. and Siskind, R.K. : Analytical Study of Approximate Longitudinal Transfer Functions for a Flexible Airframe. ASD TDR-62-279, July 1962.

39. Milne-Thomson, L.M. : Theoritical Aerodynamics. St. Martin's Press, Inc., New York 1958.

40. Etkin, Bernard: Dynamics of Flight. John Wiley & Sons, Inc., New York, 1959.

41. Balcerak, J.C., and White, R.P., Jr. : Ground Vibration Tests, AF/TIFS Convair 580 Airplane. Calspan Flight Research Department TIFS Memo No. 569, May 1971.

42. CTIFS Memo No. 217, 16 January 1970.

43. Memo Report ASI-2220-12, 13 March 1970: Status of TIFS Aircraft as of January 2, 1970.

44. Memo : C/TIFS VSS Checkout - to R.P. Harper., Jr. from J.Dittenhauser, dated 28 May 1974.

45. Memo : Completion of AT/TIFS - to R.P. Harper, Jr., from R.D. Till, dated 13 September 1974.

46. Memo : Cost of Digital Computer for the TIFS Aircraft - to R.P. Harper, Jr., from R.D. Till, dated 27 August 1974.

47. Memo : Cost of Collective Aileron Modification to TIFS for ACT Study Program - to R.P.Harper, Jr., from R.D. Till, dated 26 November 1974.

NASA CR-132614

DISTRIBUTION LIST
NAS1-13329

	No. Copies
NASA Langley Research Center Hampton, VA 23665	
Attn: Report & Manuscript Control Office, Mail Stop 180A	1
Raymond L. Zavasky, Mail Stop 115	1
Active Controls Project Office, Mail Stop 173	58
NASA Ames Research Center Moffett Field, CA 94035	
Attn: Library, Mail Stop 202-3	1
NASA Flight Research Center Edwards, CA 93523	
Attn: Library	1
NASA Goddard Space Flight Center Greenbelt, MD 20771	
Attn: Library	1
Jet Propulsion Laboratory 4800 Oak Grove Drive Pasadena, CA 91103	
Attn: Library, Mail 111-113	1
NASA Johnson Space Center Houston, TX 77058	
Attn: JM6/Library	1
NASA John F. Kennedy Space Center Kennedy Space Center, FL 32899	
Attn: Library, IS-DOC-1L	1
NASA Lewis Research Center 21000 Brookpark Road Cleveland, OH 44135	
Attn: Library, Mail Stop 60-3	1
NASA Marshall Space Flight Center Marshall Space Flight Center, AL 35812	
Attn: Library	1
National Aeronautics & Space Administration Washington, DC 20546	
Attn: KSS-10/Library	1
RE/NASA Headquarters	1
NASA Scientific & Technical Information Facility P. O. Box 33 College Park, MD 20740	30 plus reproducible